

**Soil Moisture Droughts
in Germany:
Retrospective Analysis,
Parametric Uncertainty, and
Monitoring**

Dissertation

zur Erlangung des akademischen Grades doctor rerum naturalium
(Dr. rer. nat.)

vorgelegt dem Rat der Chemisch-Geowissenschaftlichen Fakultät der
Friedrich-Schiller-Universität Jena

von Dipl.-Hydrol. Matthias Zink
geboren am 31. März 1983 in Hoyerswerda

Betreuerin: Prof. Dr. Sabine Attinger
Ko-Betreuer: Dr. Luis E. Samaniego

Diese Dissertation ist während meiner Beschäftigung als wissenschaftlicher Mitarbeiter im Department Hydrosystemmodellierung am Helmholtz-Zentrum für Umweltforschung - UFZ in Leipzig entstanden. Die hier dargestellten Erkenntnisse wurden im Rahmen der Projekte *Water and Earth System Science Cluster (WESS)*, *Regionale Klimaänderung (REKLIM)* und *Earth Systems Dynamics der Helmholtz Gemeinschaft (HGF-EDA)* erlangt. Diese Dissertation wurde von der *Helmholtz Interdisciplinary Graduate School for Environmental Research (HIGRADE)* unterstützt.

Gutachter:

Prof. Dr. Sabine Attinger
Friedrich-Schiller-Universität Jena

Prof. Dr. Ralf Merz
Martin-Luther Universität Halle-Wittenberg

Die Dissertationsverteidigung fand am 08. September 2016 in Jena statt.

Contents

Danksagung	VII
Zusammenfassung	IX
Abstract	XVII
1 Introduction and Scope of the Study	1
1.1 Background	1
1.2 Hydrologic Models	3
1.3 Uncertainty in Hydrologic Modeling	5
1.4 Droughts	6
1.5 Research Objectives	8
2 A High-Resolution Dataset of Water Fluxes and States for Germany Accounting for Parametric Uncertainty	11
2.1 Abstract	13
2.2 Introduction	13
2.3 Study Domain and Datasets	15
2.3.1 Land Surface Properties	17
2.3.2 Meteorological Forcings	18
2.4 Methodology	19
2.4.1 The mesoscale Hydrologic Model mHM	19
2.4.2 Derivation of Representative Parameter Sets	20
2.4.3 Validation Data	21
2.4.4 Uncertainty of Ensemble Model Simulations	23
2.5 Results and Discussion	24
2.5.1 Discharge Evaluation in Major German River Basins	24
2.5.2 Discharge Evaluation at Non-calibrated Basins	27
2.5.3 Evapotranspiration and Soil Moisture Evaluation at Eddy Covariance Stations	29
2.5.4 Evaluation of Groundwater Recharge	31
2.5.5 Spatial Patterns of Ensemble Means and Uncertainties	33
2.5.6 Spatio-temporal Distribution of Uncertainties	35
2.5.7 Propagation of Uncertainty Through Model Internal Com- ponents	36
2.6 Summary and Conclusion	38
2.7 Data Availability and Data Format	39

3	Implications of Parameter Uncertainty on Soil Moisture Drought Analysis in Germany	41
3.1	Abstract	43
3.2	Introduction	43
3.3	Soil Moisture Data	47
3.3.1	The mesoscale Hydrologic Model mHM	47
3.3.2	Ensemble Description and Experimental Design	49
3.4	The Soil Moisture Index	51
3.4.1	Aggregation and Normalization	51
3.4.2	Estimation of the Soil Moisture Index	51
3.4.3	Identification of Drought Events	52
3.4.4	Quantification of Drought Characteristics	54
3.5	Results and Discussion	55
3.5.1	mHM Evaluation	55
3.5.2	Retrospective Reconstruction of Soil Moisture Fields	56
3.5.3	Comparison with Other Indices	60
3.5.4	Sensitivity of the Parameter Uncertainty Related to Precipitation Interpolation	61
3.5.5	Overall Parameter Uncertainty of the Soil Moisture Index	62
3.5.6	Identification of Major Drought Events based on Mean Duration, Mean Areal Extent and Total Magnitude	65
3.5.7	Uncertainty of Large Events Occurring in Summer and Winter	69
3.5.8	Uncertainty of the Severity-Area-Duration Curves	71
3.5.9	Drought Persistence and Trends of the Soil Moisture Index	72
3.6	Summary and Conclusions	73
4	Calibration of a Hydrological Model using Patterns of Satellite Derived Land Surface Temperature	75
4.1	Abstract	77
4.2	Introduction	77
4.3	Study Domain and Data	80
4.3.1	Meteorological Data	80
4.3.2	Study Domain and Land Surface Properties	81
4.4	Methodology	82
4.4.1	The mesoscale Hydrologic Model mHM	82
4.4.2	Development of a Land Surface Temperature Module	83
4.4.3	Optimization of the Coupled mHM-Land Surface Temperature Model	87
4.4.4	Experimental Design	92
4.5	Results and Discussion	94
4.5.1	The Predictive Skill of Land Surface Temperature Regarding River Runoff	94
4.5.2	Calibration of mHM with River Runoff and Land Surface Temperature	98

4.6	Summary and Conclusions	104
5	The German Drought Monitor	107
5.1	Abstract	109
5.2	Introduction	109
	5.2.1 Existing Drought Monitoring Systems	111
	5.2.2 Justification for a German Drought Monitor	112
5.3	Operational Drought Monitoring Framework	113
5.4	Benchmark for the Recent 2015 Drought Event	116
5.5	Conclusion and Outlook	118
6	Discussion and Outlook	121
6.1	Discussion	122
6.2	Outlook	124
	References	127
	List of Figures	i
	List of Tables	vii
	Selbstständigkeitserklärung	xi

Danksagung

Mein erster Dank gilt Prof. Sabine Attinger, die mir die Möglichkeit gab diese Dissertation anzufertigen und immer zur Stelle war, wenn man sie brauchte.

Mein besonderer Dank gilt Dr. Luis E. Samaniego für die Betreuung dieser Arbeit. Seine Begeisterung für die Hydrologie war sehr inspirierend und ansteckend. Falls nötig, wurden Blumentöpfe, Salzstreuer oder sonstige verfügbare Materialien genutzt, um einen Sachverhalt zu verdeutlichen. Luis war stets auf ein hohes Maß an wissenschaftlicher Stringenz bedacht, was die Qualität meiner Arbeit und auch meine berufliche Entwicklung positiv beeinflusste. Er ermutigte mich meine Arbeit auf Konferenzen zu präsentieren und zu diskutieren, wodurch der Grundstein für internationalen wissenschaftlichen Austausch gelegt wurde.

Jule - vielen Dank für die enge Zusammenarbeit und vor allem für unsere Freundschaft. Unsere Mathematiker-Hydrologen-Diskussionen waren immer sehr erleuchtend und kurzweilig. Große Teile meines Wissen habe ich dir zu verdanken, wie z.B. die Erörterung der Frage "Wie entstehen Zufallszahlen?"

Auch Matthias möchte ich an dieser Stelle ein großes Dankeschön sagen. Ohne dich hätte sich mir vermutlich nie die wundervolle Welt von Bash und Unix ergründet. Auch an so manch anderen Problemen hätte ich mir ohne deine Hilfe wohl die Zähne ausgebissen.

Dir, Rohini, danke ich für unermüdliche Diskussionen, konstruktive Ratschläge und deine stets gute Laune. In noch so schwierigen Situationen hast du mit deinem Optimismus Projekte voran getrieben.

Auch der stetige Austausch mit euch, Stephan und Andreas, haben mir sehr geholfen und zum Entstehen dieser Arbeit beigetragen.

Ich möchte mich bei Corinna Rebmann, David Schäfer und dem gesamten Kollegium des Departments Hydrosystemmodellierung für eine inspirierende und freundliche Arbeitsumgebung bedanken. Danke an Ben Langenberg, Thomas Schnicke und Christian Krause für eure Hilfe bei Arbeiten auf unserem Cluster "EVE".

Nicht zuletzt ist auch eine gute Portion moralische Unterstützung nötig, um solch eine Arbeit anzufertigen. Vor allem dafür, aber auch für dein unermüdliches Korrekturlesen, möchte ich mich bei dir, Edna, bedanken. Auch ohne eure Unterstützung und Bestärkung, Mutti, Vati und Sebastian, wäre diese Arbeit niemals möglich gewesen.

Zusammenfassung

Motivation

Dürren sind nach Hochwasserereignissen die schwersten Naturkatastrophen weltweit. Zwischen 1950 und 2014 waren 2.2 Milliarden Menschen von Dürreereignissen betroffen. In Europa sind Dürren die kostenintensivsten Naturereignisse. Eine durchschnittliche Schadenssumme von 621 Mio. EUR pro Ereignis macht diese Naturkatastrophen zu einer ernstzunehmenden Gefahr. Das letzte, große Dürreereignis in Europa trat 2003 auf. Allein in Deutschland gab es im Zusammenhang mit diesem Ereignis 7000 Todesfälle und einen wirtschaftlichen Schaden von 1,5 Milliarden EUR infolge von Ernteaufschlägen. Diese agro-ökonomischen Auswirkungen begründen die Bedeutung eines operationellen Monitorsystems für landwirtschaftliche Dürren. Solch ein System bietet die Möglichkeit negativen Auswirkungen von Bodendürreereignissen entgegenzuwirken.

Das Monitoring landwirtschaftlicher Dürren kann nicht auf der Basis von beobachteten Daten realisiert werden, da großräumige Messungen von Bodenfeuchte sowohl technisch als auch wirtschaftlich nicht umsetzbar sind. Mittels hydrologischer Modellierung kann Bodenfeuchte jedoch auch weiträumiger, z.B. auf nationaler Ebene, ermittelt werden. Hydrologische Modelle berücksichtigen meteorologische Beobachtungsdaten, um Abschätzungen der Größen des hydrologischen Kreislaufs, wie z.B. der Bodenfeuchte, geben zu können. Jedoch unterliegen diese Abschätzungen verschiedenen Unsicherheiten. Diese entstehen aus Unsicherheiten in den Modelleingangsdaten, der Modellstruktur, den Anfangsbedingungen und den Modellparametern. Die Parameterunsicherheit in hydrologischen Modellen ist einer der Untersuchungsgegenstände dieser Arbeit.

Die Zielstellung dieser Studie ist es, ein operationelles Monitoringsystem für landwirtschaftliche Dürren in Deutschland zu entwickeln. Um ein solches System in den operationellen Einsatz zu bringen, sind folgende Herausforderungen zu bewältigen: Erstens, die Berechnung eines räumlich kontinuierlichen Bodenfeuchtedatensatzes für Deutschland mittels hydrologischer Modellierung unter Einbeziehung der Unsicherheiten, welche durch die Abschätzung von Modellparametern entstehen. Zweitens, die Bestimmung der Unsicherheiten von Dürrecharakteristika (z.B. Intensität, Dauer) bei der Identifizierung historischer Dürreereignisse. Diese geben Auskunft über die Unsicherheiten eines Dürremonitoringsystems. Drittens, die Erforschung eines Ansatzes um Parameterunsicherheiten mittels satellitengestützter

Landoberflächentemperatur zu reduzieren. Und viertens, die Entwicklung und Implementierung eines Dürreinformationssystems, welches in fast-Echtzeit Karten des Bodenfeuchtezustands in Deutschland liefert. Die Gliederung dieser Studie orientiert sich an diesen vier Teilaufgaben.

Methodik

Die nachfolgend dargestellten Untersuchungen wurden mit Hilfe des mesoskaligen Hydrologischen Modells mHM durchgeführt. mHM ist ein prozess-basiertes hydrologisches Modell, das Gitterzellen als hydrologische Einheiten betrachtet (räumlich explizites Modell). Es grenzt sich vor allem durch den Multiscale Parameter Regionalization-Ansatz von anderen hydrologischen Modellen ab. Dieser Parametrisierungsansatz stellt die Berücksichtigung von kleinskaligen Variabilitäten sicher. Dadurch ist es möglich mit mHM hydrologische Flüsse und Zustandsvariablen sowohl auf unterschiedlichen Skalen als auch in unterschiedlichen Einzugsgebieten ohne erneute Kalibrierung verlässlich zu simulieren. Das Modell wird durch Niederschlags- und Temperaturdaten angetrieben. Diese Daten werden als Stationsdaten vom Deutschen Wetterdienst bereitgestellt und mittels external drift kriging auf ein hochaufgelöstes $4 \times 4 \text{ km}^2$ Gitter interpoliert.

Das Untersuchungsgebiet ist die Bundesrepublik Deutschland. Diese wird in hydrologische Untersuchungsgebiete - die großen innerdeutschen Flusseinzugsgebiete Mulde, Ems, Neckar, Saale, Main, Weser und Donau - unterteilt. mHM wird in diesen Flussgebieten kalibriert. Die Validierung erfolgt in 222 zusätzlichen, deutschen Einzugsgebieten, welche bei der Kalibrierung nicht berücksichtigt wurden. Ein Teil dieser Einzugsgebiete liegt innerhalb der großen sieben Flussgebiete. Weiterhin wird die simulierte Evapotranspiration anhand der Daten von sieben Eddy-Kovarianz-Stationen validiert.

Das hydrologische Modell mHM wurde für die zuvor genannten Einzugsgebiete aufgesetzt. Die räumliche Auflösung entsprach der Auflösung der meteorologischen Eingangsdaten ($4 \times 4 \text{ km}^2$). Die Simulationsperiode belief sich auf einen Zeitraum von 1950-2010. Um die Vergleichbarkeit mit den Eddy-Kovarianz-Messungen sicherstellen zu können, musste das Modell auf eine räumlichen Auflösung von $100 \times 100 \text{ m}^2$ gebracht werden. Diese Auflösung entspricht dem footprint der Eddy-Kovarianzmessungen. Die Übertragbarkeit des Modells ist durch seine Skalenunabhängigkeit gewährleistet.

Die erste im Rahmen dieser Arbeit durchgeführte Studie befasst sich mit der Berechnung räumlich kontinuierlicher hydrologischer Flüsse und Zustandsvariablen mittels mHM (Kapitel 2). Dieser in sich konsistente Datensatz besteht aus täglichen Daten von Evapotranspiration, Bodenfeuchte, Grundwasserneubildung und pro-Gitterzelle-generiertem Abfluss in Deutschland über einen Zeitraum von 1950

bis 2010.

Um räumliche konsistente Felder der zuvor genannten Variablen zu erhalten, wurde ein zweistufiges Parameterschätzverfahren entwickelt. In einem ersten Schritt wird mHM in jedem der sieben großen deutschen Flusseinzugsgebieten kalibriert. Im zweiten Schritt werden die einzugsgebietspezifischen Parameter in die anderen sechs Einzugsgebiete übertragen. In einer Validierungsperiode wird deren Vorhersagegüte bezüglich des Durchflusses bestimmt. Nur Parametersätze die eine Nash-Sutcliffe Effizienz größer 0,65 aufweisen, werden für die darauffolgenden Ensemble-Simulationen auf dem gesamten Bundesgebiet herangezogen. Dieses Kriterium wird von 100 Parametersätzen erfüllt.

Die Unsicherheiten dieser Ensemble-Simulationen werden auf zwei verschiedenen Ebenen betrachtet. Auf der Einzugsgebietsebene werden die Unsicherheiten der Durchflusssimulationen analysiert. Auf Ebene der Gitterzellen werden die Unsicherheiten von Evapotranspiration, Bodenfeuchte, Grundwasserneubildung und pro-Gitterzelle-generiertem Abfluss hinsichtlich ihrer räumlichen und zeitlichen Verteilung analysiert.

Die zweite hier vorgelegte Studie beschäftigt sich mit der Identifikation von Dürreereignissen (Kapitel 3). Diese basiert auf den zuvor modellierten Bodenfeuchtedaten. Bodendürrebedingungen werden mittels eines neu entwickelten Bodenfeuchteindex identifiziert. Dieser stellt das Perzentil der Bodenfeuchte im betrachteten Monat und der betrachteten Gitterzelle dar. Er wird durch das Anpassen einer nicht-parametrischen, Kernel-basierten, kumulativen Verteilungsfunktion an den historischen Bodenfeuchtedatensatz (1951-2010) berechnet. Dürrebedingungen werden angenommen, sobald der Bodenfeuchteindex einen Grenzwert von 0,2 unterschreitet.

Um Benchmark-Ereignisse zu identifizieren werden Dürrebedingungen sowohl räumlich als auch zeitlich mit Hilfe eines Clusteralgorithmus konsolidiert. Diese Benchmark-Ereignisse werden bezüglich ihrer Ausdehnung, Dauer, Schwere, Intensität und Magnitude klassifiziert. Die Identifizierung der Benchmark-Ereignisse und deren Charakteristika werden bezüglich ihrer Unsicherheiten, stammend aus dem Ensemble-Bodenfeuchtedatensatz, analysiert.

Die nachfolgende Studie untersucht Möglichkeiten zur Reduktion der Parameterunsicherheiten (Kapitel 4). Es wird die Hypothese aufgestellt, dass die Modellparameter besser eingeschränkt werden können, wenn mHM mit satellitenbasierter Landoberflächentemperatur und Durchfluss gemeinsam kalibriert wird. Dabei stellt die Kalibrierung mittels Durchfluss die korrekte Aufteilung des Niederschlagswassers auf die einzelnen Komponenten der Wasserbilanz für das gesamte Einzugsgebiet sicher. Diese Methodik hat jedoch keine Aussagekraft über die räumliche Verteilung der hydrologischen Flüsse und Zustandvariablen innerhalb des Einzugsgebiets. Daher soll die Berücksichtigung räumlich verteilter Landoberflächentemperatur bei der Kalibrierung die räumliche Repräsentanz des Modells

verbessern.

Um mHM mit Landoberflächentemperatur kalibrieren zu können, wird ein eigenständiges Modul zur Berechnung der Landoberflächentemperatur entwickelt und an mHM gekoppelt. Dieses Modul kann an verschiedene Umweltsystemmodelle gekoppelt werden. Weiterhin wurde ein Kriterium zur Erkennung räumlicher Muster entwickelt, um explizit die räumliche Struktur der Landoberflächentemperaturen bei der Kalibrierung zu berücksichtigen. Dieses Kriterium wurde so gewählt, dass es nicht sensitiv bezüglich eines Biases ist.

In einer zweiten Hypothese wird postuliert, dass die Kalibrierung von mHM mit Landoberflächentemperaturen zu einem gewissen Maße zur Simulation von Durchfluss eingesetzt werden kann. Die Parameter, welche durch einen solchen Ansatz geschätzt wurden, werden zur Verifizierung dieser Hypothese in den 222 kleineren Einzugsgebieten validiert.

Schlussendlich wurde ein operationelles System zum Monitoring von landwirtschaftlichen Dürren in Deutschland entwickelt (Kapitel 5). Dieses System basiert im Wesentlichen auf vier Arbeitsschritten: (1) der täglichen Aktualisierung der meteorologischen Datenbasis mit Messdaten des Deutschen Wetterdienstes einschließlich Konsistenzprüfung und Ausreißertest, (2) der Simulation der Bodenfeuchte mittels mHM, (3) der Berechnung des Bodenfeuchteindex und (4) der Klassifizierung des Bodenfeuchteindex in fünf Dürreklassen die von “ungewöhnlich trocken” bis “außergewöhnliche Dürre” reichen.

Ergebnisse und Diskussion

Bevor die 100 Ensemble-Parametersätze auf nationaler Ebene eingesetzt werden konnten, wurden sie bezüglich ihrer Vorhersagegüte für Durchfluss untersucht. In den 222 Validierungseinzugsgebieten konnte eine ausreichende Qualität der Durchflusssimulationen beobachtet werden. Die mittlere Nash-Sutcliffe Effizienz (NSE) ist 0,68 für diese Einzugsgebiete. Dieses Ergebnis zeigt, dass mittels der Ensemble Parametersätze hinreichend genaue Durchflusssimulationen durchgeführt werden konnten, ohne das Modell im jeweiligen Einzugsgebiet kalibrieren zu müssen. An den Eddy-Kovarianz-Stationen bildete das Modell die Magnitude, die Dynamik und die Varianz der Evapotranspirationmessungen gut ab. Die größten Differenzen zwischen mHM und den Messungen traten im Frühling auf. Die Implementierung eines dynamischen Vegetationswachstumsmodells in mHM könnte diese Abweichungen vermutlich reduzieren. Zusammenfassend ist zu sagen, dass sich die Ensemble-Parametersätze für die Simulation auf nationaler Ebene als geeignet erwiesen.

Die modellierten Felder für Evapotranspiration, Bodenfeuchte, Grundwasserneubildung und pro-Gitterzelle-generiertem Abfluss spiegeln hauptsächlich das räum-

liche Muster des Niederschlags wieder. Der Trockenheits-Index (Budyko's dryness index) dominiert die räumliche Verteilung der Unsicherheiten in Bodenfeuchte, Grundwasserneubildung und generiertem Abfluss. Große Unsicherheiten in der Evapotranspiration korrelierten zusätzlich mit hohen Porositätswerten des Bodens. Unter den vier betrachteten Variablen zeigte die Evapotranspiration die geringste Unsicherheit in Bezug auf die Größenordnung. Weiterhin unterlag die Unsicherheit kaum Schwankungen im Laufe des Jahres. Die Unsicherheit der Grundwasserneubildung zeigte die größte Magnitude und eine ausgeprägte Dynamik innerhalb eines Jahres. Bei der Bodenfeuchte variierte sowohl die Magnitude als auch die unterjährliche Dynamik der Unsicherheit in Abhängigkeit der geografischen Lage innerhalb Deutschlands.

Die Analyse von Dürreereignissen in den vergangenen 60 Jahren in Deutschland basiert auf diesem Bodenfeuchtedatensatz. Als die drei schwersten Dürren bezüglich ihrer Magnitude wurden die Ereignisse 1962-65, 1971-74 und 1975-78 identifiziert. Interessanterweise rangiert die Dürre 2003-2005 nur auf Platz 7, obwohl dieses Ereignis schwerwiegende Schäden in Europa nach sich zog. Dies ist damit zu begründen, dass das Dürreereignis von einer Hitzewelle intensiviert wurde, welche eine Rekordmarke der Temperaturen der vergangenen 500 Jahre darstellte.

Die Unsicherheiten in den Bodenfeuchtesimulation wirken sich auf die Bestimmung von Dürrecharakteristika aus. Daher entstehen signifikante Unsicherheiten bei der Klassifikation von Dürreereignissen. Für das Dürreereignis 1971-74, welches als das längste und schwerste Ereignis seit 1951 bestimmt wurde, konnte diese Einordnung nur in 67% der Ensemble-Simulationen nachgewiesen werden. Der Ensemble-Mittelwert der räumlichen Ausdehnung dieser Dürre beträgt 43% der Fläche Deutschlands. Die Ensemble-Standardabweichung der Ausdehnung beträgt hingegen 5%, was in etwa der Fläche Sachsens entspricht. Diese Ergebnisse zeigen, dass eine Betrachtung einzelner Modellsimulationen zu fehlerhaften Abschätzungen bei der Identifikation und Charakterisierung von Dürreereignissen führen kann.

Unter Zuhilfenahme zusätzlicher Daten bei der Modellkalibrierung sollen Parameterunsicherheiten reduziert werden. Neben Durchfluss wurde das hydrologische Modell mHM zusätzlich mit satellitengestützter Landoberflächentemperatur kalibriert. Diese Methodik bewirkte eine bessere Eingrenzung der Spannweite der kalibrierten Parameter, d.h. der Parameterunsicherheit, im Vergleich zu einer klassischen Kalibrierung, welche sich nur auf Durchflussdaten stützt. Insbesondere Unsicherheiten der Parameter, die mit der Evapotranspiration zusammenhängen, konnten erheblich reduziert werden. Gleichzeitig verschlechterte sich jedoch die Güte der Durchflusssimulationen in den sechs großen Einzugsgebieten (ohne Donau) um circa 6%. Demgegenüber verbesserte sich die Schätzung der Evapotranspiration an Eddy-Kovarianz-Stationen um 5%. Aufgrund dieser Kompromisslösung und vor allem der reduzierten Parameterunsicherheiten wird diese Methode als vorteilhaft gegenüber einer klassischen Kalibrierung mit Durchflusszeitreihen angesehen.

Ein zweites Experiment dieser Studie zielte auf die Bewertung der Landoberflächentemperatur hinsichtlich ihres Nutzens zur Simulation von Durchfluss. Dafür wurde das Modell alleinig mit der Landoberflächentemperatur kalibriert. Der mittlere Median der Nash-Sutcliffe Effizienz ist 0,51 in den sechs großen deutschen Einzugsgebieten (ohne Donau). Dieser Median basiert auf 20 unabhängigen Kalibrierungsläufen in den jeweiligen Einzugsgebieten. In den 222 Validierungseinzugsgebieten konnte ein mittlerer NSE von 0.4 erreicht werden. Diese Ergebnisse lassen die Schlussfolgerung zu, dass mittels Landoberflächentemperatur eine gewisse Modellgüte in der Durchflusssimulation erreicht werden kann. Die größte Diskrepanz zwischen Simulation und Messung zeigte sich bei Niedrigwasserbedingungen. Dies kann damit begründet werden, dass die Landoberflächentemperatur oberflächennahe Bedingungen gut abbildet, jedoch ungenügenden Informationsgehalt für unterirdische hydrologische Prozesse besitzt.

Die zuvor dargestellten Erkenntnisse bezüglich landwirtschaftlicher Dürren mündeten in der Implementierung des deutschen Dürremonitors (GDM). Dieser stellt der Öffentlichkeit hochaufgelöste Informationen über Dürren mittels leicht verständlicher Karten in fast-Echtzeit mit einer Verzögerung von 4 Tagen zur Verfügung (www.ufz.de/duerremonitor). Mit Hilfe des deutschen Dürremonitors konnte bereits ein Dürreereignis im Jahr 2015 beobachtet und analysiert werden. Während dieses Ereignisses etablierte sich der GDM als Informationsplattform durch zahlreiche Veröffentlichungen in regionalen und nationalen Zeitungen sowie bei Fernsehanstalten. Auch Landesbehörden begannen die Informationen des deutschen Dürremonitors zu nutzen (z.B. Sächsisches Landesamt für Umwelt, Landwirtschaft, und Geologie; Bayerische Landesanstalt für Landwirtschaft). Die Karten des Dürremonitors sind frei verfügbar und können von der Webseite heruntergeladen werden. Im Bedarfsfall werden zusätzliche Informationen, z.B. der Bodenfeuchteindex, auf Anfrage kostenfrei bereitgestellt.

Der deutsche Dürremonitor ermöglichte die Entwicklung des Dürreereignisses 2015 in fast-Echtzeit zu verfolgen. Hotspots wie Berlin, Nordbayern und Ostsachsen wurden vom GDM abgebildet. In Nordbayern und Ostsachsen wurde wegen anhaltender Trockenheit im Boden die Waldbrandbeobachtung intensiviert. In Berlin begannen bereits im August die Stadtbäume ihr Laub einzufärben. Im gesamtdeutschen Maßstab kam es zu Ernteeinbußen von 22% beim Körnermais, verglichen mit den durchschnittlichen Hektarerträgen der vorangegangenen 6 Jahre (2009-2014). Fast 75% der Fläche Deutschlands waren im Juli zumindest von moderaten Dürrebedingungen betroffen. Diese Ereignis rangiert bezüglich seiner Magnitude unter den 10 schwersten Dürren im Zeitraum 1951-2015.

Schlussfolgerungen

Diese Studie zeigt die notwendigen Schritte zur operationellen Beobachtung von landwirtschaftlichen Dürren in Deutschland. Zunächst wurden räumlich kontinuierliche und hochaufgelöste Bodenfeuchtedaten für Deutschland modelliert. Diese basierten auf deutschlandweit validen Parametersätzen. Neben Bodenfeuchte wurden Evapotranspiration, Grundwasserneubildung und per-Gitterzelle-generierter Abfluss hinsichtlich ihrer parameterbedingten Unsicherheiten untersucht. Die Unsicherheiten in Bodenfeuchtesimulationen zeigten signifikante Auswirkungen auf die Identifikation und Charakterisierung von Dürreereignissen in Deutschland. Im Folgenden wurde eine Methodik zur Reduzierung dieser Unsicherheiten erforscht.

Die hier dargelegten Arbeitsschritte führten zum ersten, frei verfügbaren, nationalen Monitorsystem für landwirtschaftliche Dürren. Dieses System ermöglicht die unverzügliche Einordnung der Schwere von Dürreereignissen durch den Vergleich mit historischen Dürren. Der deutsche Dürremonitor ist ein wichtiges Element für die Kommunikation von Dürreinformationen in die Öffentlichkeit und an Landesbehörden. Diese Informationen sind die Grundlage, um mögliche Schäden aufgrund von Bodendürren abzuwenden, wie z.B. durch Intensivierung von Waldbrandbeobachtungen. Unsicherheiten beim Dürremonitoring wurden im deutschen Dürremonitor zum jetzigen Zeitpunkt nicht berücksichtigt. Die Kommunikation solcher Unsicherheiten sowie die Auswirkung von Bodenwasserdefiziten auf landwirtschaftliche Erträge bedürfen weiterer Forschung. Diese soll in Kooperation mit sozialwissenschaftlichen Forschern und unter Einbeziehung der Stakeholder in den nächsten Jahren vorangetrieben werden.

Abstract

Motivation

Droughts are worldwide the second most severe natural disaster beside floods. They affected 2.2 billion people between 1950 and 2014. In Europe, droughts are the costliest natural disasters with average expenses of 621 million EUR per event. The last severe drought event took place in 2003. It covered extensive areas of Europe, affected many sectors of the society, and caused 7,000 fatalities. Further, it induced an agro-economic loss of 1,5 billion EUR in Germany alone. Such economical losses emphasize the need of an operational system for monitoring agricultural droughts in order to mitigate their negative consequences.

Observation-based monitoring of agricultural droughts, which are characterized by soil moisture deficits, is technically and economically not feasible on regional to national scales. Hydrologic modeling is the prime alternative to estimate soil moisture availability on large spatial domains. Such models are driven by meteorological observations and predict hydrological fluxes and states, such as soil moisture or evapotranspiration. Predictions of hydrologic models underlie several sources of uncertainties. These uncertainties arise from input data, model structure, initial conditions, and model parameters. The implications of parametric uncertainty to hydrologic predictions are analyzed herein.

The main objective of this work is to develop a monitoring system for agricultural droughts in Germany. The development of such a system includes several challenges. First, a spatially continuous dataset of soil moisture for entire Germany is derived from modeling. The parametric uncertainty of such hydrologic predictions is taken into account. Second, the propagation of parametric uncertainty of soil moisture to the identification of drought characteristics is estimated in order to evaluate the uncertainty inherent to such a monitoring system. Third, an approach to reduce the parametric uncertainty by using satellite retrieved land surface temperature data is investigated. And fourth, an operational system providing drought information in near-real time is developed and implemented. The outline of this study is organized following these objectives.

Methods

All computational experiments presented herein are conducted with the mesoscale Hydrologic Model mHM. mHM is a process-based hydrological model, which treats grid cells as hydrological units (distributed model). A key feature of mHM is the Multiscale Parameter Regionalization. This parameterization approach explicitly takes subgrid variabilities into account. It ensures mHM's transferability across locations and scales. The model is forced with observations of precipitation and temperature data, which were provided by the German Meteorological Service. These observations are interpolated to a high spatial resolution of $4 \times 4 \text{ km}^2$ using external drift kriging.

The study domain is the territory of Germany. This domain is subdivided into the seven major inner German river basins: Mulde, Ems, Neckar, Saale, Main, Weser, and Danube. mHM is calibrated within these catchments and validated in additional 222 river basins throughout Germany to assess the validity and transferability of parameter sets. Some of these 222 catchments are subcatchments of the seven major river basins. Evapotranspiration estimates of mHM are evaluated at seven eddy covariance stations.

mHM is set up for these regions using a high spatial resolution that is identical to the meteorological input ($4 \times 4 \text{ km}^2$). The temporal resolution of the model is hours, whereas the input and outputs are on daily basis. The overall simulation time period is 1950 to 2010. This period is shortened for the subbasins according to available river runoff observations. One of mHM's key features, the scale independency, is used to estimate evapotranspiration at scale of eddy covariance stations with a spatial resolution of $100 \times 100 \text{ m}^2$. This resolution is comparable to the footprint of eddy covariance observations.

A first study aims on the estimation of a consistent dataset of hydrologic fluxes and states using mHM. This dataset contains evapotranspiration, soil moisture, groundwater recharge and per-model-cell-generated runoff (Chapter 2). It is freely available for the public from 1950-2010 on a daily basis.

A two-step parameter estimation procedure was developed to derive continuous fields of the above-mentioned variables. In a first step, the hydrologic model mHM is calibrated within the seven distinct river catchments. In a second step, the catchment specific parameter sets are interchanged between the seven catchments to assess their performance in a validation period. Only parameter sets exceeding a Nash-Sutcliffe Efficiency of 0.65 in all seven catchments are retained. As a result 100 parameter sets are used for the prediction of a nationwide ensemble of hydrological fluxes and states.

The uncertainty of the ensemble simulation is assessed at two levels. On the catchment level, the uncertainty of model performance is evaluated regarding river runoff simulations. On the grid level, the uncertainty of evapotranspiration, soil moisture,

groundwater recharge and per-grid-cell-generated runoff is analyzed regarding its spatio-temporal distribution.

A second study focuses on the identification of drought characteristics (Chapter 3) based on the ensemble soil moisture of the previously generated dataset. Drought conditions are identified by a recently developed and implemented Soil Moisture Index (SMI). The SMI is defined as the percentile of soil moisture for a particular month and grid cell. It is estimated by fitting a non-parametric, kernel-based, cumulative distribution function to the historic soil moisture data. Soil moisture droughts are identified when the SMI is below a threshold of 0.2.

Benchmark drought events in Germany are identified by applying a cluster algorithm. This algorithm consolidates drought conditions in space and time. The drought events are analyzed regarding their spatial extent, duration, severity, intensity, and magnitude. The identification of benchmark events as well as their drought characteristics are reviewed regarding their uncertainties, which originate from the ensemble soil moisture estimation.

A consecutive study aims on the reduction of parametric uncertainty in mHM (Chapter 4). It is hypothesized that model parameters are better constrained if mHM is calibrated simultaneously with satellite derived land surface temperature and river runoff. The calibration with runoff ensures the right partitioning of water balance components at the catchment scale, but is insufficient to estimate the spatial distribution of water fluxes and states within the catchment. Thus, incorporating spatial distributed land surface temperature may increase the spatial representativeness of the model.

A diagnostic land surface temperature module is developed and coupled to mHM in order to calibrate mHM with land surface temperature. This module can be coupled to any environmental model. Further, a bias insensitive, non-parametric pattern matching criterion was developed to exclusively account for the spatial patterns of land surface temperature.

Beside that, it is hypothesized that parameters which are inferred by calibrating mHM with land surface temperature alone, have a certain predictive skill regarding river runoff. This skill is assessed by validating the parameters in the seven major and 222 minor river basins within Germany.

Finally, I developed an operational system for agricultural drought monitoring in Germany (Chapter 5). This system consists of four steps: (1) a daily update of observed meteorological data from the German Meteorological Service, with consistency checks and interpolation; (2) an estimation of current soil moisture conditions using mHM; (3) the calculation of the Soil Moisture Index; and (4) the classification of the Soil Moisture Index into five drought classes ranging from “abnormally dry” to “exceptional drought”.

Results and Discussion

The 100 ensemble parameter sets were evaluated regarding their capability to reproduce observed discharge before applying them to the national domain. They led to reasonable discharge estimations when validating them within the 222 catchments. The Nash-Sutcliffe Efficiency (NSE) was 0.68 for the median of daily discharge simulations within these catchments. This result confirms that the ensemble parameters are capable of sufficiently reproducing river runoff without being calibrated on a particular location. The validation with evapotranspiration observations at the eddy covariance towers revealed that the dynamics, the magnitude and the variance of the observations were captured by the model. The largest error between observations and model simulations is observed in spring which may be caused by the absence of a dynamic vegetation representation within mHM. It is concluded that the ensemble parameter sets are appropriate for the nationwide simulation.

The modeled fields of evapotranspiration, soil moisture, groundwater recharge and per-grid-cell-generated runoff mainly reflect the pattern of precipitation. I found that uncertainty of soil moisture, groundwater recharge and generated runoff are governed by the pattern of the Budyko's dryness index. The spatial distribution of high uncertainties in evapotranspiration is, however, closely related to the areas of high soil porosity. The evapotranspiration is the least uncertain variable out of the four in terms of magnitude. Its uncertainty stays almost constant over the course of a year. The highest uncertainty can be observed in groundwater recharge, which follows a distinct inter-annual dynamic. The magnitude of soil moisture uncertainties varies between different regions in Germany and times of the year.

The nationwide analysis of agricultural droughts is conducted based on this soil moisture dataset. The three most severe agricultural droughts according to its magnitude are the events 1962-65, 1971-74, and 1975-78. Interestingly, the event 2003-2005 which caused extensive negative consequences in Germany ranks only at seventh position. This event was accompanied by a severe heat wave, which exceeded the temperature records of the last 500 years and intensified the negative impacts of the drought event 2003 significantly.

The parametric uncertainty of the ensemble soil moisture propagates to drought characteristics. This leads to significant classification errors for drought events. The event 1971-74, for example, is estimated to be the longest and most severe drought event since 1951. Whereas, it was estimated to be the most severe event in only 67% of the ensemble simulations. The ensemble mean drought area of this event is 43% of Germany. The ensemble standard deviation is 5% for this event, which is almost as large as the area of Saxony. These results show that single parameter sets may lead to inconclusive results regarding drought identification and characteristics.

In a consecutive study, the reduction of the parametric uncertainty is anticipated. For that purpose, mHM is calibrated with satellite retrieved land surface temperature and river runoff. The resulting parameter ranges (parameter uncertainty) are reduced compared to those obtained by a classical calibration with streamflow alone. Especially, the uncertainty of parameters connected to the evapotranspiration is significantly reduced. Meanwhile, the error in discharge simulation of the six catchments (Danube is excluded) increased by 6% using this approach. Contrarily, the error of estimating evapotranspiration at seven eddy flux towers decreased by 5%. Despite this tradeoff, this approach is beneficial compared to the classical calibration with discharge, since the parametric uncertainty decreases.

In a second experiment, the hydrologic model mHM was calibrated with land surface temperature to investigate its predictive skill regarding river runoff. Within the major six German river basins (Danube is excluded), the average Nash-Sutcliffe Efficiency (NSE) is 0.51 for the median performance of 20 independent calibration runs in each catchment. The average median NSE is 0.4 if these parameter sets are transferred to the 222 validation locations. These results lead to the conclusion that land surface temperature has a certain predictive skill regarding river runoff. The largest deviations of observed and simulated runoff are at low flow conditions. This behavior is caused by the fact that land surface temperature characterizes the near surface and thus is a bad estimator for subsurface processes such as baseflow.

The gained knowledge on agricultural droughts led to the implementation of the German Drought Monitor (GDM). The GDM delivers high resolution, easy to understand drought information for the public in near-real time with a latency of 4 days since 2014 (www.ufz.de/droughtmonitor). A recent drought event in 2015 has already been observed and analyzed based on data of the GDM. The German Drought Monitor was recognized as a tool for public information by several print media ranging from local to national coverage and television, during this event. Furthermore, several federal state authorities started to use the GDM as an information platform for planning purposes (e.g., Saxon State Agency for Environment, Agriculture and Geology; Bavarian Agency for Agriculture). The drought maps as well as the underlying information, e.g., the Soil Moisture Index, are freely available for the public upon download or request.

The German Drought Monitor gave the unique opportunity to observe the development of the 2015 drought event in near real-time. Drought hot spots like Berlin, Northern Bavaria and Eastern Saxony were estimated by the GDM. Fire watch activities were strengthened in summer 2015 because of exceptional dry soils in Northern Bavaria and Eastern Saxony. Trees already started to shed their leaves in Berlin in mid August. Finally, this drought led to a decrease of corn yield by 22% compared to the preceding 6 years (2009-2014). In July almost 75% of the territory of Germany was at least under moderate drought conditions. The 2015 event ranks under the 10 largest drought events between 1950-2015 regarding its magnitude in Germany.

Conclusion

This study shows the steps towards the development of an operational drought monitoring system for agricultural droughts in Germany. Continuous, spatially highly resolved fields of soil moisture are determined for Germany due to the determination of nationwide valid parameter sets. Soil moisture, evapotranspiration, groundwater recharge and per-model-cell generated runoff, are analyzed regarding their parametric uncertainty and how this uncertainty propagates to the identification and benchmark of drought events. An approach to decrease such parametric uncertainties is introduced.

The herein presented work led to the first public available, national monitoring system for agricultural droughts. This system enables the immediate evaluation of drought events in the light of historic events due to the benchmarking of drought events. This system is greatly valuable for regional authorities and the public. It is an essential tool to mitigate potential impacts of soil moisture drought such as forest fires, e.g., by fire watch activities. The uncertainty in drought monitoring has not been considered in the recent version of the German Drought Monitor, yet. The communication of such uncertainties as well as the impact of soil water deficits on agricultural yields are focus of current research and have to be investigated in collaboration with social scientist under consideration of stakeholders' needs.

Chapter 1

Introduction and Scope of the Study

1.1 Background

Water is a chemical compound that is fundamental to all forms of life on Earth. It constitutes 60% of animal and 90% of plant biomass (Shuttleworth, 2012). It shapes the Earth in many aspects: for example, water forms landscapes due to erosion or weathering and is partly responsible for the Earth's surface temperature, since water vapor is the most important greenhouse gas. In consequence, investigating the spatial and temporal distribution of water resources is of big interest for humanity.

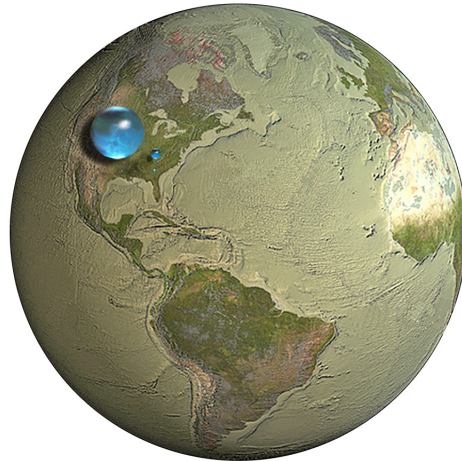


Figure 1.1: Volumetric view on the Earth's water resources. The big sphere represents the volume of available water on, in, and above Earth (fresh and salt water) compared to the Earth's volume. The middle-size sphere on its right side depicts the available liquid fresh water resources on Earth including groundwater, lakes, swamps, and rivers. The smallest sphere, located below the former, shows the volume of surface fresh water (lakes and rivers) compared to the Earth's volume (source: <http://water.usgs.gov/edu/earthhowmuch.html>).

Compared to the total volume of the Earth, all available water resources are small as shown in Figure 1.1. The 96.5% of the available water on Earth is allocated to oceans as non-potable salt water (Table 1.1). The remaining water could potentially be used as drinking water. The majority of it is stored as ice or snow in glaciers and ice caps. Only less than 1% of the Earth's water remains accessible as liquid freshwater. It constitutes a volume of approximately $10.6 \cdot 10^6 \text{ km}^3$ and is stored in rivers, lakes and the subsurface water, i.e., soil moisture and groundwater.

Table 1.1: Main water reservoirs of the earth characterized by volume and turnover times (Shiklomanov, 1993; Shuttleworth, 2012).

	Volume (10^6 km^2)	Percentage of total	Approximate residence time
Ocean	~ 1340	~ 96.5	1 000-10 000 years
Glaciers, ice, and permafrost	~ 27	~ 1.8	10-1 000 years
Groundwater	~ 23	~ 1.7	15 days - 10 000 years
Atmosphere	~ 0.013	~ 0.001	~ 10 days
Lakes, swamps, marshes	~ 0.187	~ 0.014	~ 10 days
Rivers	~ 0.002	~ 0.0002	~ 15 days
Soil moisture	~ 0.017	~ 0.001	~ 50 days

Although the volume of freshwater is marginal compared to total Earth's water resources, it is the major resource of drinking water and plant available water. Potable water would exhaust anytime soon, if it is not constantly renewed by the hydrologic cycle as shown in Figure 1.2 (Shuttleworth, 2012). Water evaporates from land and the ocean, drains as precipitation, and accumulates in rivers, lakes and subsurface reservoirs on land. Finally, it flows back to the ocean where it evaporates again. As Table 1.1 shows, surface water and atmospheric water vapor have fast turnover rates, whereas groundwater is replaced very slowly. Soil moisture, the main source of plant available water, is in between these temporal scales with an approximated turnover rate of 50 days.

Anomalies of water fluxes and states within the hydrologic cycle, either cause an excess or scarcity of water, i.e., floods and droughts. Precise knowledge on the spatio-temporal distribution of water within this cycle is essential in order to monitor and predict such hydrologic extremes.

Unfortunately, the states and fluxes of this cycle, e.g., soil moisture and evapotranspiration, are unknown at many places of the world since they are not observed. The vast majority of measured variables are meteorological observations, i.e., precipitation and climate variables. Less than $10^{-10}\%$ of the area of Germany is covered by rain gauge area despite the fact that Germany has the highest station density worldwide. Besides meteorological observations, river runoff is often

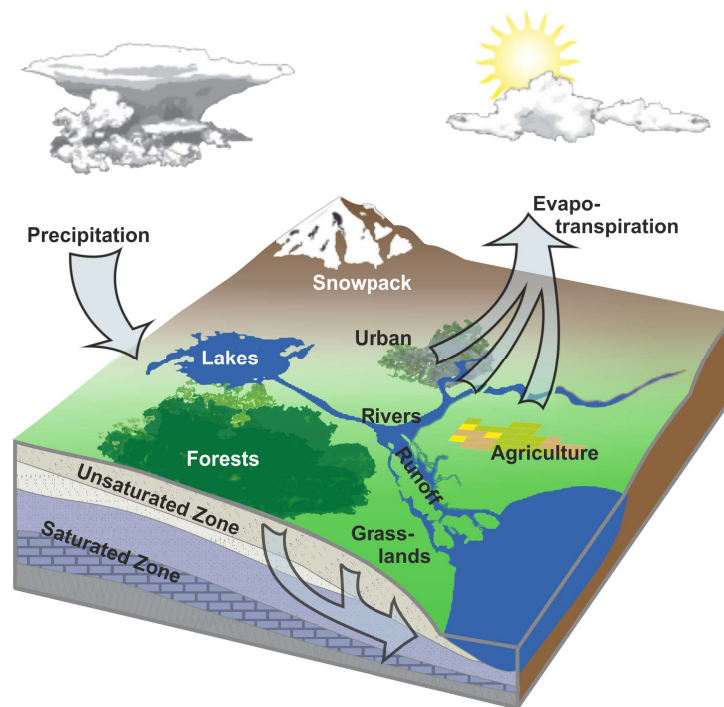


Figure 1.2: The hydrologic cycle. (adapted from: <http://hydrogeology.glg.msu.edu>)

observed. This integral variable describes the reaction of a catchment on precipitation events. Hydrologic models can be applied in order to get estimates of the spatial and temporal distribution of single variables of the hydrologic cycle using the water balance of a catchment.

The water balance describes the conservation of mass within a catchment. Based on the observed precipitation (P) and river runoff (Q) it is estimated as $\Delta S = P - Q - ET$. Given P and Q , the water balance allows the estimation of evapotranspiration (ET) and the storage term ΔS , representing soil moisture (SM) and ground water storage (G), among others.

1.2 Hydrologic Models

Hydrologic models are grouped into three different types depending on their degree of physical representativeness: 1) empirical or black box models, 2) physically based or white box models, and 3) process-based or gray box models (e.g., Xu, 2002; Beven, 2012; Rakovec, 2014).

Black box models are data driven, empirical models that are based on the analysis of the concurrent input and output time series (Abbott and Refsgaard, 1996). These models do not imply physical process understanding. Typical representa-

tives of black box models are artificial neural network models (e.g., Tokar and Johnson, 1999; Dawson and Wilby, 2001; Tongal and Berndtsson, 2016) or autoregressive moving average models (Box et al., 2008).

White box models are based on the main physical laws which are governing the hydrologic phenomena: the equations of mass, momentum and energy (Abbott and Refsgaard, 1996). The model domain is spatially and temporally discrete. Usually this discretization is based on finite elements or finite volumes. They are usually applied to gain process understanding. Disadvantages of these models are their high computational costs, their demand on a tremendous amount of data, their scale-dependency, and their overparameterization (Todini, 2007b; Beven, 2008, 2012). This makes it difficult to use them for operational purposes. For these reasons, physically based models are not yet as popular as process-based models in the hydrologic community. Examples for white box models are HYDRUS (Šimnek et al., 2008), ParFlow (Kollet and Maxwell, 2006) and MODFLOW (McDonald and Harbaugh, 1984).

The fundamental principle of process-based hydrologic (grey box) models is the fulfillment of the water balance, i.e. the conservation of mass. They are driven by meteorological forcings and output hydrologic responses of the catchment, e.g., river runoff or evapotranspiration (Beven, 2012). Usually a cascade of reservoirs characterizes these models. The reservoirs represent different states of the hydrologic cycle such as interception, snow accumulation, soil water retention, and groundwater storage. They are connected by hydrologic fluxes such as snow melting, evapotranspiration, percolation and runoff generation. Process-based models are widely used in catchment hydrologic studies because of their reasonable computational costs and low data demand. Well known process-based models are HBV (Bergrström, 1976), Variable Infiltration Capacity (VIC) model (Liang et al., 1994), LISFLODD (De Roo et al., 2000), SAC-SMA (Burnash et al., 1973), and mHM (Kumar et al., 2013b; Samaniego et al., 2010) among others.

In hydrologic models, catchments are treated differently regarding their spatial representation. Three different kinds of model approaches exist: lumped, semi-distributed, and distributed hydrologic models. Lumped models treat the entire catchment as one homogenous unit in which the hydrologic inputs, processes and outputs are averaged in space. Semi-distributed models subdivide the model domain into functional units. Distributed models work on defined, geometrical grids. The advantage of distributed models is a high spatial resolution of the estimated hydrologic fluxes and states compared to the two other approaches (Beven, 1992; Carpenter and Georgakakos, 2006; Kumar, 2010). This study is based on a spatially distributed model: the process-based hydrologic model mHM.

1.3 Uncertainty in Hydrologic Modeling

All of the aforementioned models underlie uncertainties in their hydrologic predictions. These uncertainties are attributed to four different sources: initial conditions, model structure, input data, and model parameters (Wagener and Gupta, 2005; Liu and Gupta, 2007; Beven, 2008).

Running a hydrologic model simulation without knowledge of the initial conditions, e.g., state of the soil moisture, will lead to biased model simulations. Hydrologic models need a certain amount of simulation time to adapt to the conditions within the catchment at the start of the simulation period if the initial conditions are unknown. A decent amount of observational data should be reserved for model spin-up to avoid initialization errors. Climatological values of the model states can be used for initialization, to minimize this spin-up time.

The model structural uncertainty depends on the decision for a particular model or modeling concept. This choice is usually based on subjective criteria, e.g., the modeler's preference for a particular model (Wagener et al., 2003). Different models will produce different results at the same location because of the model design. Hydrologic models differ in the mathematical description of processes, the parameterization of these processes, and in the hydrologic processes that are considered within the model (Beven, 2012). A multi-model setup for the area under investigation can expose model structural uncertainties in hydrologic predictions.

The third source of uncertainty arises from the input data. Usually, hydrologic models are driven by spatially distributed fields of meteorological variables. Besides the measurement errors, the interpolation approach is another source of errors. Predictions of the future behavior of hydrologic systems depend on forecasts of global or regional climate models (Beven, 2008). These climate models underlie predictive uncertainties themselves which are propagated to the hydrologic model (e.g., Thober et al., 2015).

The fourth source of uncertainty is connected to the model parameters. All of the aforementioned models are mathematical abstractions of nature and usually depend on parameters which allow the model to adapt to local conditions of the watershed or grid cell (Kuczera and Mroczkowski, 1998). These parameters do not necessarily represent physical entities due to model conceptualization and a lack of observations of hydrologic processes on the relevant scale, e.g., mesoscale (Beven, 2012). Further, every hydrologic model, regardless of its spatial explicitness (lumped or distributed), is to some degree the approximation of a heterogeneous world (Wagener and Gupta, 2005). Consequently, the parameters of hydrologic models can be seen as effective parameters that are usually determined by calibration. A calibration is the backward estimation of the model parameters aiming to reproduce an observed response of the hydrologic system, e.g., river runoff at the catchment outlet.

Two different approaches of estimating model parameters can be differentiated: the manual calibration and the automatic calibration (Gupta et al., 1999). The manual calibration needs to be conducted by an experienced hydrologist whose judgment of the model skill may be subjective. Automatic calibration routines, such as the Shuffled Complex Evolution (SCE) algorithm (Duan et al., 1992) or the Dynamically Dimensioned Search (DDS) algorithm (Tolson and Shoemaker, 2007), are searching for the best fit between the model and observations based on an objective criterion or objective function. The objective function quantifies the error of the model with respect to a particular observation. Typical error metrics in hydrologic modeling are the root mean square error or the Nash-Sutcliffe efficiency criterion (Nash and Sutcliffe, 1970). The parametric uncertainty is the inability to adequately locate a “best” parameter set (Wagner and Gupta, 2005). Calibration can lead to multiple or equifinal parameter sets, which perform equally satisfactorily compared to observations (Beven and Freer, 2001).

Within this study, the effect of parameter uncertainties that arise from running independent calibration runs for the hydrologic model mHM is analyzed. The herein used automatic calibration algorithm is the DDS algorithm, which is broadly applied in hydrology. This algorithm converges faster to good calibration results compared to, e.g., the SCE algorithm (Tolson and Shoemaker, 2007). It terminates after a fixed number of iterations rather than after a convergence criterion. The uncertainties of different hydrologic fluxes and states are analyzed regarding their spatio-temporal distribution, and are reviewed regarding their implications on soil moisture drought analyzes in Germany. An approach is presented to reduce parameter uncertainties by calibrating the model against additional data, i.e., satellite retrieved land surface temperature.

1.4 Droughts

Droughts are natural phenomena that are caused by precipitation amounts below the expected or normal (Wilhite, 2005). They can occur in all climatic zones irrespectively of the typical amount of rainfall in a region (Wilhite and Glantz, 1985). They are creeping events, which can easily last several years and reach national to continental spatial coverage (Andreadis et al., 2005; Sheffield and Wood, 2011; Sheffield et al., 2014).

Droughts are the second most severe natural disaster beside floods. They affected worldwide 2.2 billion people between 1950-2014 (Guha-Sapir et al., 2015). Its consequences reach from economic losses, mass migrations, and famines to casualties, among others (Hodell et al., 1995; Field, 2000; Wilhite et al., 2007). For example, in Germany the 2003 heat wave and drought event caused 7,000 fatalities (European Commission, 2007). On the European level death toll was estimated to exceed 70,000 (Robine et al., 2008). This severe drought event im-

pacted many socio-economic fields such as agriculture, forestry or inland navigation. The agro-economic loss in Germany was estimated to 1.5 billion EUR (COPA-COGECA, 2003). In entire Europe the agricultural sector had to cope with losses of 15 billion EUR.

According to the fifth assessment report of the International Panel on Climate Change (IPCC) "there will be a marked increase in extremes in Europe, in particular, in heat waves, droughts, and heavy precipitation events" (IPCC, 2012). The European Commission reported that the frequency of droughts has already increased and will further increase (EEA, 2012a). Additionally, Trenberth et al. (2014) discuss that anthropogenic factors of climate change will speed up the establishment of droughts and increase drought intensities. This makes droughts an important field of research in Central Europe.

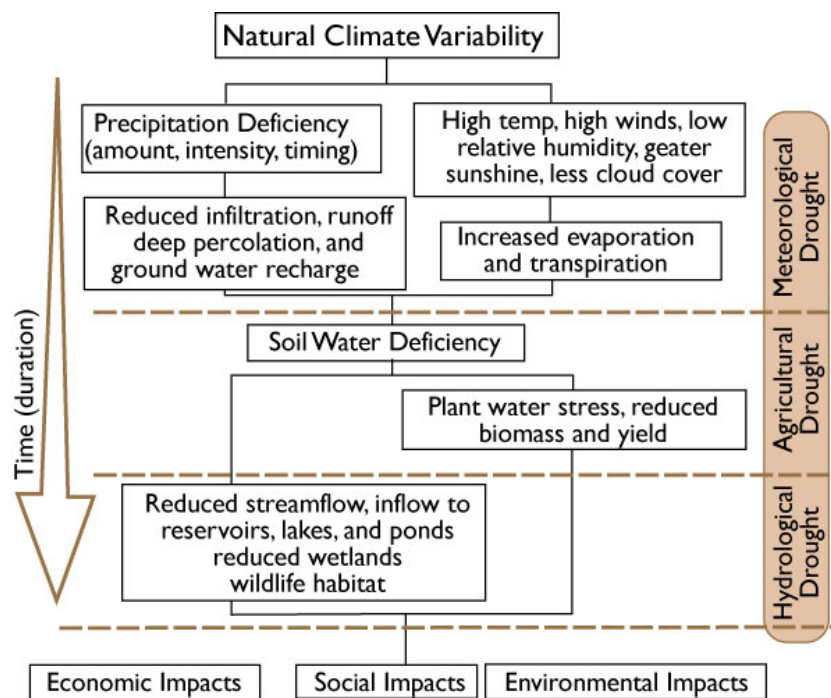


Figure 1.3: The four different types of drought and their sequence of occurrence. (source: National Drought Mitigation Center, University of Nebraska-Lincoln, USA)

Since droughts have an impact on many parts of society, there is no generally accepted definition of droughts (Wilhite, 2005). Different disciplines, e.g., water resources management or agriculture, focus on different variables of the hydrologic cycle, e.g., river runoff or soil moisture, respectively. This led to the classification of droughts into four types: meteorological, agricultural, hydrologic, and socio-economic drought as shown in Figure 1.3 (Wilhite and Glantz, 1985; WMO, 2006). The meteorological drought is usually defined as a deficiency of precipitation amount in a defined period of time. The hydrologic drought is characterized

by exceptional low surface and subsurface water availability, such as reduced river runoff and low groundwater levels. A low availability of soil moisture, which is the major water resource for plants in most regions of the world, is termed agricultural drought. All of the aforementioned drought types can lead to a shortfall in water supply leading to monetary losses, which characterizes the socio-economic impacts.

A drought monitoring system which delivers timely information about onset, extent and intensity, could help to reduce drought related fatalities and economic losses (Wilhite, 1993). Within this study, such a system is developed for Germany. It focuses on the analysis of soil moisture droughts, because of their high agro-economic relevance for Germany (e.g., Schindler et al., 2007; Döring et al., 2011).

1.5 Research Objectives

The main objective of this study is the development of an operational drought monitoring system for agricultural droughts in Germany. Therefore, spatially continuous fields of soil moisture are derived with a hydrologic model, i.e., mHM. Hydrologic models are uncertain in hydrologic predictions due to uncertainties in the parameter estimation process, amongst others. These uncertainties need to be considered if predicting drought characteristics, such as drought severity or duration. Further, the ability of spatially distributed fields of satellite derived land surface temperature is explored to reduce parameter uncertainties. Finally, the operational framework of the German Drought Monitor is presented.

Hydrologic modeling is usually conducted at the catchment scale. Catchment borders have to be crossed when conducting predictions on the national domain. In consequence, the parameters of the hydrologic model need to be sufficient and stable for application in distinct catchments. Additionally to the equifinality problem, transferring calibrated model parameters to remote locations will lead to uncertainties in the model simulation. A framework to determine such parameters is presented in Chapter 2 in order to address the following research objectives:

- Derive highly resolved and spatially consistent estimations of hydrologic states and fluxes, i.e., evapotranspiration, soil moisture, groundwater recharge, per grid cell generated runoff, for Germany between 1950 and 2010.
- Analyze the spatio-temporal distribution of parametric uncertainties of these variables.

A retrospective drought analysis from 1950 to 2010 is anticipated based on the soil moisture fields of these estimations. An algorithm for the estimation of a Soil Moisture Index (SMI) is developed and implemented for performing drought

analyzes. Based on the SMI, the following research objectives are addressed in Chapter 3:

- Reconstruction of agricultural drought conditions and identification of benchmark events.
- Investigate the effect of parametric uncertainty on drought characteristics, such as duration, spatial extent, severity, and magnitude.

Chapter 4 will deal with the reduction of parametric uncertainties observed in the above-mentioned studies. Using satellite derived land surface temperature and a newly developed and implemented land surface temperature module for mHM, the following research objectives will be addressed:

- Reduction of parameter estimation uncertainties by calibrating a hydrologic model with spatial patterns of satellite derived land surface temperature.
- Assessment of the predictive skill of satellite land surface temperature regarding river runoff.

Finally, the operationalization of a drought monitoring system for Germany is presented in Chapter 5. The research question addressed is:

- How to deliver timely information about agricultural droughts to the decision makers and the public to potentially mitigate negative impacts?

The last chapter summarizes and discusses the major findings of this work and provides an outlook for further improvements of the drought monitoring framework.

Chapter 2

A High-Resolution Dataset of Water Fluxes and States for Germany Accounting for Parametric Uncertainty

This chapter is largely based on the manuscript:

Zink, M., Kumar, R., Cuntz, M., and Samaniego, L. (2016): A High-Resolution Dataset of Water Fluxes and States for Germany Accounting for Parametric Uncertainty, *Hydrology and Earth System Sciences Discussions*, doi:10.5194/hess-2016-443, in review.

2.1 Abstract

Long term, high-resolution data of hydrologic fluxes and states are needed for many hydrological applications. Since long-term, large-scale observations of such variables are not feasible, hydrologic or land surface models are applied to derive them. This study aims to analyze and provide a high-resolution dataset of land surface variables over Germany, accounting for uncertainties caused by the estimation of equifinal model parameters. Furthermore, the spatiotemporal distribution of uncertainties in various hydrological variables as well as the propagation of uncertainties through different model compartments is investigated. The mesoscale hydrological model (mHM) is employed to create an ensemble (100 members) of daily fields of evapotranspiration, groundwater recharge, generated discharge and soil moisture at a spatial resolution of 4 km in the period 1950-2010. The model is evaluated with observed runoff in 222 catchments, which have not been used for calibrating the model. In these catchments the mean and the standard deviation of the ensemble median *NSE* for daily discharge are 0.68 and 0.09, respectively. The modeled evapotranspiration, which is evaluated with observations at eddy covariance stations, exhibits a five times larger error in spring during the onset of the vegetation period compared to the other seasons. Our analysis indicates the lowest uncertainty for evapotranspiration, while the largest uncertainty is observed for groundwater recharge. The uncertainty of the hydrologic variables varies throughout the course of a year with exception of evapotranspiration, which stays almost constant. The uncertainties in soil moisture and recharge are recognized to propagate to the modeled discharge. Our study emphasizes the role of accounting for the uncertainty due to equifinal parameter sets when reconstructing high-resolution, model-based datasets.

2.2 Introduction

Consistent, long-term data of meteorological and hydrological variables at high spatial resolution are needed for applications like i) impact assessment studies such as drought, flood or climate change analyzes (Sheffield and Wood, 2007; Samaniego et al., 2013; Huang et al., 2010), ii) studies that need spatially and temporally continuous observation based data, e.g., for temporal disaggregation (Thober et al., 2014) or downscaling of climate model data (Wood et al., 2004), Ensemble Streamflow Prediction (Day, 1985), or reverse Ensemble Streamflow Prediction (Wood and Lettenmaier, 2008).

Continuous observations of hydrologic fluxes and states are economically and logistically not feasible on regional to national scales (Vereecken et al., 2008). Soil moisture observations, for example, are scarcely conducted. Additionally, these measurements are usually only representative for a small control volume of a few

cm³. Evapotranspiration measurements at eddy covariance stations have a footprint of ten to hundreds of meters, but are available at only 827 stations worldwide (<http://fluxnet.ornl.gov>, April 2016).

Alternatives are remote sensing or reanalysis data. These data are broadly available, but do not consider the conservation of mass, i.e., the closure of the water balance. Apart from that reanalysis data have spatial resolutions of at most 1/4° (Dee et al., 2016). Continuous remote sensing products are not available due to their addiction to cloud free conditions (Mu et al., 2007; Liu et al., 2012). However, hydrologic models driven by observational data are the prime alternative to derive consistent water fluxes and states on large spatial domains.

Observational driven datasets are estimate by Maurer et al. (2002); Zhu and Lettenmaier (2007); Livneh et al. (2013); Zhang et al. (2014) on the national scale. These data are based on the Variable Infiltration Capacity (VIC) model (Liang et al., 1994) having at most a spatial resolution of 1/16° and cover the United States, Mexico and China. Studies, like Nijssen et al. (2001); Fan and van den Dool (2004); Berg et al. (2005); Sheffield et al. (2006), are focusing on the global domain and thus already cover Germany. But the spatial resolution of these data is at most 1/2° and most of these studies are focusing on meteorological forcings rather than on hydrologic variables. The Hydrological Atlas of Germany (HAD) (Federal Ministry for the Environment Nature Conservation Building and Nuclear Safety, 2003) provides long-term averages of many water fluxes and states as maps. The underlying data for some of these maps are freely available. The maps of the HAD have been derived independently from each other and are thus not necessarily consistent between each other.

The resolution of the above mentioned model-derived datasets are coarse according to Wood et al. (2011), who stated that a need exist to have higher spatially resolved data and models for purposes like flood and drought forecasting. Moreover, Bierkens et al. (2014) states that water resources or river basin managers will favor highly resolved data, i.e., 1-5 km.

Further, land surface hydrologic models are subject to different sources of uncertainties, i.e., input, model structural and parametric uncertainty. These uncertainties are often not considered when deriving hydrologic or hydro-meteorological datasets (e.g., Huang et al., 2010; Livneh et al., 2013; Zhang et al., 2014). In consequence, predictive uncertainties are often not addressed but may have substantial implications on subsequent studies as shown by Samaniego et al. (2013).

Another challenge is to derive continuous fields of hydrologic variables on large spatial domains. Since hydrologic models are commonly applied on the catchment scale the parameters are often calibrated to perform good in this particular catchment. The aim of this study is to derive a national dataset for Germany, which is exceeding the domain of a single catchment. To estimate continuous data for Germany, this paper is based on compromise parameter sets. These are derived by

transferring parameters among seven catchments, which cover a large part of the study domain. Subsequently, the results are screened for satisfactory performances in all of those catchments.

Additionally, we address the issue of predictive uncertainties by considering an ensemble of equifinal parameter sets (Beven, 1993). This uncertainty is understood as the uncertainty in hydrologic fluxes and states emerging from multiple parameter sets which perform equally satisfactory if evaluated with discharge. For this particular study, the input uncertainty is very little compared to the parameter uncertainty, because of the high quality and density of meteorological observations. The application of multiple models or modeling concepts is out of the scope of this study.

Summarizing, the objective of this study is to derive a continuous and consistent dataset of hydrologic fluxes and states between 1950 and 2010 in Germany with a high temporal and spatial resolution. This model derived dataset consists of evapotranspiration, soil moisture, groundwater recharge and per-grid-cell-generated runoff. Additionally, we provide the forcing dataset of the model including precipitation, temperature, and potential evapotranspiration. To our knowledge such a consistent dataset is not freely available up to now for Germany. We address the need for highly resolved data by conducting simulations at the spatial resolution of $4 \times 4 \text{ km}^2$ ($1/25^\circ$). Spatial continuity is ensured due to the estimation of 100 independent parameter sets which are valid on the entire domain of Germany.

We evaluate the 100 parameter sets in 222 catchments, which have not been used for parameter inference. Additionally to streamflow, the ensemble simulations are evaluated with evapotranspiration and soil moisture observations at seven eddy covariance stations. Therefore, model simulations are obtained on a resolution of $100 \times 100 \text{ m}^2$, which is comparable to the footprint of the evapotranspiration measurements.

An additional objective, is the investigation of the 100 ensemble simulations regarding their temporal and spatial distribution of parametric uncertainties. Moreover, the propagation of uncertainties through different compartments of the hydrologic model is scrutinized.

2.3 Study Domain and Datasets

The study is conducted on the territory of Germany, which covers an area of about $357,000 \text{ km}^2$ (Figure 2.1). The region, located in Central Europe, is mainly characterized by a humid climate, but nonetheless has a north to south and east to west climatic gradient. The topography varies from low-altitude, flat areas in the north (North German Plain) over mid-altitude mountains in Central Germany (Central Uplands) to the high altitude Alpine Foothills and the Alps in the south.

Whereas the northwestern part of Germany is still under maritime influence, the eastern part has a more continental climate, characterized by colder winters and less precipitation.

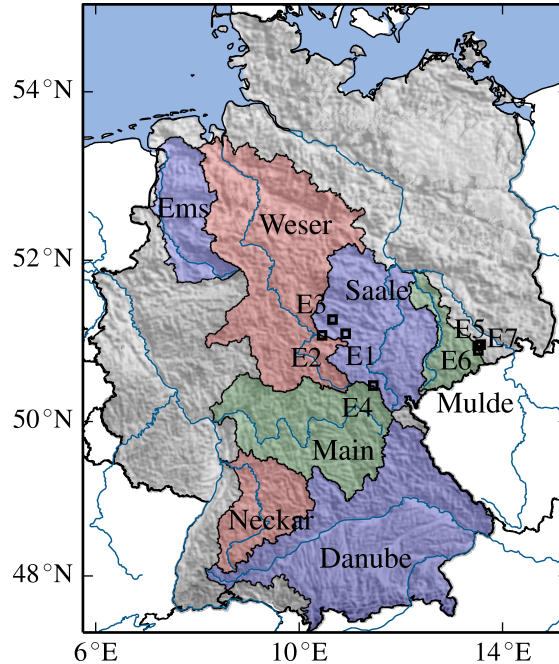


Figure 2.1: Study area showing the seven catchments used for estimation of common parameter sets for Germany. The points E1-E7 denote eddy covariance stations which are used for the evaluation of evapotranspiration and soil moisture.

The assessment of water fluxes and states is restricted to the national borders of Germany, since meteorological data and land surface characteristics have been available on this domain. Thus, only catchments fully covered by German territory are used to derive parameters for the hydrologic model. These seven, major catchments are depicted in Figure 2.1. These basins represent the topographic and hydro-climatic gradient within Germany (see Table 2.1). They are ranging in size from 6,000 km² to 48,000 km² and are characterized by mean elevations ranging from 60 m.a.s.l. (Ems catchment) to 560 m.a.s.l. (Danube catchment). All catchments have a comparable degree of urbanization ranging between 6% to 10%. A remarkable low amount of forest is observed in the Ems catchment, where agriculture and pasture are the dominating land use.

Due to different climatic regimes the average discharge of the seven catchments ranges from 161 mm a⁻¹ to 469 mm a⁻¹. The low-lying Ems reaches a remarkable high discharge due to maritime influence, whereas the Saale river is characterized by the lowest discharge. The runoff coefficient of the Saale differs significantly from the other catchments, which originates from the high degree of anthropogenic influence within this basin. Three out of the ten biggest dams in Germany are located

Table 2.1: Catchment properties and water balance characteristics of the seven major German river basins. The geographical location of the catchments is depicted in Figure 2.1.

	catchment area [km ²]	elevation [m]				land cover [%]			water balance [mm a ⁻¹]			dryness index [-] E _p /P	runoff coeff. [-] Q/P
		avg	std	min	max	forest	urban	mixed	P	Q	E _a		
Mulde	6 200	386	201	75	1 212	26	10	64	798	344	454	0.88	0.43
Ems	8 400	60	36	10	383	13	8	79	802	312	490	0.89	0.39
Neckar	12 700	445	153	124	1 015	35	10	55	914	356	558	0.85	0.39
Main	23 700	356	113	93	1 044	39	6	55	793	247	546	0.97	0.31
Saale	24 800	287	162	56	1 139	23	8	69	645	161	484	1.13	0.25
Weser	37 700	223	165	8	1 116	34	7	59	781	276	505	0.91	0.35
Danube	47 500	558	170	302	2 329	32	6	62	948	469	479	0.80	0.49

there (Bleiloch - 215 Mio. m³, the Hohenwarte -182 Mio. m³ and the Rappbode reservoir - 109 Mio. m³). Furthermore, open pit mining has a big influence on the water budget of this catchment.

2.3.1 Land Surface Properties

The land surface characteristics required by the hydrologic model include a 50 m digital elevation model (DEM) acquired from the Federal Agency for Cartography and Geodesy (Federal Agency for Cartography and Geodesy (BKG), 2010), a digitized soil map at a scale of 1:1,000,000 (Federal Institute for Geosciences and Natural Resources (BGR), 1998), and a hydrogeological vector map at a scale of 1:200,000 (Federal Institute for Geosciences and Natural Resources (BGR), 2009). The soil map contains information on soil textural properties such as sand and clay contents of different soil horizons. The soils are classified to 72 soil types which have an average depth of 1.8 m. The hydrogeological map comprises 32 classes and gives information about saturated hydraulic conductivities and karstic areas. Based on the DEM additional information like slope, aspect, flow direction and flow accumulation are inferred. Land cover information are derived from CORINE land cover scenes of the years 1990, 2000, and 2006 (European Environmental Agency (EEA), 2009). The period prior 1990 is assumed to be static and is represented by the scene of 1990. All data sets are remapped to a common spatial resolution of 100×100 m.

The location and shape of the catchments (Figure 2.1) is derived with an automated delineation, which is based on gauging station information and terrain information (flow accumulation, flow direction). Discharge data are provided by the European Water Archive (EWA) (2011) and the Global Runoff Data Centre (GRDC) (2011). The results of the delineation are approved by comparing with the CCM River and Catchment Database (European Commission - Joint Research

center (JRC), 2007; Vogt et al., 2007). Additionally to the seven major catchments (as described above), the model is set-up in 222 additional, smaller catchments to cross-validate the model performance.

2.3.2 Meteorological Forcings

The hydrologic model is forced with daily fields of precipitation, average temperature and potential evapotranspiration. They are derived from local observations operated by the national weather service (Deutscher Wetterdienst (DWD), 2015). The station network comprises in average 3800 rain gauges and 570 climate stations per year (period: 1950-2010), which have an average minimum distance of 6 km and 14 km between neighboring stations, respectively.

These local observations are interpolated on a regular grid of 4×4 km² using external drift Kriging. The terrain elevation (DEM) is used as external drift and the Kriging weights are based on a theoretical variogram. This variogram is estimated for entire Germany by fitting to a empirical variogram. To avoid discontinuities in the interpolated meteorological forcings and consecutively in the hydrologic simulation, an estimation of multiple variograms for different climatic zones or distinct morphological regions has been rejected. The spatial resolution of 4×4 km² is seen as appropriate considering the aforementioned station network density. Subsequently, daily fields of potential evapotranspiration were estimated with the Hargreaves-Samani method (Hargreaves and Samani, 1985) using interpolated temperatures (average, minimum, and maximum temperature).

The interpolation of the precipitation is evaluated with gridded precipitation data (REGNIE) provided by the German Meteorological Service (Deutscher Wetterdienst (DWD) (2013); Rauthe et al. (2013)). The REGNIE data are based on the same observations and have a spatial resolution of 1 km. They are derived by applying a multiple linear regression approach, which takes daily atmospheric conditions and terrain properties, such as elevation, slope, and aspect, into account (Rauthe et al., 2013). After remapping the REGNIE data to the aforementioned 4×4 km² grid by bi-linear interpolation a satisfactory correspondence between the interpolation and the REGNIE precipitation data is found. The spatially averaged bias of the daily fields is 0 with a standard deviation of 0.11 mm d^{-1} within the period 1950-2010.

2.4 Methodology

2.4.1 The mesoscale Hydrologic Model mHM

The hydrologic model mHM (www.ufz.de/mhm) is a distributed hydrologic model that accounts for the following main processes: snow accumulation and melt, evapotranspiration, canopy interception, soil water infiltration and storage, percolation, and runoff generation (Figure 2.2). These processes are conceptualized as water fluxes between internal model states similar to existing models like HBV (Bergrström, 1976) or VIC (Liang et al., 1994). Snow accumulation and melt processes are based on the improved degree-day method which accounts for an increased snow melt during intense precipitation events (Hundecha and Bárdossy, 2004). A three layer discretization is used to account for processes representing the root-zone soil moisture dynamics. The upper two layers are ending in 0.05 m, 0.25 m and the lowest layer is spatially variable in depth depending on the soil map. On average it is 1.8 m deep in Germany. The evapotranspiration from soil layers is estimated as a fraction of the potential evapotranspiration depending on the soil moisture stress and the fraction of vegetation roots present in each layer. The runoff generation in mHM is formalized as sum of the components direct runoff, slow and fast interflow, and baseflow. The runoff generated at every grid cell is routed to the outlet using the Muskingum routing algorithm. For a detailed model description, interested readers may refer to Samaniego et al. (2010) and Kumar et al. (2013b). To date the model has been successfully applied to various river basins across Germany, Europe, and the USA (Samaniego et al., 2013; Rakovec et al., 2016; Kumar et al., 2013a).

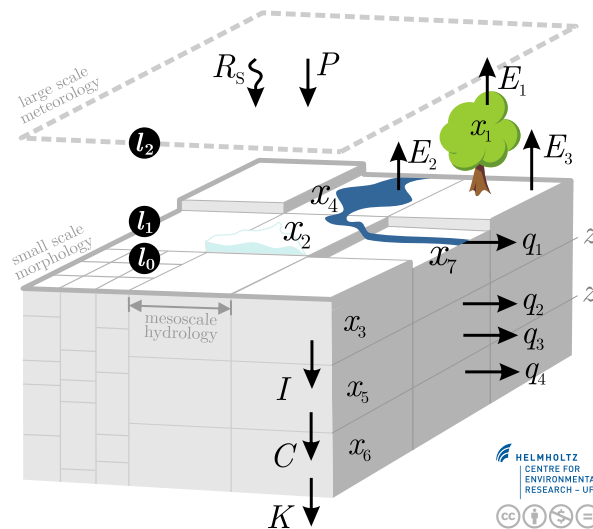


Figure 2.2: Schematic view on the distributed, mesoscale Hydrologic Model mHM (www.ufz.de/mhm).

A feature which is unique for mHM is its technique for estimating effective model parameters called Multiscale Parameter Regionalization (MPR, Samaniego et al. (2010); Kumar et al. (2013b)). Its basic concept is to estimate parameters (e.g., the porosity) based on terrain properties (e.g., sand and clay content) and transfer functions (e.g., pedotransfer functions). These transfer functions depend on transfer parameters (e.g., factors of the pedotransfer functions) which are time-invariant and location independent and are purpose to calibration (described in section 2.4.2). This parameter estimation is performed on the high-resolution of the land surface property input, e.g., $100 \times 100 \text{ m}^2$, and subsequently this parameters are upscaled to the resolution of the hydrologic simulations, e.g., $4 \times 4 \text{ km}^2$. Thus mHM explicitly accounts for the sub-grid variability of land surface properties, such as terrain or soil information.

2.4.2 Derivation of Representative Parameter Sets

One of the goals of this study is to derive consistent model parameters for performing nation-wide simulations of water fluxes and states. A two step parameter selection procedure was used for this purpose. In a first step we estimated multiple parameter sets via calibration in each of the seven inner German river basins (Figure 2.1) independently. In a next step, we transfer these calibrated parameter sets to the remaining basins and finally only those parameter sets are retained, which exhibit a sufficient model performance criteria, i.e., a Nash-Sutcliffe Efficiency (NSE) ≥ 0.65 , in all seven basins during the evaluation period (1965-1999). This parameter selection procedure ensures that the resulting ensemble parameter sets do not exhibit spatial discontinuities at catchment boundaries.

The calibration is performed using the dynamically dimensioned search (DDS) algorithm (Tolson and Shoemaker (2007)). The objective function for calibration consists of an equally weighted power law function for the NSE (Nash and Sutcliffe, 1970) of the discharge and the logarithm of the discharge to consider high and low flows within the objective function. A compromise programming technique (Duckstein, 1984) using a power law with an exponent $p = 6$ is used, to estimate the multi-objective function (Φ). This technique ensures equal improvement of the different measures ϕ_i during a multi-objective calibration. The overall objective function Φ is given as

$$\Phi = \left(\sum_{i=1}^2 w_i^p \cdot (\phi_i)^p \right)^{\frac{1}{p}} \quad \text{with } \sum w_i = 1 \quad (2.1)$$

with

$$\phi_1 = NSE(Q) = 1 - \frac{\sum_{t=1}^T (\widehat{Q}_t - Q_t)^2}{\sum_{t=1}^T (Q_t - \overline{Q})^2} \quad (2.2)$$

$$\phi_2 = NSE(\ln Q) = 1 - \frac{\sum_{t=1}^T (\ln \widehat{Q}_t - \ln Q_t)^2}{\sum_{t=1}^T (\ln Q_t - \overline{\ln Q})^2} \quad (2.3)$$

where w_i is the weight ($w_1 = w_2 = 0.5$) for a particular measure ϕ_i , \widehat{Q}_t and Q_t denote the modeled and observed discharge at a time step t , respectively. \overline{Q} is the mean of observed discharge over all time steps T .

A period of 5 years from 2000 to 2004 is chosen for model calibration. This time period reflects various hydrologic conditions ranging from a high impact flood event in Central Europe in August 2002 to a significant drought event in 2003. The remaining 35 years of available data (1965-1999) are used for model evaluation. All simulations are conducted with a 5 year spin up period to abrogate the influence of initial conditions.

Hundred independent calibration runs are performed for each of the seven catchments (Figure 2.1). Using 2000 model iterations per calibration run led to a large number of model evaluations per catchment (200,000). Finally, 100 parameter sets out of 700 are retained to derive nation-wide ensemble simulations of water fluxes and states at daily resolution.

2.4.3 Validation Data

Besides discharge in the seven major German river basins, the model performance is evaluated against discharge in 222 additional catchments and complementary data sets including evapotranspiration, soil moisture and groundwater recharge. The cross validation of ensemble parameter sets in catchments which have not been used for parameter inference should prove the ability of the model to satisfactorily estimate discharge in various regions of Germany with differing hydrologic characteristics.

The catchments for cross validation are distributed all over Germany and range in sizes from 100 km² to 8,500 km². A subset of these catchments contains sub-catchments of seven major basins. The simulation time period is adopted to the available discharge observations but is at least 10 years. The mean simulation time period of all 222 catchments is 42 years. The discharge estimation in these catchments is evaluated using the ensemble median *NSE* and its uncertainty is

characterized by the range between the 5th and 95th percentile of *NSEs* of the ensemble simulation.

Evapotranspiration observations are available at seven eddy covariance towers located in Germany (Figure 2.1; www.europe-fluxdata.eu). These towers are designed to observe carbon fluxes as well as all fluxes of the energy balance, i.e., latent heat (or evapotranspiration E_a), sensible heat H , ground heat flux G and net radiation R_n . However, the observed fluxes have discrepancies in the fulfillment of the energy balance ($R_n = E_a + H + G$) called energy balance closure gap (Foken, 2008). The source of the energy balance closure gap is still subject of research. It is closed by applying mathematical corrections to the latent heat and sensible heat flux to satisfy the energy balance equation. Here we apply a correction method preserving the fraction of latent and sensible heat. The corrected evapotranspiration values at the eddy sites are compared with the corresponding model estimates based on the root mean squared error (RMSE), the Pearson correlation coefficient (r) and the bias.

Additionally, soil moisture observations, undertaken at eddy covariance stations, are used to evaluate modeled soil moisture. Soil moisture is measured using TDR or FDR sensors, which have a control volume of a few cm^3 . This is much smaller than the model resolution of $100 \times 100 \text{ m}^2$. A direct comparison between observed and simulated soil moisture may therefore be misleading, due to differences in spatial representativeness and sampling depth. Here we aim to analyze the temporal dynamics of soil moisture by normalizing the respective soil moisture time series (Koster et al., 2009). The anomalies are calculated as

$$z = \frac{SM(t) - \mu}{\sigma} \quad (2.4)$$

where μ is the mean and σ is the standard deviation of the entire soil moisture time series SM at daily resolution. It is not possible to use deseasonalized values (normalization with monthly values) because the time periods of the available observations were too short ($\approx 6 \text{ years}$).

The mHM simulation for comparing the observations at the location of the eddy Covariance stations is conducted with deactivated lateral processes on a single grid cell. The model resolution ($100 \times 100 \text{ m}^2$) is adopted to the size of footprint of the energy flux measurements which is typically several 10 to 100 meters. Rather than downscaling the model results, the hydrologic processes are modeled at the resolution of the observations. The transferability of mHM across scales is presented in Kumar et al. (2013b).

We evaluated the model performance against long term estimates of annual recharge over Germany (1961-1990). Due to the lack of observations, the estimated recharge from the Hydrologic Atlas of Germany (Federal Ministry for the Environment Nature Conservation Building and Nuclear Safety, 2003) is taken here as a reference.

This recharge estimate is obtained using a multiple regression model accounting for terrain properties (e.g., land cover), locally observed baseflow indices and depths of the groundwater table among other variables (Neumann and Wycisk, 2003). The gridded recharge estimate is available at a $1 \times 1 \text{ km}^2$ spatial resolution, which is remapped to a $4 \times 4 \text{ km}^2$ resolution using bi-linear interpolation to be comparable to the ensemble median modeled estimates.

2.4.4 Uncertainty of Ensemble Model Simulations

The uncertainty of the modeled evapotranspiration, groundwater recharge, per-grid-cell-generated runoff and soil moisture is assessed by two different criteria. First, the spatially distributed uncertainties are presented as maps showing the coefficient of variation c_v which is defined as

$$c_v = \frac{\sigma}{\mu} \quad (2.5)$$

in which μ is the mean and σ the standard deviation of the ensemble simulations. A large c_v describes a large variance in the modeled flux or state normalized with its mean. The mean μ and standard deviation σ are derived from the 100 ensemble realizations of the hydrologic model mHM on every grid cell. The variances within the ensemble simulation are caused by predictive uncertainties. These uncertainties stem from the parametric uncertainty itself and from the transfer of parameters to locations which have not been used for model calibration. In the following the variances of the ensemble simulations are denoted as uncertainty.

Second, for assessing the temporal variation of the uncertainty throughout a year the range and the normalized range of the respective flux or state are considered. The range is defined as the difference between the 95th (p_{95}) and 5th (p_5) percentile of the ensemble simulation, whereas the normalized range is defined as

$$r = \frac{p_{95} - p_5}{p_{50}}. \quad (2.6)$$

where $p_{50}(x)$ denotes the median value of the ensemble simulation (50th percentile). The choice of the percentiles 5 and 95 was taken to exclude potential outliers from the analysis.

2.5 Results and Discussion

The model simulations are evaluated against multiple variables available at different spatial and temporal resolutions. These include daily and monthly time-series of streamflow measured at the catchment outlets, soil moisture and evapotranspiration at several eddy covariance sites, and a long term, annual recharge map. mHM simulations are carried out at a hourly time scale on two spatial resolutions, i.e., $100 \times 100 \text{ m}^2$ at the eddy covariance stations and $4 \times 4 \text{ km}^2$ at the catchment level and for the nation-wide ensemble simulation. Finally, a analysis of the model runs for the nation-wide water fluxes and states including per-grid-cell-generated runoff (Q_G), evapotranspiration (E_a), groundwater recharge (R) and soil moisture (SM) is presented. The focus here is to provide a comprehensive overview on regional scale water fluxes and states over Germany and to analyze the uncertainty in modeled variables due to an ensemble of model parameters. The uncertainties are investigated with respect to its temporal and spatial distribution and its triggering sources. Finally, the propagation of uncertainties through the different model states and fluxes is analyzed.

2.5.1 Discharge Evaluation in Major German River Basins

The discharge simulations of the hydrologic model mHM are evaluated based on the NSE of daily and monthly discharge values for a validation (1965-1999) and a calibration (2000-2004) period. The daily discharge of the major German catchments is sufficiently estimated revealing mean $NSEs$ of 0.89 and 0.84 using on-site calibrated parameters in the calibration and the validation period, respectively (Figure 2.3). Note that the ensemble parameter sets are common to all basins (grey boxes in Figure 2.3). They are chosen as compromise parameter sets, which should perform well in all of the seven basins (see section 2.4.2). The median model performance of the ensemble parameters is dropping by approximately 6% compared to on-site estimated parameters. This performance loss can be attributed to changes in basin climatic and land-surface conditions including terrain, soil, and vegetation properties. The ranges of $NSEs$, which correspond to the 100 on-site and ensemble parameter sets, are comparable across the investigated basins which indicates that the application of the ensemble parameter sets did not significantly increase the uncertainty of estimated discharge.

The model performance is lower during the validation period in comparison to the calibration period (Figure 2.3). Such deterioration of model performance, common to other hydrologic model applications too, is caused by differences in hydro-meteorological regimes between the calibration and validation period and constraining (over-fitting) of the parameters to compensate for errors in model structure. The model exhibited improved performance for monthly streamflow simulations with an average median NSE of 0.97 and 0.92 for on-site calibrated

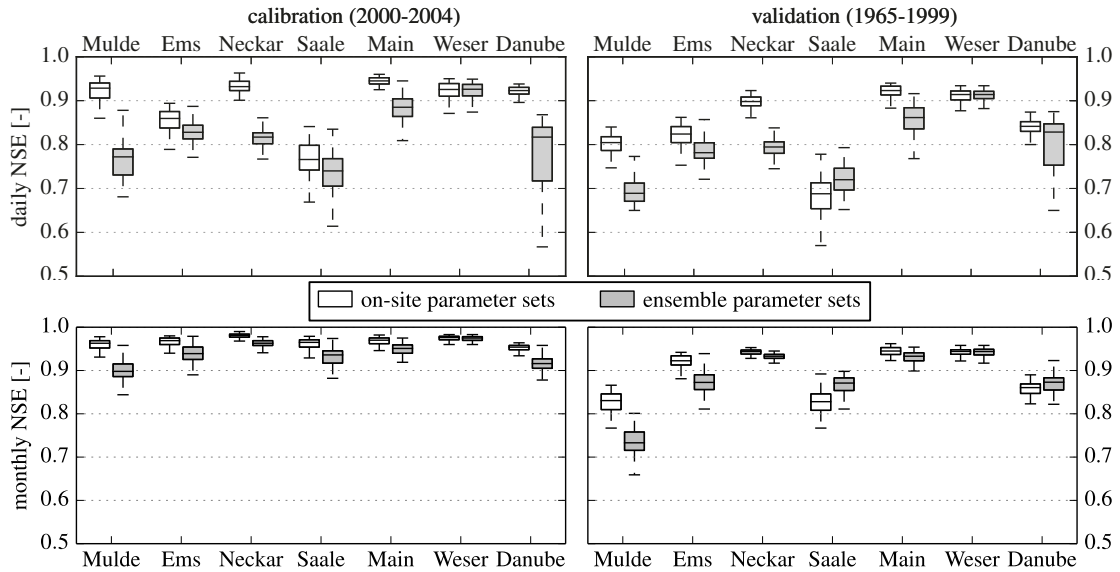


Figure 2.3: Model performance expressed as Nash Sutcliffe Efficiency (NSE) at daily (upper row) and monthly (lower row) resolution for the calibration period 2000-2004 (left hand side) and validation period 1965-1999 (right hand side). The white box plots show the results of the on-site calibration, whereas the gray box plots are simulations using the 100 ensemble parameter sets for Germany. Note that the y-axis starts at $NSE=0.5$

parameter sets during the calibration and validation period, respectively. The corresponding $NSEs$ with the transferred parameter sets were 0.94 and 0.87, respectively. The spread of $NSEs$ for the monthly streamflow is considerably narrower compared to the daily flows (Figure 2.3). Unsurprisingly, the high variabilities of daily streamflow are smoothed when averaged over a longer (monthly) time scale leading to an overall better correspondence between observed and simulated flows.

Heavy human interactions lead to lower model performances for the Saale river basin, especially on daily timescale. The highly regulated discharge in the headwaters of the Saale river (see section 2.3) is difficult to capture and thus leads to lower performances, since mHM has no reservoir operation included. The main discharge mechanisms of Saale are considered as adequately captured, since the median $NSEs$ are exceeding 0.85 at monthly and 0.7 on the daily resolution for the ensemble parameter sets (Figure 2.3).

Interestingly, this catchment shows equal or higher performances for the ensemble parameter sets compared to the on-site parameter sets in the evaluation period. A similar behavior can be observed for the Weser catchment. We conclude that discharge simulations in some catchments improve by gaining knowledge from remote locations.

2. Water Fluxes and States Dataset Accounting for Parametric Uncertainty

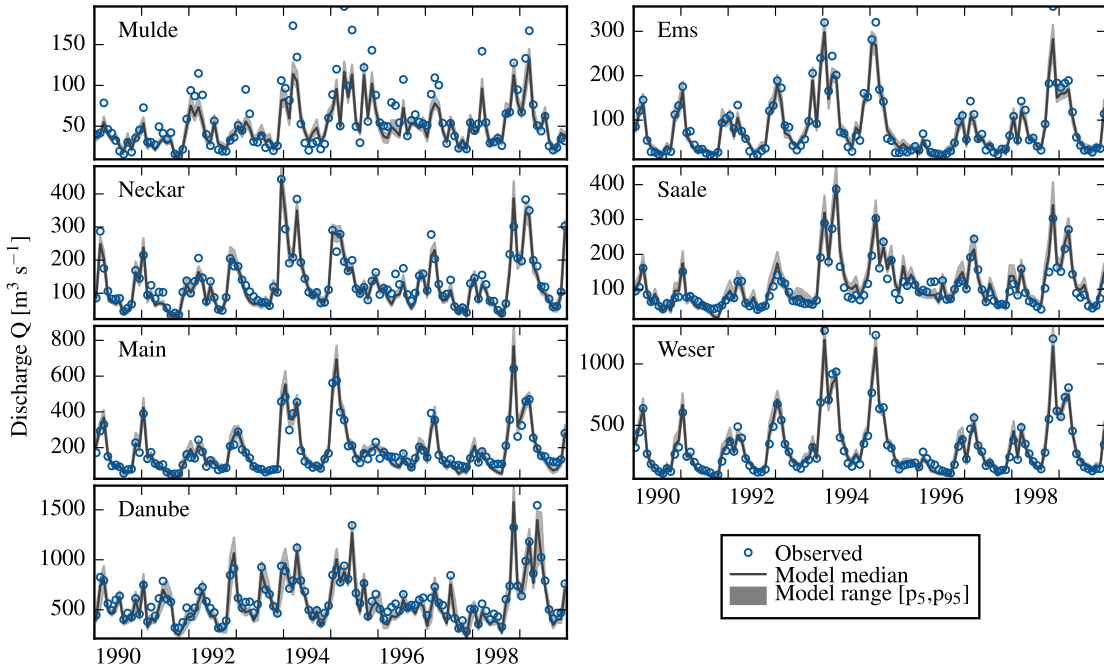


Figure 2.4: Observed and modeled monthly discharge for the seven catchments, which were used for parameter inference. The figure shows one decade (1990-1999) of the evaluation period. The solid dark gray line depicts the median model results and the light gray band depicts the range between the 5th and 95th percentile of the 100 ensemble simulations.

The filtering of transferred parameters for determining the ensemble parameters introduced a notable degree of uncertainty in some of the catchments, e.g., the Danube. This stems from the fact that different catchments are sensitive to different parameters. For example, the Ems, located in the maritime influenced north, are not as sensitive to snow parameters as the alpine influenced Danube. In consequence, parameters which originate from the Ems deteriorate ensemble predictions in the Danube. A simultaneous calibration of multiple, distinct catchments would be beneficial for deriving hydrological fluxes and states on national or continental scales.

The Mulde basin has a tendency to underestimate peak flows (Figure 2.4). This could be attributed to our precipitation product. The headwaters of the Mulde basin are located in the Ore mountains at the border between Germany and the Czech Republic (Figure 2.1). Besides a sparse network of rain gauges in these mountainous area, a lack of information on meteorological variables from the neighboring country (i.e., the Czech Republic) lead to an underestimation of precipitation by the interpolation, especially for orographic driven events. In other basins, the model is able to capture both high and low flows adequately well (Figure 2.4).

The results presented in this section show that the method for determining ensemble parameter sets (section 2.4.2) lead to satisfactorily estimations of discharge in the catchments used for parameter inference. However, the model performances shown within this section compare well to those of other studies, like Huang et al. (2010). A further investigation of the applicability of the ensemble parameter sets on additional, smaller catchments is shown in the next section.

2.5.2 Discharge Evaluation at Non-calibrated Basins

Following Klemeš (1986), the model performance is evaluated across 222 catchments diverging in size and geographical location. The streamflow data of these proxy locations have not been used during the model calibration. This cross-validation test focuses on evaluating the model performance against discharge simulations along a diverse range of climatic and land-surface conditions. The evaluations shown in Figure 2.5, indicate a satisfactory agreement between simulations and observations. The daily discharge simulations (Figure 2.5, panels A, B) reveal a median NSE value of at least 0.5 across the investigated basins based on the ensemble parameter sets. The overall average NSE value is 0.68. Expectedly, the model exhibits a better skill in capturing monthly discharge dynamics, with the ensemble median NSE averaged across all basins of approximately 0.81 (Figure 2.5, panels D, E). Furthermore, the ensemble median NSE exceeded a value of 0.75 in more than 20% of the basins for the daily flows and 80% for the monthly flows. The spatial variability of the median NSE across the investigated basins is low with a standard deviation of around 0.09 for both daily and monthly flows.

Different climatic regimes can be expressed in terms of the dryness index E_p/P of a basin (Budyko, 1974). The model performances of the 222 catchments are plotted in panel A and D of Figure 2.5 using this index. It separates the catchments into energy ($E_p/P < 1$) and water limited conditions ($E_p/P > 1$). Various studies investigated the relationship between dryness and evaporative index E_a/P (Schreiber, 1904; Ol'dekop, 1911; Budyko, 1974; Gerrits et al., 2009). The simulated evapotranspiration E_a is used for deriving the Budyko plot to identify potential errors in the water balance closure (Figure 2.5 panels A, D). All catchments under investigation lie perfectly within the uncertainty ranges of the reported theoretical curves. In conclusion the water balances of those basins are well closed with a mean closure error of 1% for the median simulation. The performances are comparable for catchments in different climatic regimes. However, a tendency to better perform in large catchments is observed.

The uncertainty for the individual basins caused by the ensemble parameter sets is expressed as the range between the 95th and 5th percentile of $NSEs$ (Figure 2.5, panels C, F). Substantial performance differences occur in 70% (45%) of the basins exceeding a range of 0.1 for the daily (monthly) flow simulations. A geographical dependency of the uncertainty can not be found as no spatial clustering is observed.

2. Water Fluxes and States Dataset Accounting for Parametric Uncertainty

Whereas, daily flows show almost no relation between median $NSEs$ and the uncertainty range, i.e., worse performing catchments reveal high uncertainties, monthly $NSEs$ are less uncertain if their NSE is high.

The evaluation of the ensemble parameter sets presented in this section support the hypothesis that the ensemble parameter sets are valid on the national scale. In the following, evapotranspiration, soil moisture and groundwater recharge estimates are evaluated.

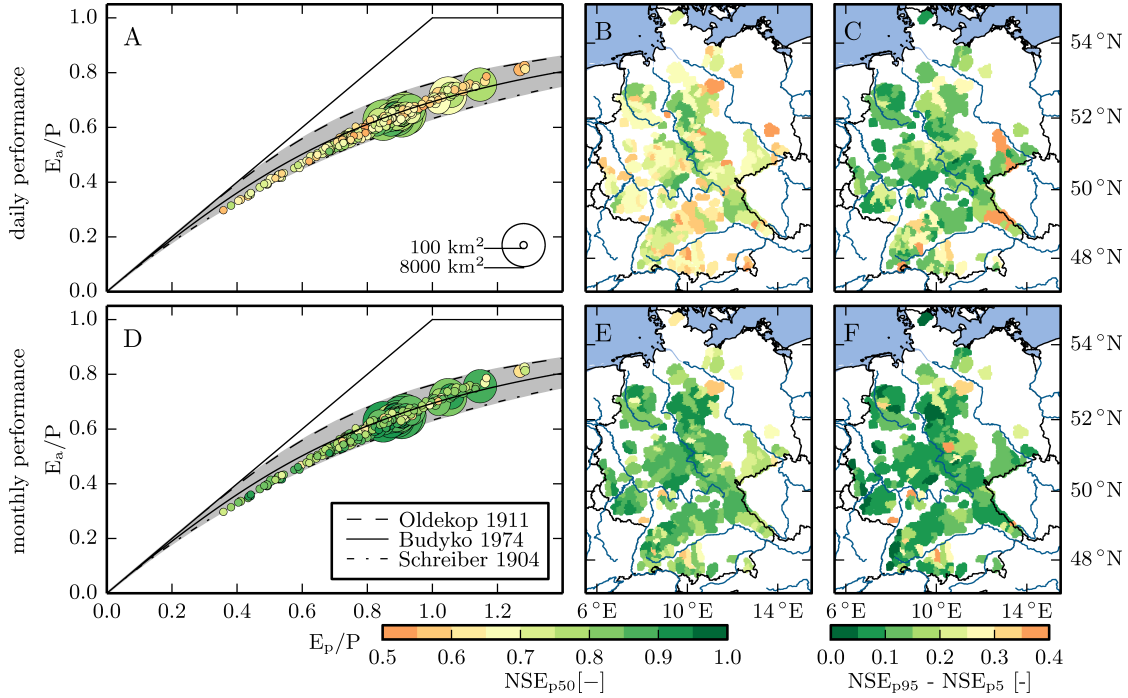


Figure 2.5: Budyko plot and performance maps for ensemble parameter sets at 222 catchments spread over Germany. The upper row depicts evaluations based on daily values (panels A, B, C), whereas the lower row depicts monthly discharge evaluation (panels D, E, F). In the first column the catchments are presented as Budyko plots (panels A, D) which are color-coded based on the ensemble median NSE for daily (panel A) and monthly (panel D) discharge values. The gray band envelops different estimations of the Budyko curve (Schreiber, 1904; Ol’dekop, 1911; Budyko, 1974). The center column depicts the location of the 222 catchments shown in the Budyko plots using the same color-code (panels B, E). The right column shows the range of the 5th and 95th ensemble percentiles for the NSE on daily (panel C) and monthly (panel F) basis. Panels A, B, D, E share the left color bar and panels C and F share the right color bar. The simulation period is adopted according to the available discharge observations, but is at least 10 years (average=42 years).

2.5.3 Evapotranspiration and Soil Moisture Evaluation at Eddy Covariance Stations

The ensemble model simulations are further evaluated with evapotranspiration (E_a) and soil moisture (SM) observed at seven eddy covariance stations (Figure 2.1) to assess the model ability to represent other fluxes and states next to streamflow. The ensemble median of the daily sum of evapotranspiration is plotted against the corresponding observations in Figure 2.6 and the resulting error statistics are summarized in Table 2.2.

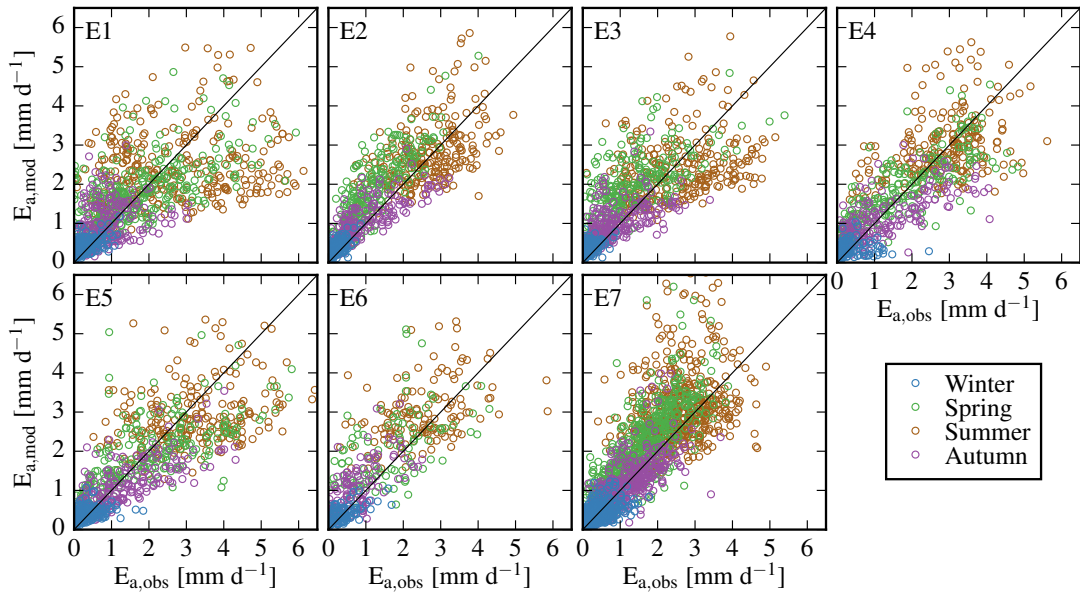


Figure 2.6: Observed ($E_{a,obs}$) versus ensemble median modeled evapotranspiration ($E_{a,mod}$) at seven eddy covariance stations (Figure 2.1).

The results of the scatter plot shown in Figure 2.6 indicate no systematic over or under estimation of the observed evapotranspiration. The highest deviation in terms of RMSE is observed during summer, when the highest fluxes occur, and the lowest during winter in which the contribution of E_a is lowest among all seasons. The average bias estimated across all stations during spring is 0.34 mm d^{-1} , while it is 0.08 mm d^{-1} , 0.04 mm d^{-1} and 0.04 mm d^{-1} for winter, summer and autumn, respectively. The slight overestimation of modeled E_a during spring is likely to be caused due to a lack of a dynamic vegetation growth module in mHM. Thus, the onset of the vegetation period may not be captured adequately by the model. With respect to the vegetation class, the stations E1 and E6 covered by crops have the largest errors with RMSEs of E_a of 19.4 mm mon^{-1} and 15.4 mm mon^{-1} for monthly evapotranspiration, respectively (Table 2.2). This errors arise because of the high impact of human interactions on croplands, e.g., due to seeding, harvesting or irrigation, compared to other vegetation classes. Additionally, the land cover

2. Water Fluxes and States Dataset Accounting for Parametric Uncertainty

class cropland is not explicitly represented within the model, rather it is generalized within a mixed land cover class, representing all land cover types different from urban and forest.

In general, errors of local evapotranspiration estimates can be attributed to the Hargreaves-Samani approach for estimating the potential evapotranspiration. This approach may be inappropriate for local weather conditions. Since this method approximates the net radiation based on the minimum and maximum daily temperatures, local phenomena like short term cloudiness are not accounted. Especially in summer this effect is high, which causes the lowest correlations between observations and simulations during this period. Be aware of the observational error caused by the energy balance closure gap which is in average 33% for the herein considered stations if reviewing the errors of modeled evapotranspiration.

Table 2.2: Evaluation of evapotranspiration E_a and soil moisture SM at seven eddy stations. The evaluation is based on daily and monthly values for the available observation period. The location of the eddy flux stations is depicted in Figure 2.1.

ID	Station name	Period	Land Cover	monthly E_a			daily E_a			daily SM
				[mm mon ⁻¹]	[-]	[r]	[mm d ⁻¹]	[-]	[r]	[-]
E1	Gebesee	2003-2008	cropland	19.14	0.61	0.85	1.01	0.02	0.67	0.62
E2	Hainich	2000-2007	DBF*	11.72	6.99	0.95	0.62	0.23	0.87	0.68
E3	Mehrstedt	2003-2006	grassland	12.44	5.78	0.94	0.74	0.18	0.79	0.80
E4	Wetzstein	2004-2008	ENF**	9.86	1.58	0.96	0.73	0.05	0.84	0.80
E5	Grillenburg	2004-2008	grassland	13.93	-4.19	0.94	0.89	-0.14	0.8	0.93
E6	Klingenberg	2004-2008	cropland	15.39	9.38	0.93	0.86	0.31	0.77	0.53
E7	Tharandt	1997-2008	ENF**	13.39	7.71	0.96	0.72	0.26	0.83	0.82

* deciduous broadleaf forest, ** evergreen needleleaf forest

In terms of temporal dynamics the model is able to capture the observed evapotranspiration quite well across the different eddy covariance sites as exemplarily shown in Figure 2.7 in the upper panel. The model is able to adequately represent the observed monthly dynamics with an average correlation of approximately 0.93 (Table 2.2). The correlation between the observed and the simulated daily evapotranspiration is at least 0.77, with exception of the cropland site E1.

The lower panel of Figure 2.7 shows the performance of mHM for representing the daily soil moisture anomalies which are generally in good correspondence with observations. The temporal dynamics of observed soil moisture anomalies during the wetting and drying phases are well captured by the model. The resulting correlation shown in Table 2.2 at different eddy stations ranges between 0.53 and 0.93. The lowest values are observed at cropland sites, which is due to the above mentioned human interaction and land cover class representativeness. Still some peaks are not captured satisfactorily by the model, which could be reasoned in the

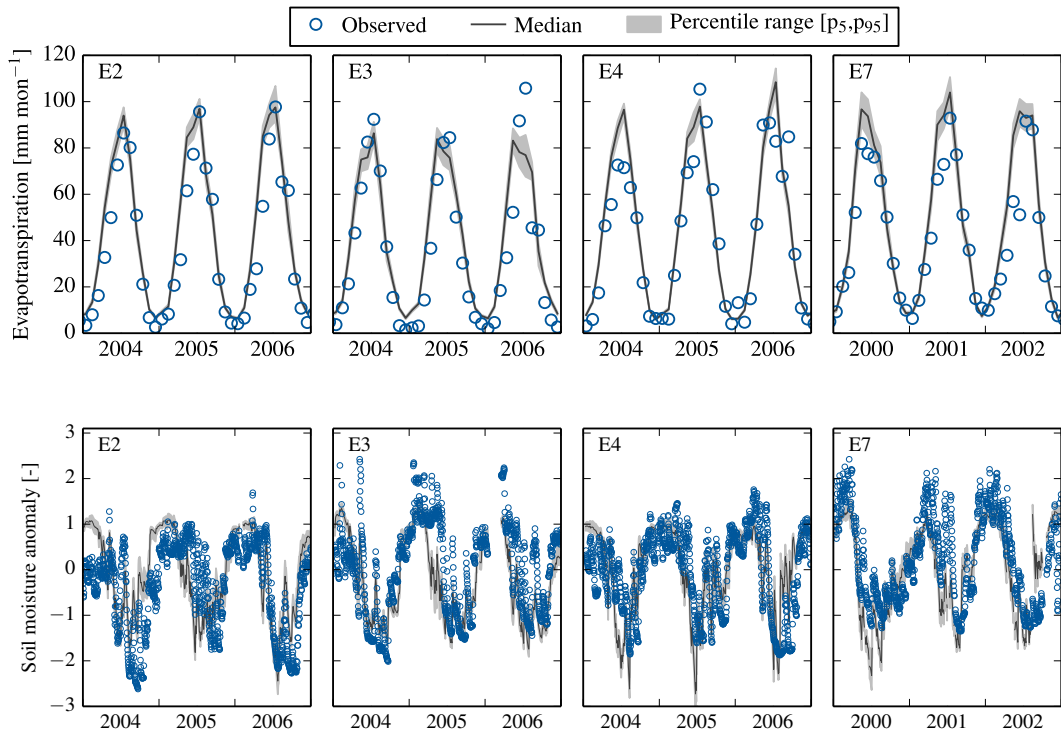


Figure 2.7: Exemplary time series of observed and modeled monthly evapotranspiration and daily soil moisture anomalies at four eddy covariance stations. The solid dark gray line depicts the median model results and the light gray band depicts the range between the 5th and 95th percentile of the 100 ensemble simulations.

non-representativeness of $100 \times 100 \text{ m}^2$ grid cells of the model for TDR/FDR soil moisture measurements. Thus the simulated soil moisture is smoother compared to the observation, since it represents the effective soil moisture of the entire grid cell.

2.5.4 Evaluation of Groundwater Recharge

Finally, the ensemble simulations are evaluated with the long-term annual groundwater recharge from the Hydrologic Atlas of Germany (HAD) (Federal Ministry for the Environment Nature Conservation Building and Nuclear Safety, 2003). mHM's long term recharge estimate implicitly represents the baseflow component of the total runoff, based on the assumption that the underground catchment is closed and there are no external losses (e.g., irrigation or pumping). Consequently, this analysis serves as a proxy for assessing the model skill for partitioning the total runoff into interflow and baseflow. The comparison of the spatial pattern of the recharge shows good accordance between the two maps with a correlation

coefficient of approximately 0.8 (Figure 2.8). The spatial pattern of the recharge follows the known climatology of Germany with high recharge rates being observed in areas with high precipitation amounts (e.g., secondary mountains or Alps).

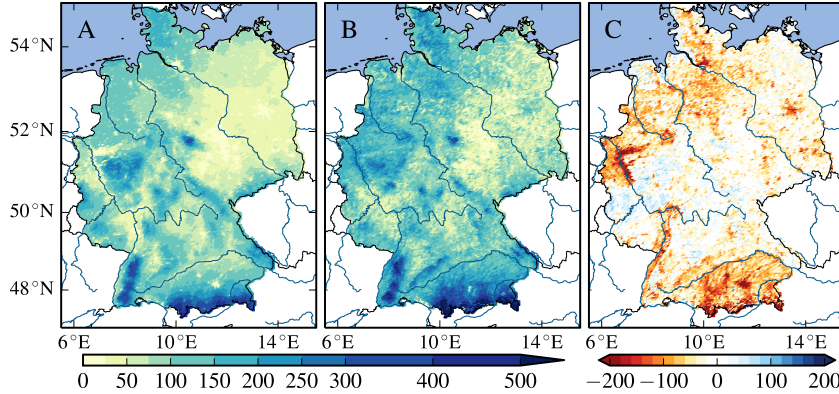


Figure 2.8: Comparison of mean annual groundwater recharge (R) modeled with A) mHM and from B) the Hydrologic Atlas of Germany (Federal Ministry for the Environment Nature Conservation Building and Nuclear Safety, 2003; Neumann and Wycisk, 2003). Panel C shows the difference (A-B) between both data sets. Units are $[\text{mm a}^{-1}]$ for all panels.

There are some significant differences between the modeled and the HAD groundwater recharge particularly at cells characterized by urbanization (i.e., Munich, Hamburg, Berlin, and the metropolises of Ruhrgebiet in the north-west). The model tends to underestimate the HAD recharges with differences as high as around 200 mm a^{-1} . Notably, the herein used version of mHM treats urban areas as almost impermeable which is unrealistic. This issue has been resolved in recent mHM versions (5.0 and higher). In general the HAD estimate of recharge is in average 31 mm a^{-1} higher compared to the ensemble mean simulation. This mismatch arises from the differences in potential evapotranspiration (E_p), which were used for both estimates. The E_p estimates used for the HAD (Federal Ministry for the Environment Nature Conservation Building and Nuclear Safety, 2003) are lower than those used for mHM simulations and result in higher water amounts remaining in the underground. Besides these mismatches, overall the spatial pattern of the modeled recharge compares well with the HAD estimates (Figure 2.8), which to some degree provides a first-order confidence regarding the representation of the runoff separation scheme used by mHM.

2.5.5 Spatial Patterns of Ensemble Means and Uncertainties

The ensemble means and coefficients of variation of evapotranspiration (E_a) and per-grid-cell-generated runoff (Q_G) as well as the climatology of the meteorological forcing and some land surface properties are presented in Figure 2.9. The high precipitation amounts above 1000 mm a^{-1} in panel A correspond to mountainous areas in Germany. The driest region is located in the northeastern part of Germany. This is on the one hand due to its distance to the sea (continental climate) and on the other hand due to the secondary mountains in the western and central part of Germany. These mountains, especially the Harz mountains (center of Germany), capture most of the precipitation events brought from the west. The low amounts of precipitation in the east lead to lower amounts of evapotranspiration (Figure 2.9, panel B) and generated runoff (Figure 2.9, panel C) in this region compared to the rest of Germany. Thus the northeastern part of Germany is characterized by high dryness indexes of 1.2 and above. The uppermost dryness indexes up to 1.4 are located in the lee of the Harz mountains. The average dryness index in Germany is 0.98. Another region characterized by high dryness indexes is the Upper Rhine Graben which is known to have a locally warmer climate compared to its neighboring regions. Mountainous regions are characterized by stronger energy limitation due to high precipitation amounts, which result in dryness indexes lower 0.65.

The uncertainty, i.e., the coefficient of variation (see section 2.4.4), in the simulation of evapotranspiration (Figure 2.9, panel F) and generated runoff (Figure 2.9, panel G) is varying in space and is highest in the regions of high dryness. Especially the northeastern part of Germany is prone to large uncertainties in evapotranspiration and runoff generation estimates compared to other locations. The spatial patterns in evapotranspiration are not exclusively caused by the high degree of water limitation, they are also connected to soil properties (Figure 2.9, panel E and F). In regions with dominating high sand contents in soils, which are characterized by high porosities, high uncertainties in E_a can be observed. Especially, the spatial patterns of high uncertainties in E_a in the northwestern and northeastern part of Germany are corresponding to the regions of high porosity (Figure 2.9, panel E). In contrast the spatial structures of uncertainties of per-grid-cell-generated runoff (Q_G) in the northeastern part of Germany and the Upper Rhine Graben are corresponding to high values in the dryness index in those regions.

In conclusion the spatial distribution of uncertainty in evapotranspiration in the north of Germany is partially caused by the parameterization of the soil whereas the main pattern is governed by the dryness index. Since in the regions of high dryness the water amount entering the soil is significantly lower than in other regions of Germany, the model is highly sensitive to the partitioning of the water between the model internal reservoirs, i.e., surface, soil water and ground water reservoir. Thus slight changes of parameters effect the partitioning of water in the subsurface and lead to changes in the modeled fluxes and states.

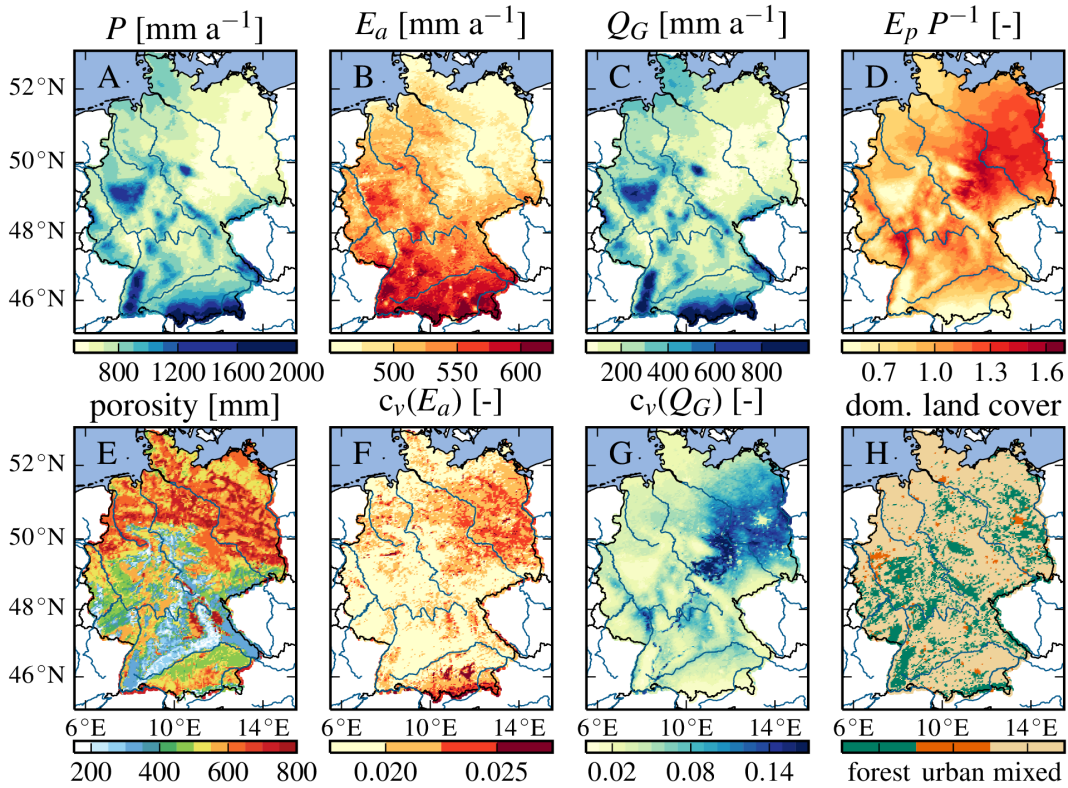


Figure 2.9: Water balance variables, their coefficients of variation as well as land surface characteristics for Germany. A) Mean annual precipitation P , B) ensemble mean annual evapotranspiration E_a , C) and per-grid-cell-generated runoff Q_G , D) dryness index E_p/P , E) sum of porosities (saturated soil water content) of all model layers, F) coefficient of variation from the ensemble of annual evapotranspiration and G) discharge, H) dominating land cover class on $4 \times 4 \text{ km}^2$ grid. The mean values and coefficients of variation are based on the period 1950-2010.

The patterns appearing in the evapotranspiration and generated runoff at the location of big cities (orange areas in panel H of Figure 2.9) are caused by the above mentioned inappropriate representation of urban areas within mHM lower version 5.0.

2.5.6 Spatio-temporal Distribution of Uncertainties

This section focuses on the spatio-temporal differences of uncertainties caused by the 100 equifinal ensemble parameter sets. The temporal variation is analyzed based on monthly, climatological values. Figure 2.10 shows the normalized ranges of the respective variables (see section 2.4.4), evapotranspiration (E_a), soil moisture (SM), groundwater recharge (R) and generated runoff (Q_G). The plots refer to different environmental zones in Germany (Federal Environmental Agency, 2005), which are depicted in the upper left corner of Figure 2.10.

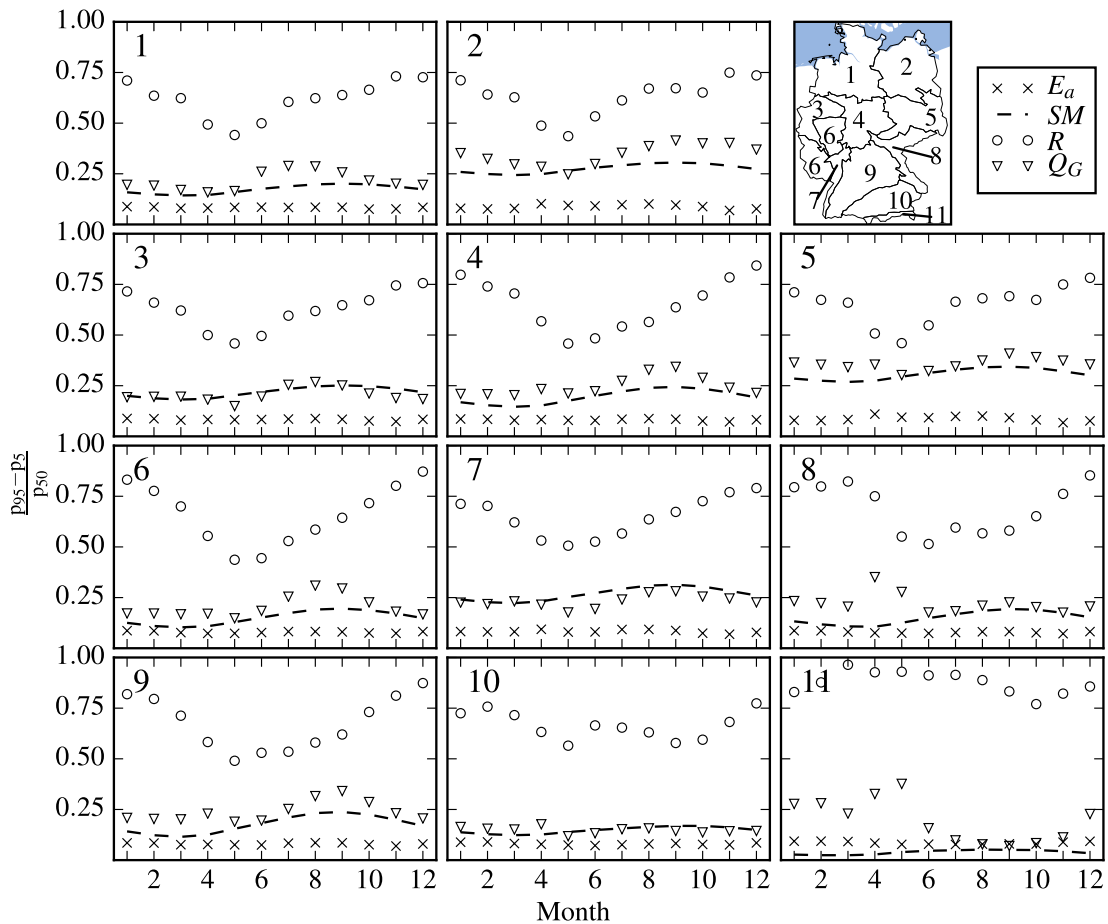


Figure 2.10: Normalized ranges of ensemble monthly climatology of hydrologic variables for different environmental zones within Germany. The locations of 11 environmental zones are depicted on the map on the upper right. The normalized ranges are determined as the differences of the 5th and 95th percentiles divided by the median (50th percentile) of the ensemble. The hydrologic variables presented are evapotranspiration E_a , soil moisture SM , per-grid-cell-generated runoff Q_G , and groundwater recharge R .

The uncertainty of evapotranspiration is almost constant throughout the year and is lowest among the four hydrologic variables. The recharge is highly uncertain and highly variable compared to the other variables. Its minimum is usually in the end of spring when the groundwater reservoirs are starting to deplete. The uncertainty of per-grid-cell-generated runoff and soil moisture estimates show similar dynamics. It is reaching its maximum in the end of summer, when the water in below ground reservoirs (ground water, soil water) is lowest and thus the steadiest behaving discharge components baseflow and slow interflow are lowest. So, the uncertainties are dominated by the response to precipitation events. The amplitude of soil moisture uncertainty is lower than the uncertainty of generated runoff because soil moisture has a high persistence, whereas runoff generation quickly reacts to precipitation events.

Additionally, to the different magnitude and variability over time, regional variations in dynamics of uncertainty can be observed. The most contrasting region is zone 11 (the Alps). In this region the uncertainties in recharge are highest (average normalized range 0.88) compared to the other environmental zones. Furthermore, the uncertainty of per-grid-cell-generated runoff has a pronounced peak in spring (zone 8 behaves similar). This peak is caused by water from snow melting, which is largest during spring in these regions.

2.5.7 Propagation of Uncertainty Through Model Internal Components

The interplay between the climatology of the hydrologic variables and its uncertainty is presented in Figure 2.11. In this figure only those environmental zones (depicted Figure 2.10) revealing the most significant differences as well as a north to south gradient are chosen. In Figure 2.11 zone 2 represents the area of high dryness index in the northeast, zone 4 the central part of Germany including secondary mountains, zone 10 the Alpine Foothills and zone 11 the Alps.

The uncertainty of evapotranspiration among these locations is comparable in its dynamics and uncertainty. The magnitude of uncertainty and its variability are changing from north to south and thus from low to high altitudes for soil moisture. This is caused by decreasing soil porosity and increasing amount of precipitation. Soils with high sand contents can be found in the northern part of Germany (ground moraine). These soils are highly permeable and hence have a lower water holding capacity, which leads to a more distinct dynamic. The highest uncertainties occur when the soils are driest (end of summer). For recharge the opposite behavior can be observed. If the recharge amount is high its uncertainty is high, too. The shape of the per-grid-cell-generated runoff is quite similar to the recharge flux, but its normalized uncertainty ranges are much lower.

For example in zone 4, is the uncertainty of Q_G quite stable at the beginning

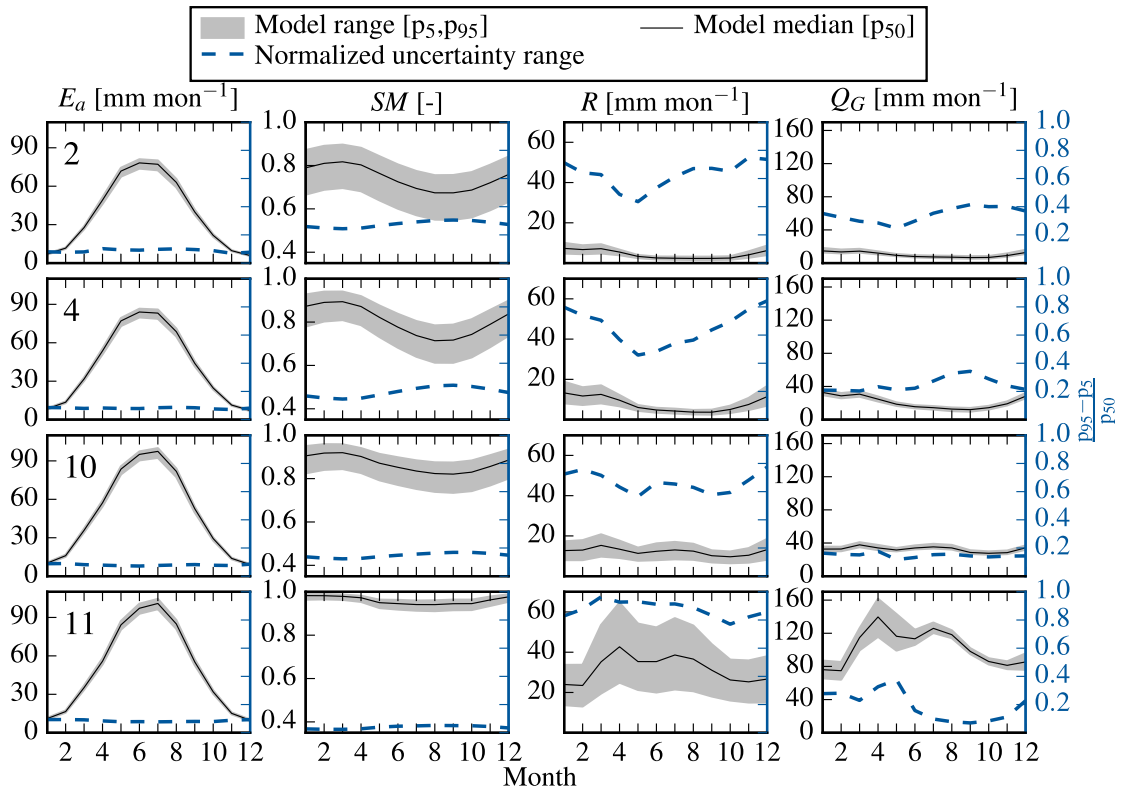


Figure 2.11: Superposition of parameter uncertainty through different model fluxes and states based on monthly, climatological values of E_a - evapotranspiration, SM - soil moisture, R - groundwater recharge, and Q_G - per-grid-cell-generated runoff. The uncertainty ranges and the median refer to the left ordinate, whereas the normalized uncertainty range refers to the right ordinate (blue). The geographical location of region 2, 4, 10, and 11 are depicted in Figure 2.10.

of the year. Soil moisture uncertainties show a similar behavior at that time of the year. Q_G uncertainty gets a little depleted in month 5, which is occurring in recharge, too. Afterward, it starts increasing until September as in soil moisture and recharge, but with a slope which is a compromise of both. Until the end of the year uncertainty of per-grid-cell-generated runoff is decreasing again comparable to the uncertainty in soil moisture, whereas it is increasing for groundwater recharge. This behavior shows that the uncertainty in generated runoff is triggered by different variables throughout the year. In summer when major discharge contributions come from the baseflow, the uncertainty of the groundwater component gets more important. In autumn and winter, when fast interflows, and thus the precipitation driven model components, have major contributions to Q_G , the uncertainty of the near surface water becomes more important.

It is noticed that the highest uncertainty in recharge corresponds to the lowest

uncertainty in soil moisture (zone 11). The reason for this behavior are the parameters controlling the snow accumulation and melting within mHM. Since the soils are almost close to saturation over the course of a year in this zone, water drains quickly to layers underneath the root zone. In this layer the interflow and groundwater recharge is determined within mHM. Since the ensemble parameters have been derived in different regions of Germany, snow parameters from regions where snow doesn't have a big impact on the water balance are involved. But snow processes have a major influence on the water balance in the Alps. To derive more appropriate parameter sets a calibration considering multiple catchments is necessary. Currently we are developing such a framework.

2.6 Summary and Conclusion

In this study we present the derivation and evaluation of a high-resolution ($4 \times 4 \text{ km}^2$) dataset of hydrologic and hydro-meteorological fluxes and states for Germany covering the period 1950-2010, which is made freely available. The dataset incorporates 100 spatially consistent ensemble simulations, which are analyzed regarding their uncertainty caused by the parameter estimation. The parameter sets of the ensemble simulations are determined by a two step parameter selection method. The model is calibrated in seven catchments and the parameters sets are filtered based on cross-validation results in all of the basins. Thus, the uncertainty is composed of the uncertainty in parameter estimation and the uncertainty stemming from transferring these parameters in to remote locations. The ensemble simulations are evaluated with streamflow observations, recharge data, evapotranspiration and soil moisture observations.

The evaluation regarding discharge at 222 additional catchments revealed a median NSE of 0.68. Thus the 100 ensemble parameter sets are considered to be representative for Germany. The evaluation with evapotranspiration from eddy covariance stations showed deficiencies in mHM. Especially in spring, deviations of modeled and observed E_a indicate room for improving the representation of vegetation dynamics within mHM. The sites covered by cropland showed the largest deviations from evapotranspiration observations, since croplands are highly human influenced (seeding, harvest, or eventually irrigation), which makes it difficult to model their dynamics at the local scale. Additionally, cropland is generalized in mixed land cover class in mHM. Soil moisture estimations at the same locations have been in good agreement with the observed dynamics.

The second part of the study is focusing on the uncertainty of the simulated hydrologic fluxes and states due to uncertainties in parameter estimation. It is shown that uncertainty is varying in time, location and magnitude between hydrologic variables. The uncertainty was lowest for evapotranspiration, among all variables, and highest for recharge. Its spatial distribution was similar to the spatial distri-

bution of the dryness index. But, for example uncertainty of evapotranspiration estimates were additionally caused by soil properties. In general, the highest uncertainties occur in the northeastern part of Germany, which is characterized by low precipitation amounts and high soil porosities. The temporal variation of uncertainties is almost constant for evapotranspiration, medium for per-grid-cell-generated runoff and high for groundwater recharge and soil moisture depending on geographical location.

Based on this results we suggest to incorporate additional data, e.g., soil moisture or satellite observations, to the calibration procedure to better constrain the model internal states. The results of this study emphasizes the importance of the consideration of uncertainties in parameter estimation for historical analyzes, now- and forecasting in hydrology.

2.7 Data Availability and Data Format

The dataset consists of daily values of precipitation, average temperature, potential evapotranspiration, evapotranspiration, soil moisture, groundwater recharge and discharge. Whereas the latter four are provided as ensemble of 100 simulations. The data format is the Net Common Data Format (NetCDF version 3). Additionally, the ensemble means and standard deviations are provided. The dataset is freely accessible under <http://www.ufz.de/index.php?en=41160>.

Chapter 3

Implications of Parameter Uncertainty on Soil Moisture Drought Analysis in Germany

This chapter is identical to the publication:

Samaniego, L., Kumar, R., and Zink, M. (2013): Implications of Parameter Uncertainty on Soil Moisture Drought Analysis in Germany. *Journal of Hydrometeorology*, 14(1):47-68. doi:10.1175/JHM-D-12-075.1. © American Meteorological Society. Used with permission.

3.1 Abstract

Simulated soil moisture is increasingly used to characterize agricultural droughts but its parametric uncertainty, which essentially affects all hydrological fluxes and state variables, is rarely considered for identifying major drought events. In this study, a high-resolution, 200-member ensemble of land surface hydrology simulations obtained with the mesoscale Hydrologic Model is used to investigate the effects of the parametric uncertainty on drought statistics such as duration, extension, and severity. Simulated daily soil moisture fields over Germany at the spatial resolution of $4 \times 4 \text{ km}^2$ from 1950 to 2010 are used to derive a hydrologically consistent soil moisture index (SMI) representing the monthly soil water quantile at every grid cell. This index allows a quantification of major drought events in Germany. Results of this study indicated that the large parametric uncertainty inherent to the model, did not allow discriminating major drought events without a significant classification error. The parametric uncertainty of simulated soil moisture exhibited a strong spatio-temporal variability, which significantly affects all derived drought statistics. Drought statistics of events occurring in summer with at most six months duration were found to be more uncertain than those occurring in winter. Based on the ensemble drought statistics, the event from 1971 to 1974 appeared to have 67% probability of being the longest and most severe drought event since 1950. Results of this study emphasize the importance of accounting for the parametric uncertainty for identifying benchmark drought events as well as the fact that using a single model simulation would very likely lead to inconclusive results.

3.2 Introduction

Drought is a recurrent and extensive climatic phenomenon characterized by below-average water availability whose duration might last for several years. It is considered as one of the most costly natural disasters because it often induces huge socio-economic losses (Wilhite et al., 2000) as well as environmental degradation. During the summer of 2003, for instance, several parts of Europe endured the highest temperatures of the last 500 years (Luterbacher et al., 2004; Fink et al., 2004) and one of the most extensive and severe drought in records. In Germany alone, the estimated loss in the agricultural sector was 1.5 billion Euros (COPA-COGECA, 2003). In extreme cases, prolonged drought spells might lead to unprecedented environmental disasters often associated with the decline of human societies (Hodell et al., 1995; Haug et al., 2003) or the trigger for mass migrations and famine (Field, 2000). Droughts occur indifferently in high and low rainfall areas and in virtually all climatic zones (Dracup, 1991; Mishra and Singh, 2010), although the most severe human consequences happen in arid regions.

Currently, hydro-meteorologic mechanisms originating droughts are relatively well understood. In general, droughts are driven by extreme macroclimatic variability originated by atmospheric interactions and feedback between the atmosphere, the oceans, and the land surface (e.g. Nicholson, 2000; McCabe and Palecki, 2006). This variability is, in turn, related to the solar activity as well as atmospheric composition, and strongly affected by anthropogenic activities (Sheffield et al., 2009).

Our ability to make reliable drought predictions, however, is not satisfactory (Wilhite et al., 2000) although there is vast scientific literature on this topic. One of the main reasons is related to the insufficient knowledge regarding the processes controlling drought development and persistence, as well as, its spatio-temporal variability (Sheffield et al., 2009). Another reason stems from the fact that there is no clear definition of this phenomenon (Wilhite and Glantz, 1985) since it depends upon the variable that is used for its quantification.

Droughts have been mainly classified into three types: (1) meteorological drought, usually defined as an extreme anomaly of precipitation; (2) hydrological drought, which is related to a deficit in the supply of surface and subsurface water, and (3) agricultural drought, being a combination of meteorological and hydrological droughts leading to deficits in root zone soil moisture available to vegetation (Wilhite and Glantz, 1985). Since precipitation and discharge data are widely available, a plethora of drought indices have been proposed in the scientific literature to quantify meteorological and hydrological droughts, for instance: the Palmer Drought Severity Index (Palmer, 1965), the Standard Precipitation Index (McKee et al., 1993), the Regional Deficiency Index (Stahl and Demuth, 1999), among others.

It is widely accepted, however, that these empirical indices are not adequate to represent extreme water stress conditions that would lead to a significant reduction of biomass and crop yield (Keyantash and Dracup, 2002; Mishra and Singh, 2010). In Germany, for example, Döring et al. (2011) have shown that empirical drought indices based only on available data such as precipitation, temperature do not constitute adequate measures to describe agricultural drought stress because they do not explicitly account for the available water stored in the root zone, which is ultimately the plant's life supporting substance.

Direct soil moisture observations, on the other hand, are not available at regional level because measuring this variable at large scales is not logistically and economically feasible (Vereecken et al., 2008). This implies that hydrologic or land surface models would have to be employed for the estimation of the soil water content. Soil moisture, in contrast to precipitation or discharge, constitutes a good index for quantifying agricultural drought because it controls the proportion of the rainfall that percolates, runs off or evaporates from the earth surface (i.e. root zone). Concisely, it integrates precipitation and evapotranspiration as well as the delays introduced by interception, snow accumulation, and melting over periods of days

to weeks. In other words, soil moisture in the root zone is a governing factor sustaining vegetative growth and thus it is a direct indicator of agricultural drought (Keyantash and Dracup, 2002). Land surface models such as VIC-3L (Liang et al., 1996) and SIM (Soubeyroux et al., 2008), for example, have been used recently to assess agricultural drought characteristics in the USA and France, respectively (Sheffield et al., 2004; Andreadis et al., 2005; Vidal et al., 2010). There are, however, several key issues that should be considered, if simulated soil moisture is chosen for quantifying agricultural droughts.

Modeling soil moisture dynamics at large-scales (e.g. grid cells greater than 500 m) is difficult and uncertain as was demonstrated by the PILPS project (Chen et al., 1997). In this project, 23 land surface models (LSMs) exhibited significant differences between modeled and measured soil moisture (among other variables) although all models were based on fundamental principles of mass and energy conservation and forced with identical atmospheric conditions. This experiment also indicated the existing interplay between this state variable and other fluxes such as latent heat as well as the substantial parameter uncertainty that is related with these physical processes. At larger scales, the sub-grid variability of the variables involved and the nonlinearity of the processes make the modeling of soil moisture even more complicated because parametrization schemes might become scale dependent (Nykanen and Foufoula-Georgiou, 2001). It should be noted that effective model parameters (e.g. saturated soil water content or porosity) at large scales can only be estimated but not measured. This, in turn, constitutes a new source of uncertainty that should be taken into account when modeling soil moisture dynamics. Consequently, a drought monitoring and early warning system based on a soil moisture index, which does not fully take into account the predictive uncertainty of the simulation model, might be inadequate for real applications and/or for impact assessment.

Most of the soil moisture drought studies (Andreadis and Lettenmaier, 2006; Vidal et al., 2010; Shukla et al., 2011) found in the literature have not addressed the epistemic uncertainty related to parametrization, model structure, and input data. More recently, Wang et al. (2011) argued that state variables, such as soil moisture, are strongly dependent on the parametrization of the LSMs and the quality of the meteorological forcing data. Similar results have been found by Mo et al. (2012), who concluded that the primary source of uncertainty between two drought monitoring systems operated in the USA is originated from precipitation data, and in a minor degree from air temperature, shortwave and longwave radiation, and wind speed. As a result, substantial discrepancies with in-situ measurements have been found (Entin et al., 2000), which are mainly attributed to the variability of topography, soil, vegetation, and root structure, but could also stem from uncertainty sources mentioned above. Specifically, finding a robust parametrization scheme for a LSM or a hydrological model, which is able to produce reliable estimates of water fluxes at high spatial resolution over large domains, is one of the grand challenges of contemporary hydrology (Beven and Cloke, 2012).

It has been noted, however, that multi-model ensembles are able to describe the anomalies and seasonal variability of soil moisture. Wang et al. (2009, 2011) successfully applied this technique to reproduce agricultural drought characteristics in the continental United States and China. In both studies, six LSMs were used to generate soil moisture fields for a period of almost 100 years in the USA and 56 years in China. However, in those studies, only a single simulation for each LSM was used.

In this study, we argue that a unique parameter set for a given LSM is inadequate to estimate water fluxes and related state variables at high spatio-temporal resolutions, considering that both inputs and model parameters over large modeling domains are subject to considerable uncertainties due to the reasons mentioned above (see also Rosero et al., 2011). Thus, we hypothesize that any drought characteristic (e.g. severity, duration) based on simulated soil moisture is prone to large variability due to parametric uncertainty, which, if it is not taken into account, will lead to incorrect estimates of drought characteristics.

The main objectives of this study and the rationale behind them is summarized below. 1) To obtain a consistent ensemble of daily soil moisture fields for Germany since 1950 at a spatial resolution of 4×4 km. Such reconstruction is fundamental to characterize historical drought events and their related characteristics. To the best of our knowledge, this is the first study to perform nationwide agricultural drought reconstruction for Germany. Long-term soil moisture simulations are also fundamental for initializing hydrologic or regional climate models and the basis to fulfill the remaining objectives. 2) To develop a reliable soil moisture drought index (SMI) for Germany at a high spatial resolution. Such SMI is key for implementing a monitoring system and adaptation strategies at regional scale. Available global soil moisture analyses have a spatial resolution 0.5° or larger, which is too coarse for a regional drought analysis. 3) To identify benchmark agricultural drought events occurring in summer and winter in Germany during the last 60 years and the uncertainty of their main statistical characteristics. These exceptional events are necessary to identify potential climate change effects on the hydrological cycle. The uncertainty associated with drought characteristics such as coverage area, duration, and severity, will be quantified by means of a Monte Carlo method. Ensemble model simulations would allow us to assess the reliability of the predictions which, in turn, will lead to minimize the number of false positive drought events (i.e. cases in which the SMI indicates that a given event is below a certain threshold for a given characteristic when in fact it is not). Additionally, the effect of the ensemble size on the false positive rate will be investigated. 4) To identify regions in Germany prone to strong drought persistence as well as areas exhibiting significant trends in monthly soil moisture fields. These insights would provide hints for mitigation and adaptation measures at regional scale.

3.3 Soil Moisture Data

Soil water availability in the root zone is a direct indicator of agricultural drought because it constitutes a governing factor of the state of vegetative growth through the availability of water for transpiration (Keyantash and Dracup, 2002). Measuring soil moisture content over the entire domain of Germany at a spatial resolution of 4×4 km, for example, is logistically and economically infeasible (Vereecken et al., 2008). LSMs or hydrologic models are therefore often employed to estimate this key variable over large spatial domains and longer periods (Andreadis and Lettenmaier, 2006; Sheffield and Wood, 2007; Wang et al., 2009; Mishra et al., 2010; Wang et al., 2011).

In this study, the mesoscale Hydrologic Model, mHM (Samaniego et al., 2010) was used to generate a large ensemble of daily soil moisture fields for the period from 1950 to 2010. A three layer soil scheme was used to model the soil moisture dynamics over the entire root zone depth (i.e. approximately up to 2 m below ground). The depth of the first two layers was fixed to 5 cm and 25 cm, whereas the depth of the last one was variable according to soil characteristics provided by the soil texture map. The spatial resolution of each grid was 4×4 km (level-1). A short description of mHM and the generation of ensemble soil moisture fields are given below.

3.3.1 The mesoscale Hydrologic Model mHM

The mesoscale Hydrologic Model is a process-based water balance model (Samaniego et al., 2010) that has been developed over the last five years at the Helmholtz Centre for Environmental Research - UFZ. This spatially explicit model does not differ significantly from existing large scale hydrologic models (e.g. the HBV and the VIC-3L model) on how dominant hydrologic processes at the meso- and macro-scales are conceptualized, but on how the effective parameters of the model are quantified at a selected modeling scale and on how the sub-grid variability of physiographic characteristics provided at level-0 is taken into account for the estimation of these effective parameters. These two fundamental differences constitute the core of the multiscale parameter regionalization technique (Samaniego et al., 2010) that is embedded into mHM. Extensive numerical experiments have shown that this technique is capable of coping with the large spatio-temporal variability of the input data and as a result, mHM is able to produce quite good performance at multiple spatial resolutions and locations other than those used during calibration (i.e. proxy basin and flux-matching tests).

Currently, mHM has been evaluated in more than one hundred basins in Germany ranging from 4 km^2 to $47\,000 \text{ km}^2$ (Samaniego et al., 2010; Kumar et al., 2010, 2013b). This model is driven by disaggregated fields of daily forcings such

3. Soil Moisture Drought Analysis in Germany

as precipitation, temperature, and potential evapotranspiration. It accounts for the following hydrological processes: canopy interception, snow accumulation and melting, evapotranspiration, infiltration, soil moisture dynamics in three layers, surface runoff, subsurface storage, discharge generation, percolation, baseflow, and flood routing within the river reaches. Readers may refer to Samaniego et al. (2010) for a detailed model description as well as its parametrization.

The morphological and physiographic data required for setting up mHM include a digital elevation model (50×50 m) acquired from the Federal Agency for Cartography and Geodesy, a vector soil map containing information on soil textural properties such as sand and clay contents of different soil horizons, and a vector map of hydro-geologic formations containing properties such as saturated hydraulic conductivity. Both vector maps at a scale of 1:1 000 000 were obtained from the Federal Institute for Geosciences and Natural Resources of Germany. Three Corine land cover seamless vector data (<http://www.eea.europa.eu>) for the years 1990, 2000, and 2006 were employed to account for the changes in states of land cover over the simulation time period (1950-2010). Land cover states, prior to the year 1990, were inferred from the Corine 1990 map. Monthly variability of the leaf area index was estimated for each land cover class with MODIS scenes from 2001 to 2009. These data are freely available from https://lpdaac.usgs.gov/get_data. For a detailed description on data processing and setting up mHM in several river basins, interested readers may refer to Samaniego et al. (2010); Kumar et al. (2010). Previous data sets were re-sampled on a common spatial resolution of 100×100 m denoted as level-0. This level of information provides the sub-grid variability of all morphological and physiographic variables required to run the model at any coarser resolution denoted as level-1 (e.g. 4 km). The time series of discharge data across several gauging stations were acquired from the EURO-FRIEND program (<http://ne-friend.bafg.de>) and the Global Runoff Data Centre (<http://www.bafg.de>).

Gridded fields of daily average precipitation as well as maximum, minimum, and average air temperatures at 4×4 km spatial resolution (level-2) were estimated from their respective point measurement data from about 5600 rain gauges and 1120 meteorological stations, which are operated by the German Meteorological Service (DWD). Two interpolation techniques were used to derive the daily fields of precipitation, which are detailed in section 3.3.2. Gridded estimates for temperature fields were obtained with external drift kriging, wherein the terrain elevation was used as a drift variable. The daily fields of potential evapotranspiration were estimated with the Hargreaves and Samani method (Hargreaves and Samani, 1985) and were subsequently corrected to account for the spatial variability of the terrain aspect.

3.3.2 Ensemble Description and Experimental Design

Two major sources of parametric uncertainty were identified through sensitivity analysis. The most important one is related with the variability of the global calibration parameters of mHM (i.e. space and time independent), and the second one is related with the parameters required for the rainfall interpolation method. Consequently, the uncertainty tree was divided into two main branches, each one driven by two independent interpolation methods but both based on the same rainfall measurements. These two branches were denoted as DWD1 and DWD2. Other meteorological variables such as daily, minimum, and maximum temperature required in both branches were kept the same. This assumption was taken considering 1) that precipitation interpolation is one the most important source of error in the input data (Mo et al., 2012), and 2) that the areal coverage of snow-dominated areas in Germany is geographically limited.

The DWD1 branch was created with external drift kriging using terrain elevation as a drift and a combined variogram that comprised a nugget and an exponential part. The resolution of this product was 4×4 km, with daily time steps from 1950 to 2010. The best fit parameters (i.e. nugget, range, and sill) were found through a cross-validation procedure.

The DWD2 branch was obtained by re-sampling the original daily REGNIE product (Deutscher Wetterdienst (DWD), 2013) available at 1×1 km into a regular grid similar to that of the DWD1 data set. The k -nearest's neighbor technique and a standard geo-referencing algorithm were employed for this purpose. The DWD1 data was used to complete this set with daily fields from 1950 to 1959 since the REGNIE data set is only available from 1960 to 2010. The REGNIE data is based on multiple linear regression having elevation, geographic location, and aspect as predictors.

Within each branch, the propagation of the parameter uncertainty into the soil moisture simulations was evaluated by an ensemble of one hundred best parameter sets of mHM. The following procedure was implemented for their selection. First, in every major river basin depicted in Figure 3.1, the dynamically dimensioned search algorithm (Tolson and Shoemaker, 2007) was employed to find good sets of global parameters which exhibit an acceptable model efficiency [e.g. Nash-Sutcliffe-Efficiency of at least 0.75] during the evaluation period (for details refer to Kumar et al., 2010, 2013b). In the next step, all parameter sets found for a given basin were transferred to the remaining ones. Finally, only those sets exhibiting a model efficiency greater than or equal to 0.65 at recipient locations were retained as members of the best global parameter sets. This implies that these super sets of global parameters are able to reproduce water fluxes in all major river basins in Germany with an efficiency of at least 0.65. It may be noted that a single set of VIC-3L model parameters for a large domain in the midwestern United States was used in a study by Mishra et al. (2010) for assessing historical drought events. In

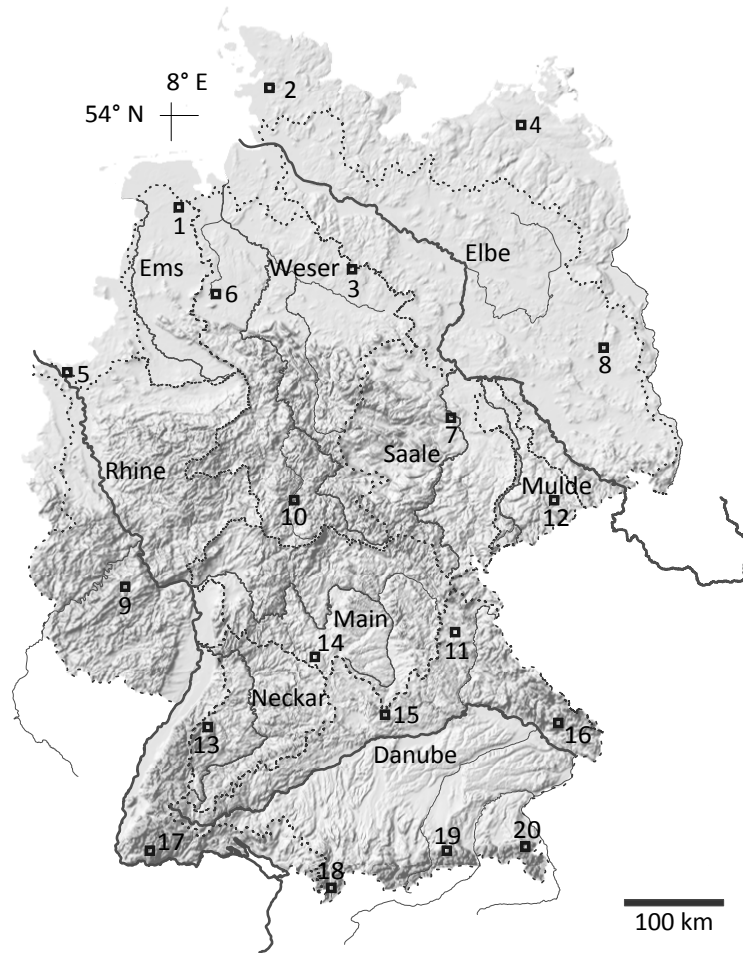


Figure 3.1: Map of Germany indicating the main river basins used for this study. Selected locations for uncertainty analysis of the soil moisture climatology are depicted with a dot.

contrast to that, in this study the ensemble of 200 model realizations was used for the subsequent analysis of historical drought events in Germany including both uncertainty branches.

In general, mHM requires at least five years of spin-up time to equilibrate. To minimize the influence of initial conditions, all state variables (e.g. water content at a given soil layer) in each ensemble member were initialized with their climatological averages corresponding to the precise time of year at the initialization (Rodell et al., 2005). The climatological average was estimated as the long term mean of a given state variable within a seven-day window around the first of January. The DWD1 precipitation estimate was employed to estimate the long term mean. This procedure allowed to reduce the spin-up time to one year without inducing large bias due to inappropriate initial conditions. Thus, model simulations during the starting year 1950 were discarded from the following analysis.

3.4 The Soil Moisture Index

The absolute values of the soil moisture states estimated with mHM do not allow a direct comparison of derived drought indices across the study domain because anomalies in absolute terms reflect climatological and morphological characteristics (Andreadis et al., 2005), rather than strong deviations from the respective normal conditions, which is the main characteristic that defines a drought event. Instead of absolute values, agricultural droughts can be quantified as “*deficit of soil moisture relative to its seasonal climatology at a location*” (Sheffield et al., 2004). The main idea behind this definition is to develop an index that varies between 0 and 1, which indicates drier to wetter conditions, respectively. The apparent selection for such an index is the conditional cumulative distribution function of the soil water content in the root zone at a given location i and time of the year m . This kind of normalization is inspired by the Standardized Precipitation Index (McKee et al., 1993). The procedure to estimate a Soil Moisture Index (SMI) based on mHM soil moisture simulations is described next.

3.4.1 Aggregation and Normalization

Daily mHM soil moisture from three soil layers was averaged for every grid cell to obtain monthly states. These monthly values were, in turn, normalized with respect to the corresponding total root zone saturated water content (i.e. porosity times the total depth of the soil layers) to estimate the monthly soil moisture fraction (x) of the total soil column, namely:

$$x = \frac{\sum_l x^l}{\sum_l x_S^l} \quad (3.1)$$

where, x^l is the monthly soil moisture at root zone layer l [mm], x_S^l is porosity or the saturated water content of root zone layer l [mm]. In the present study $l = 3$. In this case, the indexes i and m are omitted to ease the notation.

3.4.2 Estimation of the Soil Moisture Index

The monthly soil moisture fraction (Eq. 3.1) may exhibit heavily skewed, non-gaussian distributions (Koster et al., 2009) whose shape varies depending on climate and soil characteristics. The distribution of this random variable can also be multi-modal (Vidal et al., 2010), which is an indication of preferential states of seasonal soil moisture (Rodriguez-Iturbe et al., 1991; Laio et al., 2002). Consequently, describing this random variable with unimodal theoretical distribution [e.g. the beta distribution (Sheffield et al., 2004)] is not appropriate. Instead of

making assumptions regarding the theoretical distribution of this variable, which would induce an additional source of uncertainty, a non parametric technique was adopted to estimate the probability density function of the monthly soil moisture fraction at every cell within the domain, denoted hereafter as $\hat{f}(x)$. The estimation procedure is as follows.

Given a set of data from one of the ensemble members x_1, x_2, \dots, x_n that corresponds to the monthly soil moisture fractions of a given cell within the domain during month m (e.g. January), the kernel density estimate at a given value x can be obtained by

$$\hat{f}(x) = \frac{1}{nh} \sum_{k=1}^n K\left(\frac{x - x_k}{h}\right) \quad (3.2)$$

where $K(x)$ is the smoothing kernel, n the sampling size, and h the bandwidth. The sampling size in this case is equal to 60. There are various possibilities to select $K(x)$ (Wilks, 2011), however the Gaussian kernel is appealing in this case because of its unlimited support. The optimal selection of the bandwidth \hat{h} can be obtained by minimizing the unbiased cross-validation criterium (Scott and Sain, 2005) given by

$$\min_{\hat{h}} \left[\int \hat{f}(x|h)^2 dx - \frac{2}{n} \sum_{k=1}^n \hat{f}_{-k}(x|h) \right] \quad (3.3)$$

where, $\hat{f}_{-k}(x|h)$ is the leave-one-out density estimate at x when observation x_k is not taken into account. This optimization was performed with a generalized reduced gradient algorithm. Once the optimal bandwidth is found, the best fit of the empirical distribution function can be estimated \hat{f} .

Finally, the mHM soil moisture index for a given cell and month, which denotes the quantile at the soil moisture fraction value x , can be obtained by numerically integrating the expression

$$\text{SMI} = \int_0^x \hat{f}(u) du \quad (3.4)$$

3.4.3 Identification of Drought Events

Droughts are regional phenomena covering large contiguous areas over long periods. Understanding the spatial-temporal patterns and their relationships with other variables is therefore a fundamental step for drought prediction. Previous drought studies carried out in Germany, however, have been focused on statistical

analysis of readily available point observations such as river discharge or precipitation data (Demuth and Heinrich, 1997; Stahl and Demuth, 1999; Franke et al., 2004; Schindler et al., 2007; Schindler and Mayer, 2007), and in general, they are limited to a regional scale rather than to the national scale. To the best of our knowledge, studies investigating the spatial-temporal drought variability over the whole German territory are not available in the scientific literature.

The retrospective reconstruction of soil moisture analysis in Germany provides a unique data set to estimate fundamental characteristics (e.g. severity and areal extent) of the major agricultural droughts occurred in Germany since 1950 at a high spatial resolution. Drought events were identified in this continuous spatio-temporal data set with the method proposed by Andreadis et al. (2005).

First of all, regions under drought stress were identified with the threshold method (Dracup et al., 1980). This implies that cells fulfilling $SMI_t < \tau$ were selected as potential regions under drought at the monthly time step t . The selection of the truncation level τ is fundamental for this method. A common value adopted in the literature is $\tau = 0.2$ (Andreadis et al., 2005; Vidal et al., 2010). This threshold indicates that a given cell is enduring a soil water deficit occurring less than 20% of the time.

In the second step, drought clusters at every monthly time step have to be consolidated in space. This means that all clusters whose area is less than a minimum threshold area will be excluded from further analysis. This step is necessary to eliminate small isolated areas that are suffering a drought but are too small to be considered as a regional event. In this study the minimum cluster area was set to 640 km^2 (i.e. 40 cells).

The final step of the drought event identification consists consolidating independent spatial clusters over successive time steps into a regional, multi-temporal cluster. This kind of clustering is necessary because the spatial variability of a drought event is vast, composed of many branches that can either merge together or split over time. The only condition to join clusters over time is that the overlapping area should be larger than 6400 km^2 (i.e. 400 cells). Overlapping areas less than this threshold area was considered as independent drought events.

Both threshold areas (i.e. the minimum cluster area and the overlapping area) were determined through sensitivity analysis but primarily based on rules of thumb often followed in the literature (e.g. Andreadis et al., 2005; Vidal et al., 2010). The main criteria for the selection of these parameters was the stability of drought characteristics described in the following section. It should be noted that the selection of smaller areas, enduring drought conditions, leads to the proliferation of smaller clusters that are not contiguous over time and hence can not be considered as part of a regional phenomenon.

3.4.4 Quantification of Drought Characteristics

Drought characteristics such as mean duration, mean areal extent, total magnitude, intensity, and severity-area-duration curves were quantified for every drought event and every ensemble member. The *mean duration* (D) of a spatio-temporal drought event is defined as the average of the drought duration of every cell within a drought event. This statistic is given in months. The *mean areal extent* (A) is defined as the average of a region under drought from the onset until the end of the drought event, expressed as percentage of the total German surface area. The *total magnitude* (M) is defined as the spatio-temporal integral of the SMI below the threshold value τ (i.e. the deficit) over those areas which are affected by the drought event, or explicitly

$$M = \sum_{t=t_0}^{t_1} \int_{A_t} (\tau - \text{SMI}_i(t))_+ \quad (3.5)$$

where, t_0 and t_1 denote the onset and the ending months of a given drought event. A_t is the area under drought at a given time step t , expressed as the percentage of total German surface area. i denotes a given location within the domain A_t , and $(\cdot)_+$ the positive part function. Thus, M is expressed in months times percentage of total German surface area.

Above described three statistics are useful to rank drought events based on the overall impact but they do not allow to estimate the impact of the drought after some months from the onset. This could be better quantified with the *drought intensity* (I_d) at a given duration d from the onset of the event. This statistic can be estimated as

$$I_d = \frac{1}{d} \sum_{t=t_0+1}^{t_0+d} \int_{A_t} (\tau - \text{SMI}_i(t))_+ \quad (3.6)$$

This statistic would also allow to estimate the impact of various events during summer and winter, by discriminating the time step $t_0 + d$ to a corresponding season.

Another commonly used method to benchmark drought events is based on the severity-area-duration curves (SAD) proposed by Andreadis et al. (2005). The *severity* (S_d) for every cell for a given duration d in months can be estimated as

$$S_d = 1 - \frac{1}{d} \sum_{t \in d} \text{SMI}_t \quad (3.7)$$

The SAD curves for durations of 3, 6, 9, and 12 months for a given ensemble

realization were constructed as follows. Firstly, the grid cells were ranked according to their severity. The procedure starts with those cells having the maximum severity. Then, the severities of the adjacent cells were summed up progressively until a threshold area is reached. Afterwards, the average severity is estimated for those selected cells. The cumulative area and the average severity constitute the abscissas and ordinates of the SAD curves for a given duration. In this study, regular area intervals equivalent to the area of 20 grid cells were selected (i.e. every 320 km²). This procedure is repeated until the whole area of a given drought event is covered.

The monthly evolution of these statistics was estimated for every member of the ensemble. Based on the ensemble simulations, the uncertainty of the four selected statistics was analyzed.

3.5 Results and Discussion

3.5.1 mHM Evaluation

The performance of mHM was evaluated against observations of daily streamflow, latent heat and soil moisture measured at various eddy covariance (EC) stations acquired from www.fluxdata.org, as well as, with soil moisture observations obtained with a cosmic ray neutron probe (Rivera Villarreyes et al., 2011). Seven large river basins in Germany were selected to cross-validate mHM performance with respect to observed daily streamflow. In this proxy basin test, global calibration parameters of mHM obtained at every river basin were transferred to the remaining test basins. For instance, from Neckar to Danube, Main, Ems, Saale, Mulde, and Weser basins (Figure 3.1). The procedure to find the best hundred global parameter sets is described in section 3.3.2.

High efficiency in this kind of test is a good indication of model performance in ungauged locations. The ensemble mean Nash-Sutcliffe Efficiency (NSE) obtained with mHM using the best hundred global parameter sets at proxy basins during the validation period from 1965 to 1999 varied from 0.50 to 0.88, which is quite acceptable considering that these basins have significantly different hydrologic regimes. Model evaluation on those basins with at-site calibrated parameter sets during the same period exhibited on average a NSE value ranging from 0.74 to 0.93. During the calibration period (2000-2004), the NSE varied from 0.84 to 0.96. These tests indicated that mHM can be used for hydrological predictions within Germany.

The coefficient of determination between the simulated latent heat fluxes against observations across several eddy covariance (EC) stations varied between 0.50 and 0.74 during the period 2000-2002. The model domain in this case was reduced to a cell size of 100×100 m. Considering the various factors that influence the EC

measurements and the fact that mHM is driven by disaggregated hourly values of precipitation and temperature as well as known scaling issues with EC measurements, these results can be regarded as satisfactory. The soil moisture anomalies estimated with mHM were able to explain up to 75% of the variance of their observed anomalies at various EC stations during the same period. Soil moisture estimates were obtained with standard TDR probes. The model at the EC sites was forced with observed hourly precipitation and hourly temperature instead of the interpolated data as used for running the model over the whole domain.

The cosmic ray neutron probe, on the other hand, is a promising alternative because it allows an estimate of the soil water content over a control volume with a diameter of approximately 600 m and a depth of 0.3 m, which in this case, corresponds to the tillage depth setup in mHM. The coefficient of determination (r^2) between the mHM soil moisture anomaly and the cosmic ray neutron probe, reported by Rivera Villarreyes et al. (2011), was 0.57 for the period from August to September of 2011. Correspondingly, the r^2 between the simulated and the mean of soil moisture anomalies measured with 16 frequency domain reflectometry probes located within the same control volume was 0.79.

3.5.2 Retrospective Reconstruction of Soil Moisture Fields

The basis for the analysis of agricultural drought analysis in Germany was the reconstruction of daily soil moisture fields since 1950. 200 realizations of these fields were estimated for the whole of Germany at an hourly basis based on the premise that a single simulation is not sufficient for such analysis because of parameter uncertainty. For the subsequent analysis, simulated hourly fields were aggregated to daily and monthly time steps. Monthly soil moisture values were then normalized as indicated in Eq. 3.1 to ease comparison across locations. The ensemble long-term mean for each month (Figure 3.2) is the most evident statistic to evaluate these results and to verify whether the annual variability of soil moisture corresponds to the known climatology of major geographic regions in Germany. The variability of the spatial patterns shown in Figure 3.2 indicate almost saturated conditions the whole year round in mountainous areas such as the Black Forest, the Harz mountains, and the Bavarian Alpine Foreland. Quasi-permanent dryer conditions have been observed on the North German Plain. The variability of the long term mean of the soil moisture fraction x with respect to its standard deviation indicates a clear seasonality describing wetter and less variable conditions in winter opposed to less wet but highly variable conditions in summer (Figure 3.3).

Results indicated that not only the ensemble monthly climatology of the soil moisture fraction x , depicted in Figure 3.2, but also other statistics such as the 10th and 90th percentiles of x (P_{10} , P_{90}) exhibits seasonality and strong dependency to geographic location. The annual variability of these two percentiles for selected cells within Germany is depicted in Figure 3.4. The geographic location of the

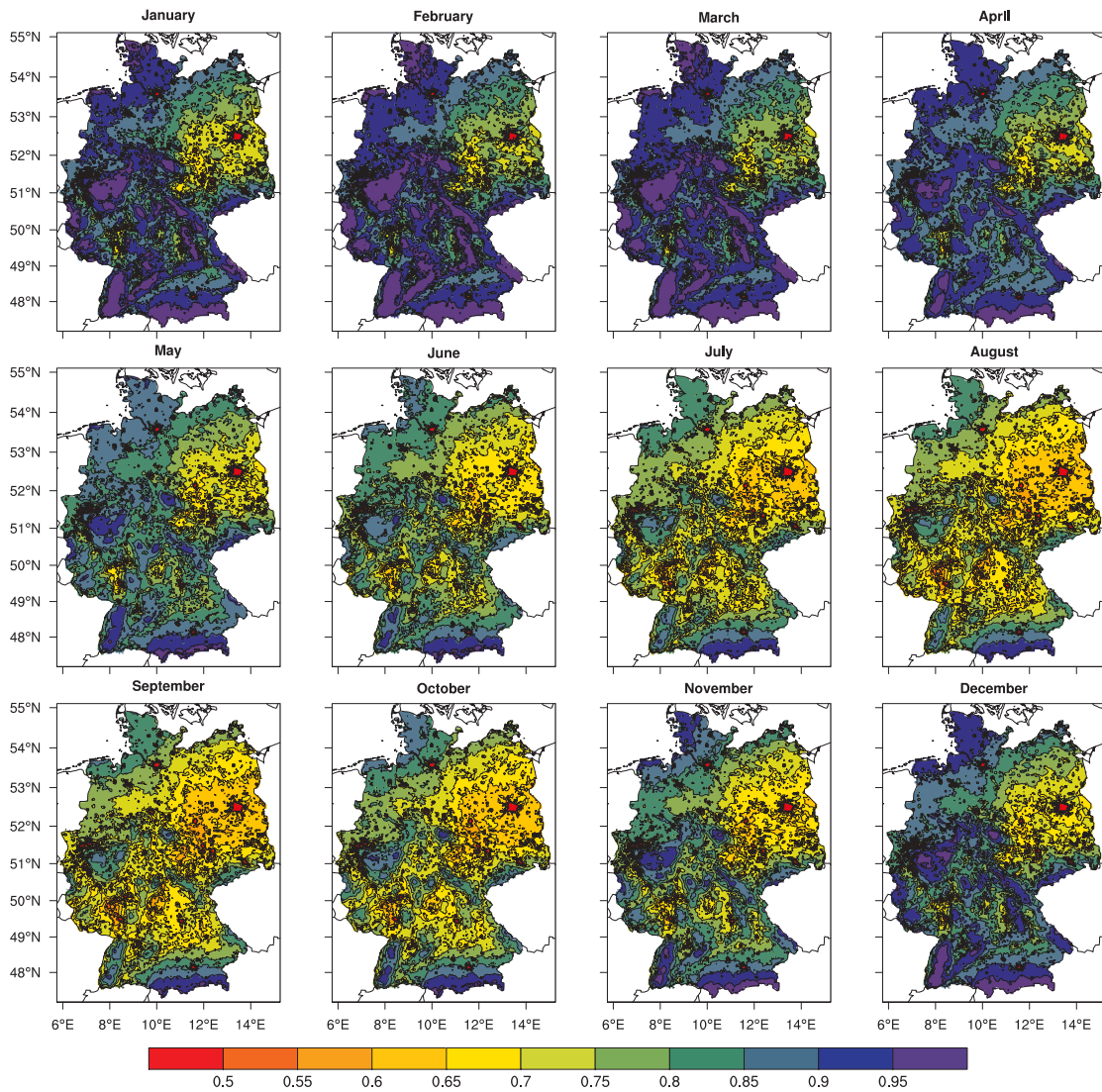


Figure 3.2: Ensemble monthly mean soil moisture fraction over Germany for the period 1950 to 2010.

selected cells is shown in Figure 3.1. The variability and the value of both percentiles indicate marked hydro-climatic regimes in Germany, for instance, humid regions with moderate seasonality on the North Sea (cells 1 and 2), very humid regions with very little seasonality in the alpine regions (cells 18-20), very humid regions with marked seasonality on the Black Forest (cells 13 and 17), moderately dry regions with marked seasonality in the North German Plain (cells 7 and 8), and regions with large seasonality in the pre-alpine regions (cells 14 and 15). In general, the standard deviation of the 90th percentile of x is less than that of the 10th percentile based on the 200-member ensemble. This corroborates the findings of Schaake (2004); Meng and Quiring (2008) which point out that the parametric uncertainty in drier regions (cells 7, 8, 11, 15) is much higher than in humid re-

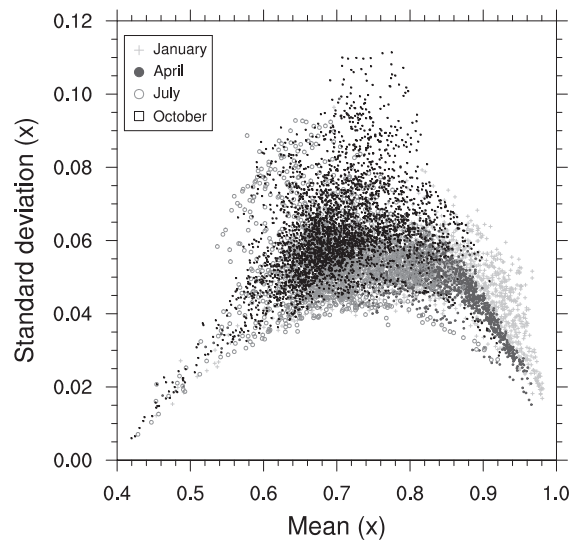


Figure 3.3: Seasonality of the long-term soil moisture fraction x in the Rhine basin. Each point denotes the mean and the standard deviation of x at a given grid cell within this basin.

gions (cells 17-20). The standard deviation of both percentiles exhibits not only seasonal variability, clearly depicted in cell no. 15 shown in Figure 3.4, but also strong geographic dependency. This indicates that there is a complex interplay between climatic conditions and parametrization of the soil moisture processes.

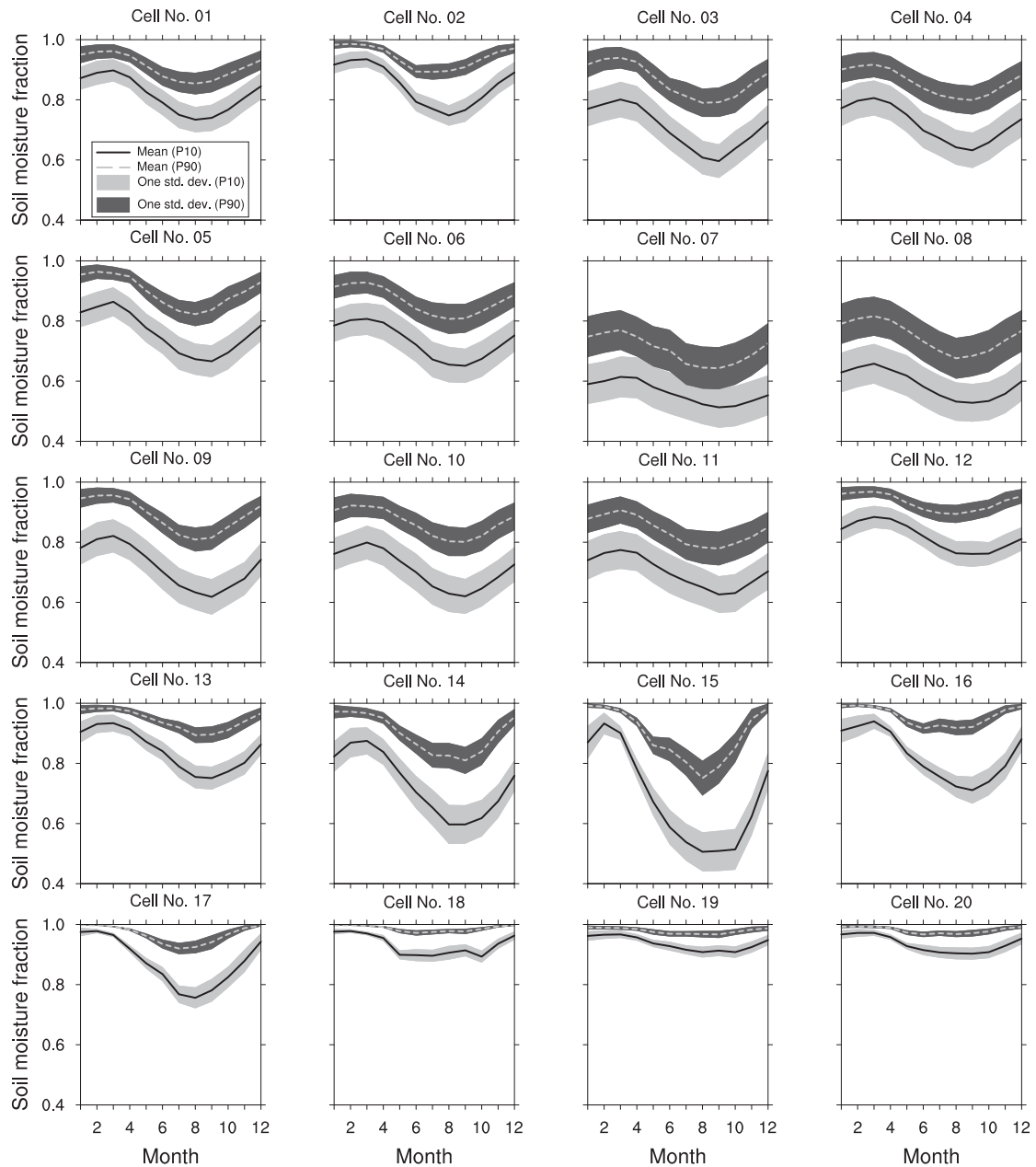


Figure 3.4: Parameter uncertainty of percentiles P_{10} and P_{90} of x at selected cells in Germany. The ensemble mean of these statistics is shown with a continuous line whereas their standard deviation is depicted in solid color. The location of the grid cells are shown in Figure 3.1. The position of the panels approximately resembles the geographic location of these grid cells.

3.5.3 Comparison with Other Indices

The same method proposed in section 3.4 to estimate the SMI can be used to estimate drought indices based on precipitation and surface runoff generated at each cell before routing (Shukla et al., 2011). The results of these three drought indices are shown in Figure 3.5 for one of the ensemble realizations obtained with DWD1. The three upper panels of this figure indicate how different the spatial distribution of the drought index might become depending on the variable used to describe a drought event. Among the three variables, the drought index based on precipitation exhibits the largest spatio-temporal variability due to the lack of memory of the precipitation process, which is one of the main reasons for considering it not appropriate for describing water stress in vegetation (Döring et al., 2011). The drought index based on surface runoff is correlated to the SMI but still quite weak due to fast runoff generation processes. The SMI, as compared with the other two indices, exhibits the largest persistence.

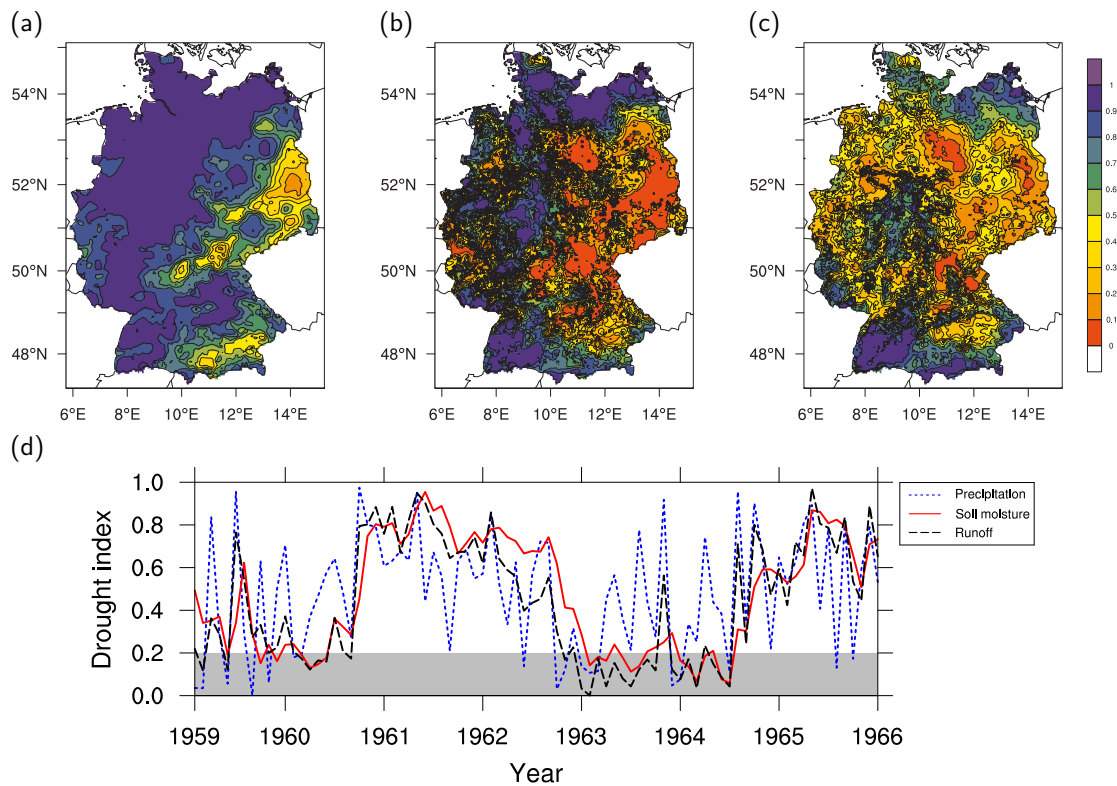


Figure 3.5: Drought indices estimated with precipitation (a), runoff (b) and soil moisture (c) at 1960-08. Panel (d) depicts the time series of the averaged values over Germany from 1959 to 1969. The solid grey area indicates the drought occurrence.

3.5.4 Sensitivity of the Parameter Uncertainty Related to Precipitation Interpolation

Among the two sources of parametric uncertainty investigated in this study, the first one was related to the interpolation methods used to regionalize rainfall point data. For this purpose, two methods were employed to estimate the gridded fields of precipitation data, as denoted by DWD1 and DWD2 (see section 3.3.2 for details). Since both methods use the same input data, any possible variation in soil moisture simulations —*ceteris paribus*— could be attributed to the kriging weights and the variogram parametrization used in DWD1, or the linear weights of the multi-linear regression method employed in DWD2. In this respect, two questions were pursued in this study. (1) How important is this source of uncertainty for the estimation of soil moisture? And, (2) how is this uncertainty distributed over space?

To answer these questions, the Pearson correlation coefficient (r) of the monthly soil moisture fractions at every grid cell obtained with both precipitation products (i.e. DWD1 and DWD2) were estimated separately for all 100 global parameter sets. From these r values, the ensemble mean (\hat{r}) and the coefficient of variation of r were calculated for every cell within the domain. These statistics are depicted in panels (a) and (b) of Figure 3.6, respectively.

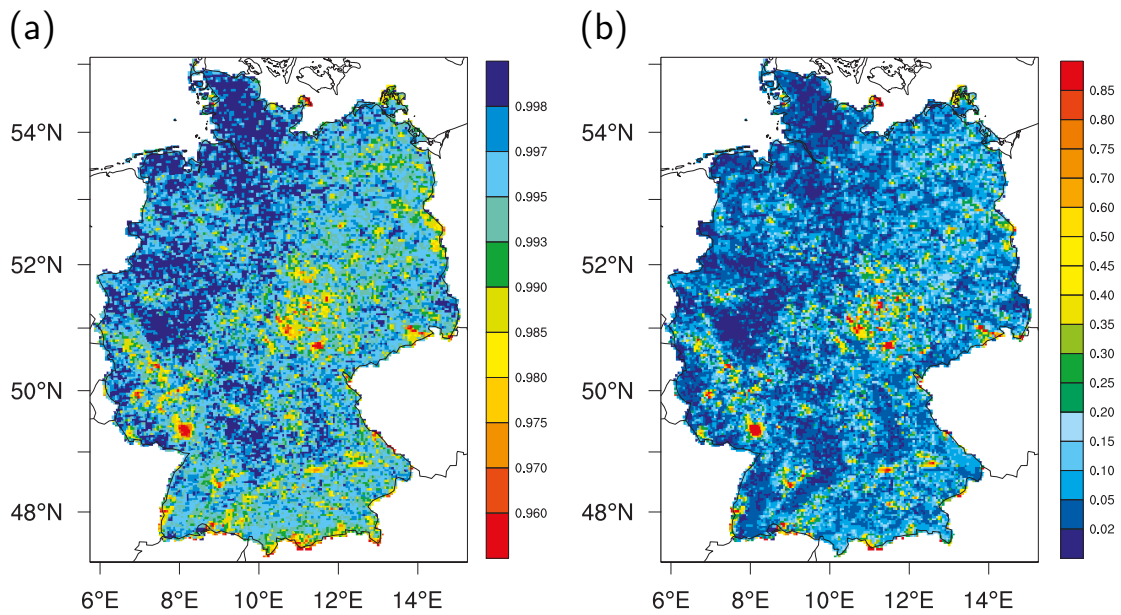


Figure 3.6: Ensemble mean of the Pearson correlation coefficient (a) and mean coefficient of variation (b) between monthly soil moisture fraction estimated with rainfall products DWD1 and DWD2 but same model parameters.

In general, most of the grid cells within Germany exhibit a \hat{r} value greater than

0.98, which indicates a high degree of agreement between any pair of simulations driven by DWD1 and DWD2 forcings but having the same global model parameters. There are very few places where this statistic is less than 0.98, but in every case greater than 0.95. This finding along with the very low coefficient of variation indicated a quite low sensitivity of the monthly soil moisture fraction to the precipitation interpolation parameters. The lower values of \hat{r} were obtained mainly in cells located in and around mountainous regions such as the Harz, the Alps, and the Swabian Jura (Figure 3.6).

3.5.5 Overall Parameter Uncertainty of the Soil Moisture Index

The two major sources of parametric uncertainty described above induced considerable variability into the SMI as shown in Figure 3.7, which depicts the areal average of the SMI over major German river basins, denoted hereafter as $\langle \text{SMI} \rangle$. It can be noticed from this figure that the overall parameter uncertainty of $\langle \text{SMI} \rangle$ is neither constant in space nor over time. The $\langle \text{SMI} \rangle$ obtained with each ensemble member exhibited a large variability within the interquartile range of SMI but a relatively small one at its extreme quartiles (Figure 3.7). This behavior is closely related with the high variability of the standard deviation of the soil moisture fraction around the middle ranges of its mean value (e.g. between 0.6-0.8 as depicted in Figure 3.3).

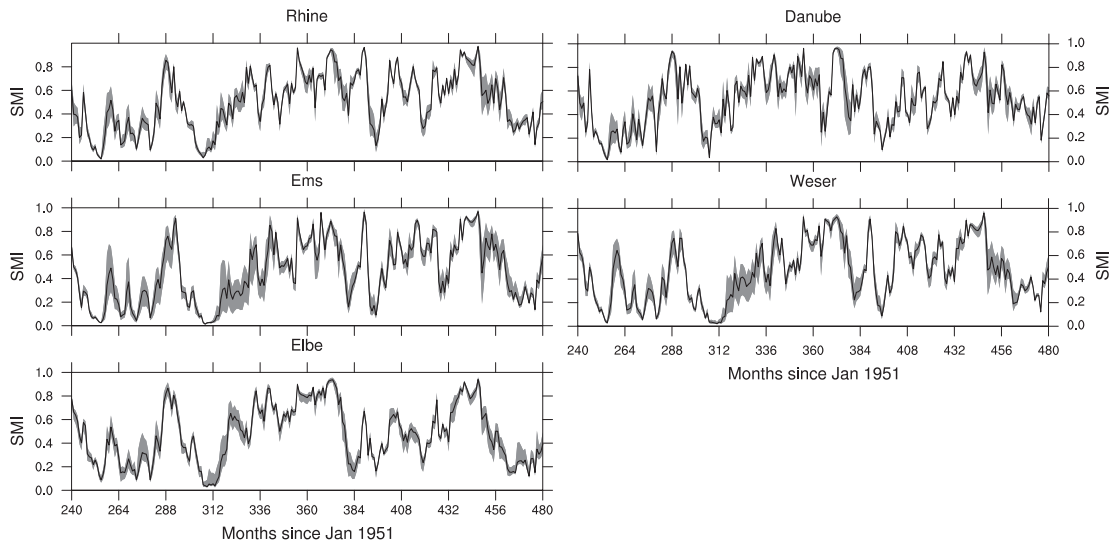


Figure 3.7: Parameter uncertainty of SMI averaged over six major basins in Germany from 1971-01-01 to 1991-12-31. The light grey depicts the variability of the ensemble $\langle \text{SMI} \rangle$ and the black line represents the ensemble mean $\overline{\langle \text{SMI} \rangle}$.

For further analysis, the temporal variability of $\langle \text{SMI} \rangle$ within the ensemble simu-

lations is estimated by its range $R(t) = \langle \text{SMI}(t) \rangle_{\max} - \langle \text{SMI}(t) \rangle_{\min}$, at every point in time t . $R(t)$ denotes the ensemble uncertainty of the soil moisture index over a given domain at time t . The long-term average of $R(t)$ is approximately 0.124 with a standard deviation of 0.014. The correlation coefficient estimated between the range of time series $R(t)$ for every pair of major basins, depicted in Figure 3.1, varied from 0.25 to 0.88. This implied that the uncertainty of the SMI is not only the result of independent errors arising from model parametrization, but also the result of systematic interdependencies between soil moisture and climatic variables

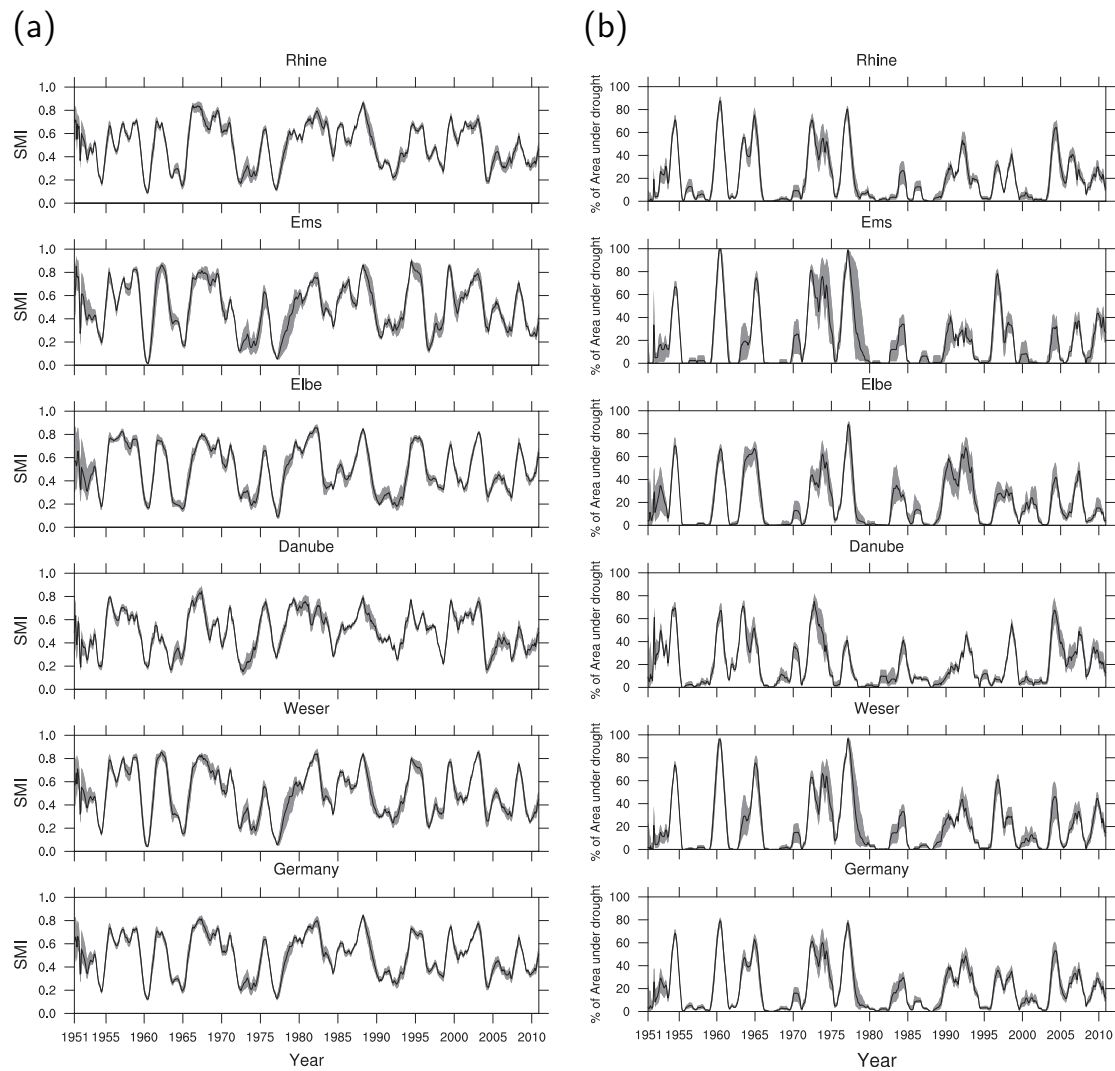


Figure 3.8: Panel (a): 12-month moving average of $\langle \text{SMI} \rangle$ over Germany and major river basins including uncertainty during the period from 1951-01-01 to 2010-12-31. Panel (b): Area under drought. The light grey line depicts the variability of the ensemble $\langle \text{SMI} \rangle$ and the black line represents the ensemble mean $\overline{\langle \text{SMI} \rangle}$.

3. Soil Moisture Drought Analysis in Germany

such as precipitation (P) and potential evapotranspiration (E_p). Based on these results, it was determined that the standard deviation of $R(t)$ tends to decrease as the ratio E_p/P increases. Moreover, given the data provided for each major basin (Figure 3.7), the null hypothesis that the time series of the ensemble uncertainty $R(t)$ constitutes white noise can be safely rejected provided that the p-value of the Fisher's Kappa statistic was less than 0.001.

The 12-month moving average of $\langle \text{SMI} \rangle$ depicted in panel (a) of Figure 3.8 over the reconstruction period (1951-2010) showed a considerable reduction in uncertainty compared with the monthly values of $\langle \text{SMI} \rangle$, but still not small enough to be considered negligible. The 12-month moving average of the percentage of area under drought (with respect to the surface area of Germany) exhibited a considerable uncertainty at the peaks of the events (panel (b) of Figure 3.8). This result, however, allows preliminary identification of major drought events covering at least 50% of the German territory, namely those in the periods 1953-1954, 1959-1960, 1964-1965, 1972-1973, 1976-1977, 1992-1993, 2003-2004.

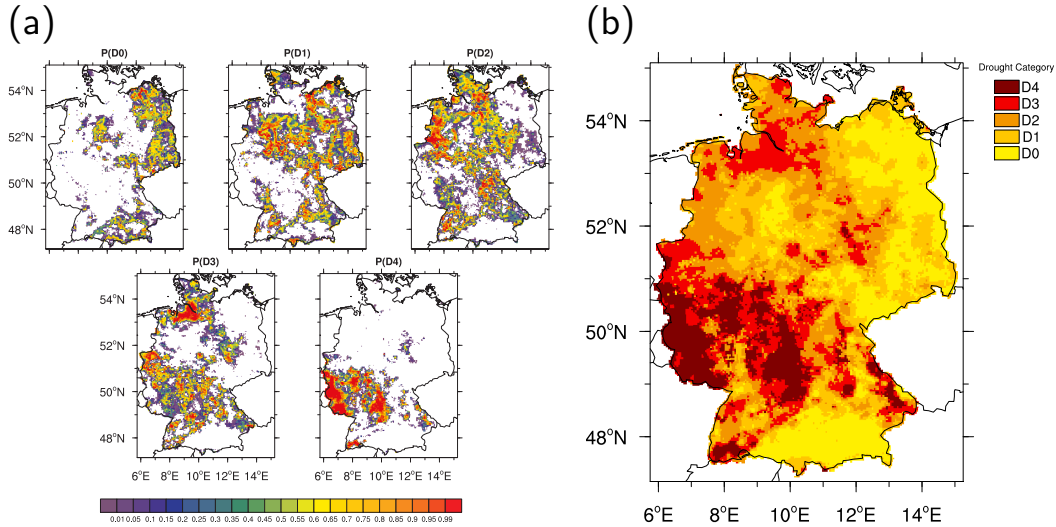


Figure 3.9: Panel (a): Probability of being at a drought severity class D0,...,D4 for May 1976. Panel (b): Most likely drought severity class based on the ensemble simulations. Classification according to the US Drought Monitor (<http://droughtmonitor.unl.edu>).

The parametric uncertainty of the SMI also has a strong influence on drought severity classes commonly used for monitoring purposes. Panel (a) of Figure 3.9 depicts the probability of finding a cell, at a given point in time, under one of the five drought severity classes used by the United States Drought Monitor (<http://droughtmonitor.unl.edu>). These classes denote abnormal (D0), moderate (D1), severe (D2), extreme (D3), and exceptional (D4) dry conditions, which correspond to: $0.2 < \text{SMI} \leq 0.3$, $0.1 < \text{SMI} \leq 0.2$, $0.05 < \text{SMI} \leq 0.1$, $0.02 < \text{SMI} \leq 0.05$, and $\text{SMI} \leq 0.02$, respectively. This figure shows also that there are areas, in

which, no unique drought class can be assigned due to parametric uncertainty. A possibility to assign a unique class to a cell is to choose a class with the largest probability, as shown in the panel (b) of Figure 3.9 for May 1976.

3.5.6 Identification of Major Drought Events based on Mean Duration, Mean Areal Extent and Total Magnitude

Major drought events were found in this study using the technique described in section 3.4.3. These benchmark events are required for the future analysis of possible consequences of climate change on agricultural droughts. The drought clustering algorithm was applied to every ensemble realization to find the spatio-temporal evolution of all drought events during the reconstruction period from 1951-2010. For every event, drought characteristics such as mean duration (D), total magnitude (M), and mean areal extent (A), among others, were evaluated using the procedure illustrated in section 3.4.4. The ensemble average of these characteristics, i.e. \hat{D} , \hat{M} , and \hat{A} are depicted in Figure 3.10. The corresponding uncertainty of these characteristics is presented in Table 3.1.

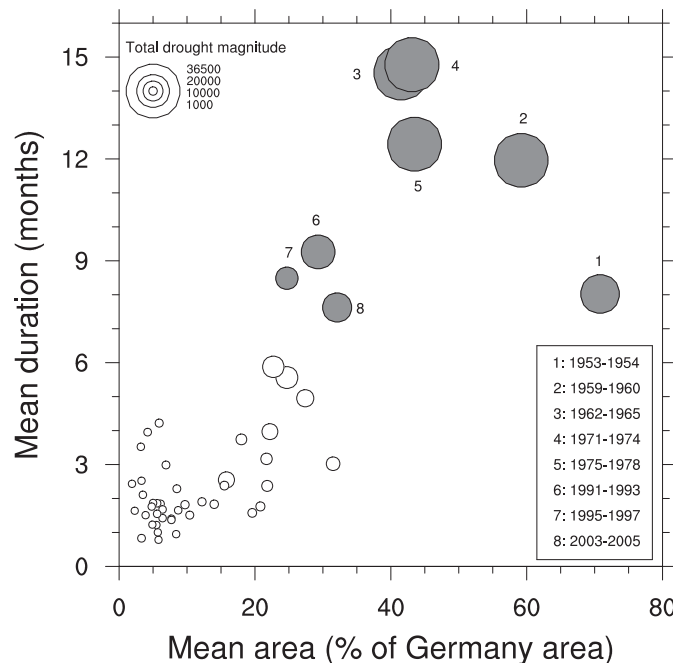


Figure 3.10: Area under drought, duration, and magnitude of the eight largest events in Germany since 1950 based on the ensemble $\langle \text{SMI} \rangle$.

The eight largest drought events identified during the last 60 years in Germany are the following periods: 1962-1965, 1971-1974, 1975-1978, 1959-1960, 1953-1954, 1991-1993, 2003-2005, and 1995-1997. It is worth noting that the event from 2003-2005, appears in this overall ranking in the 7th position. Vidal et al. (2010) also

3. Soil Moisture Drought Analysis in Germany

noticed this fact and concluded that 2003 hardly appears as a benchmark event in France. This is a rather controversial conclusion because in this year the highest temperatures during the last 500 years were recorded (Luterbacher et al., 2004). In Germany alone, great losses in the agricultural sector (COPA-COGECA, 2003) were reported. A likely explanation for this paradox is provided in section 3.5.7.

Table 3.1: Uncertainty of characteristics of major drought events in Germany since 1950. Uncertainty of the characteristics and mean \pm standard deviation.

Period	Duration [month]	Area [%]	Magnitude [% area \times month $\times 10^3$]
1953-1954	8.0 ± 0.2	70.8 ± 3.0	24.6 ± 1.0
1959-1960	12.0 ± 0.2	59.2 ± 2.3	36.3 ± 0.7
1962-1965	14.5 ± 0.9	41.5 ± 1.5	36.8 ± 2.0
1971-1974	14.8 ± 4.6	43.1 ± 5.0	36.7 ± 12.9
1975-1978	12.4 ± 0.8	43.5 ± 4.9	36.5 ± 1.9
1988-1991	5.9 ± 0.2	22.7 ± 2.0	11.1 ± 1.1
1991-1993	9.3 ± 1.5	29.3 ± 4.2	20.7 ± 3.6
1995-1997	8.5 ± 2.3	24.7 ± 6.7	11.8 ± 3.2
2003-2005	7.6 ± 0.5	32.1 ± 4.5	17.1 ± 1.6
2005-2007	5.6 ± 1.0	24.7 ± 3.4	11.5 ± 2.2

The three drought characteristics D , M , and A depicted in Figure 3.10, are highly correlated with each other. The Pearson correlation coefficient between D and M , is the highest, and equal to 0.97, whereas those between (D and A) and (M and A) are 0.80 and 0.87, respectively. This indicates that this triplet has low dimensionality. In fact, the first eigenvector of the correlation matrix of this triplet alone explains 92% of the total variance.

Using the k -means cluster analysis, three main groups of drought events were distinguished, 1) events with a large areal extent and duration, i.e. events 1962-1965, 1971-1974, 1975-1978, and 1959-1960; 2) events with the largest areal extent and moderate duration, i.e. 1953-1954; and 3) events with moderate areal extent and duration, i.e. 1991-1993, 2003-2005, and 1995-1997. Based on the ensemble SMI mean ($\overline{\text{SMI}}$), the event from 1971-1974 exhibited the longest duration, and the event from 1953-1954 covered the largest area. The events from 1962-1965 and 1971-1974 reached the two largest magnitudes.

The absolute ranking of these extreme drought events is rather difficult due to the parameter uncertainty as illustrated in Table 3.2. This table presents an estimate of the probability to order every event into the eight top ranks using a linear, equal-weighted, normalized indicator composed of D and A , as an example. The results presented in this table indicate that the maximum probability of finding

Table 3.2: Probability of finding a drought event in any of the top eight ranks. Here, only the eight largest events in Germany since 1950 were selected. The sum of the likelihood is not necessarily one due to the truncation of the table up to only the eighth rank. Values in bold represent the largest likelihood based on the ensemble simulations.

Event	Ranking likelihood							
	1	2	3	4	5	6	7	8
1953-1954		0.04	0.31	0.56	0.09			
1959-1960	0.34	0.51	0.15					
1962-1965		0.43	0.48	0.08	0.01			
1971-1974	0.67				0.03	0.19	0.10	0.01
1975-1978		0.02	0.06	0.36	0.56			
1991-1993						0.59	0.09	0.08
1995-1997						0.07	0.53	0.29
2003-2005					0.03	0.10	0.23	0.59

an event in one of the top ranks is not greater than 0.67. The ranking of a given event spans at least over three categories. Low ranking events tend to have a much larger ranking spread than the top ones, though.

The size of the ensemble also played a very important role to estimate the probability of finding an event in a given rank ($1 - \alpha$), where α denotes the false positive rate. Figure 3.11, for example, shows the probability of not identifying the event from 1971-1974 as the largest since 1951. This figure clearly shows that the variance of the false positive rate is strongly dependent on the ensemble size. These results were obtained by bootstrapping the 200 ensemble simulations without replacement and limiting the number of realizations to 1000 for a given sample size. This figure showed also that the first two moments of α tend to stabilize with ensemble sizes larger than 50. Consequently, it is safe to conclude that small ensemble sizes would lead to misleading results. An ensemble with 200 members, as realized in this study would lead to safer results. These Monte Carlo realizations clearly highlighted the role of parametric uncertainty in identifying the benchmark drought events which should be handled carefully.

The spatial distribution of severity (S_d) based on $\overline{\text{SMI}}$ at the peak of the eight largest drought events is shown in Figure 3.12. It can be observed from this figure that each event has its own peculiarities with respect to the spatial distribution of the affected areas. The drought event during December 1954 has the largest areal coverage, with 93.5% of the German territory under water stress, whereas the event during April 1996 had the lowest coverage with 46.5%. The latter drought event at its peak was particularly concentrated on the north-west part of Germany.

3. Soil Moisture Drought Analysis in Germany

The event of 1976, with its peak in August, had spread over whole Germany with an exception of the Alpine Foreland. The latter areas endured the highest severity during August 2003.

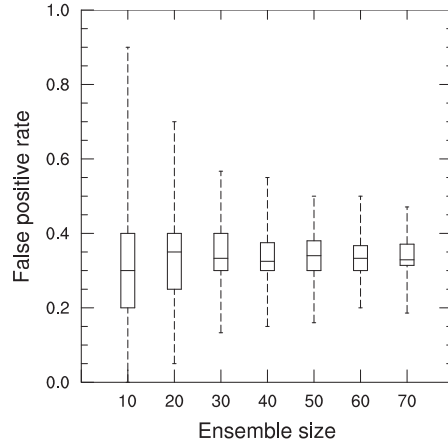


Figure 3.11: Sensitivity of the false positive rate (α) to ensemble size. In this example, α denotes the probability of rejecting the null hypothesis that the event from 1971-1974 ranks 1st among all drought events from 1950 to 2010. The size of the bootstrapping realizations was 1000.

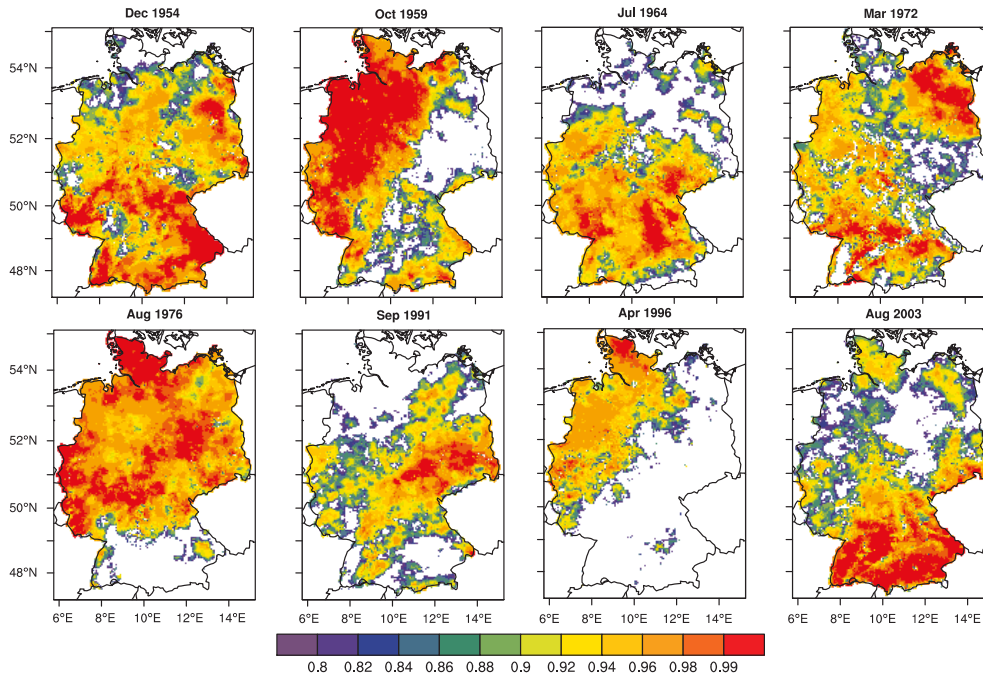


Figure 3.12: Severity at the peak of the eight largest drought events from 1951-01-01 to 2010-12-31 based on the ensemble mean SMI.

3.5.7 Uncertainty of Large Events Occurring in Summer and Winter

As mentioned before, the ranking of drought events based on ensemble characteristics (D , M , and A) does not allow the identification of their impact at a given point in time from their onset, nor to differentiate them according to their level of incidence in a particular season. The drought intensity proposed in Eq. 3.6 enables estimating the transient evolution of a drought event from its onset, and by so doing, it allows quantifying how fast a drought event covered a given area and by what magnitude. Panel (a) in Figure 3.13 shows the results of plotting drought intensity versus duration from the onset (d) of a given event for the ten largest events since 1950. Panel (b) in the same figure depicts the results obtained by ranking the drought intensities of all events at various durations from their onsets (e.g. 3, 6, ... months). The classification of an event into summer or winter was estimated with the procedure illustrated in section 3.4.3 (Eq. 3.6). The ensemble SMI mean (i.e. $\overline{\text{SMI}}$) was used instead of individual realizations for both analyses because the former is an unbiased estimate of the SMI, and thus leads to a robust estimate of the evolution of the drought intensity.

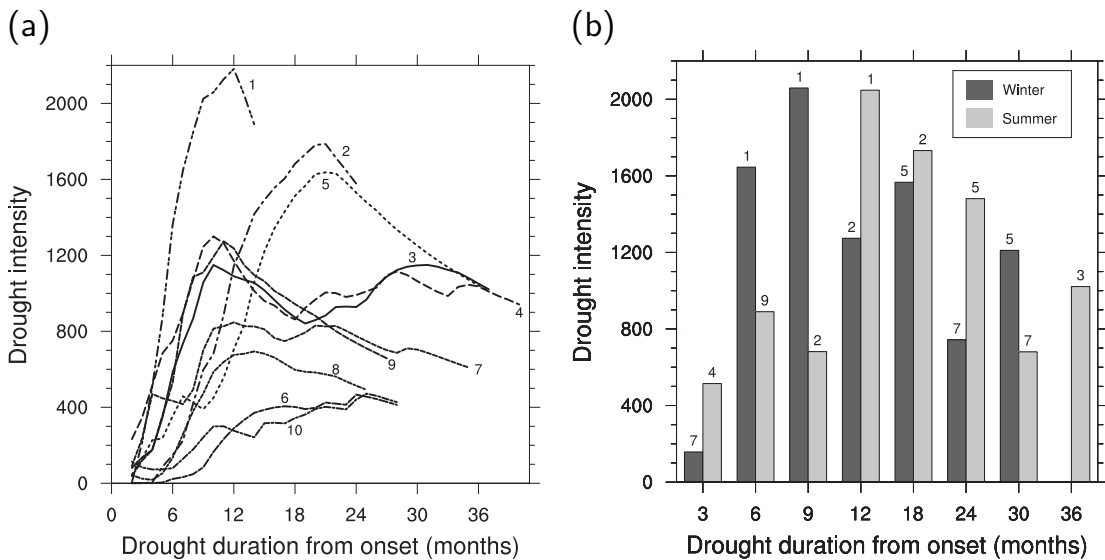


Figure 3.13: Panel (a): Drought intensity evolution for the 10 largest drought events since 1950. Panel (b): Major drought events for a given duration and season of occurrence. The numbers denote the following events: 1: 1953-1954, 2: 1959-1960, 3: 1962-1965, 4: 1971-1974, 5: 1975-1978, 6: 1988-1991, 7: 1991-1993, 8: 1995-1997, 9: 2003-2005, 10: 2005-2007.

Based on the results described above and shown in Figure 3.13, it was found that at 3 month duration, summer events have much larger drought intensity than the

corresponding ones in winter. At 6 and 9 months duration, the opposite happens. The events with more than a 9 month duration mostly reach their higher intensities during summer as compared to winter ones. However, droughts having a duration of 30 months or more are more intense during winter months. The event 1953-1954 not only exhibits the largest intensities at 6 and 9 month durations during winter months (Nov-Apr), but also the largest intensity in summer at 12 months duration. The event 2003-2005 is, according to these results, the summer event with the largest intensity at 6 months duration. Among the 10 largest drought events in Germany during last 60 years, the 1953-1954 event had the largest intensity peaking within a relatively short period of time (less than 12 months). This event, however, lasted for only one and a half years. Four drought events, namely, 1962-1965, 1971-1974, 1975-1978, and 1991-1993, spanned over the period of more than 30 months (i.e. two and a half years). According to this analysis, the decade of 1970 could be regarded as the most severe drought period in Germany. The drought events 1962-1965 and 1971-1974 clearly exhibited more than one peak over their whole life span. The analysis also indicated that most of the historical drought events in Germany have their peaks during 6 to 12 months of duration.

The empirical bivariate density function between the average drought area (A) and the total magnitude (M) was constructed to analyze the uncertainty in overall drought characteristics (D , M , and A) based on the ensemble realizations. The large number of model runs also allowed to assess the uncertainty in time evolution of these characteristics. The four most intense drought events with 6 months and at least 30 months duration after its onset were selected to illustrate this procedure, namely: the events 1953-1954 and 2003-2005 for shorter duration, and the events 1975-1978 and 1962-1965 for longer duration, respectively (Figure 3.14). It is worth noting that the events 1953-1954 and 2003-2005 are classified as winter and summer events, respectively, at 6 months duration (Figure 3.13 (b)). Likewise, the events 1975-1978 and 1962-1965 peaked in winter and summer, respectively. Droughts that are peaking within a relatively short time (up to 6 months) from their onset are quite relevant because they have large repercussion on socio-economic activities.

Based on the ensemble results, the density function for each event was estimated independently with a bivariate Gaussian kernel smoother algorithm. The estimation of the bandwidths in both directions was carried out in a similar way as presented in section 3.4.2. The results of this analysis are depicted in the top panels (a) to (d) of Figure 3.14, which clearly supports the research hypothesis that the parametric uncertainty of soil moisture has a strong implication for drought characterization. Most events exhibit multimodal behavior which is the combined result of the uncertainty of the model parametrization and drought identification (e.g. clustering, threshold).

Events having shorter durations and peaking in winter (1953-1954) appear to be more certain than those peaking in summer (2003-2005) as can be noted by the larger spread of the respective distribution (Figure 3.14 (a) and (b)). Consequently,

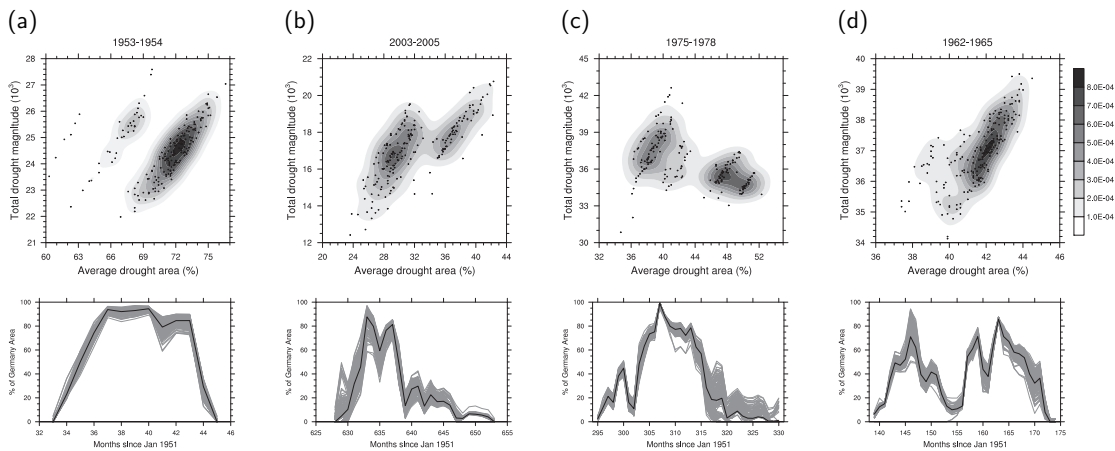


Figure 3.14: Top: Bivariate density functions between drought area and total drought magnitude of four major events. Panels (a) and (b) depict the most intense drought events with 6 months duration after its onset in winter and summer, respectively. Panels (c) and (d) correspond to the most intense drought events having a drought duration of at least 30 months, in winter and summer, respectively. Bottom: Predictive uncertainty and evolution of the area under drought for the selected events.

the probability density values for the summer event are lower than those of the winter event. However, at longer durations no conclusive comparison could be drawn from this analysis because longer events experience various seasons over many years. The time evolution of the area under drought $A(t)$ for each events, as depicted in bottom panels of Figure 3.14, also supports the assertion that a single model realization would lead, very likely to a high rate of false alarms for drought monitoring.

3.5.8 Uncertainty of the Severity-Area-Duration Curves

SAD curves obtained with the ensemble SMI mean ($\overline{\text{SMI}}$) for the eight largest drought events in Germany at duration 3, 6, 9, and 12 months are depicted in panel (a-d) of Figure 3.15. From this analysis, the event from 1975-1978 appears to be the most severe and extensive event at durations ranging from 3 to 9 months. Based on this measure, the 2003-2005 event, however, hardly appears as a benchmark event at longer durations and area coverage. The event from 1953-1954 is quite severe at 3 and 6 months, but not at longer durations. The apparent contradiction of these results, can be clarified with the individual evolution graphs presented in Figure 3.13.

SAD curves have often been used to rank drought events (Andreadis et al., 2005;

3. Soil Moisture Drought Analysis in Germany

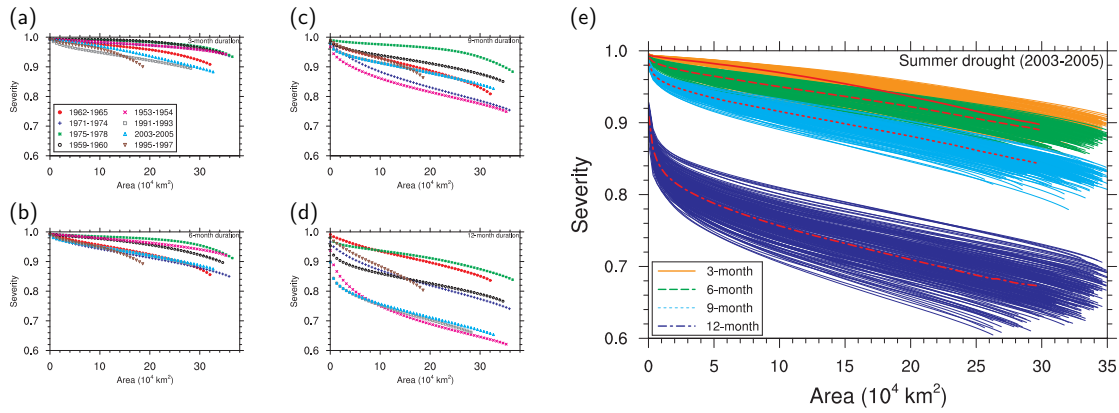


Figure 3.15: Panels (a) to (d): Ensemble averaged Severity-Area-Duration (SAD) curves of eight major drought events for 3, 6, 9, and 12 months duration since 1950 over Germany. Panel (e) depicts the predictive uncertainty of the SAD curves obtained for the event 2003-2005. In this panel, lines in red denote the ensemble mean.

Sheffield et al., 2009). Due to parametric uncertainty, however, they exhibit large variability as shown in panel (e) of Figure 3.15. This, again, corroborate our hypothesis that a single model run would lead to unsatisfactory conclusions and event ranking. These results indicate that the SAD variability increases as the area under drought and duration increase. The variability of the SAD curve with a 12-month duration is almost twice as much as that for 3 months. The variability of SAD curves for summer events is higher than that estimated for winter at any duration.

3.5.9 Drought Persistence and Trends of the Soil Moisture Index

Characterizing areas prone to remain under severe drought conditions when they are already suffering one constitute a relevant piece of information for water resources planning. The level of persistence of the severe drought events can be quantified with a two-state Markov chain with two states: $SMI \leq 0.2$ and $0.2 < SMI \leq 1$. The persistence of severe drought can be estimated for each ensemble member as the probability $\pi_{00} = \Pr(SMI(t+1) \leq 0.2 | SMI(t) \leq 0.2)$, $\forall t$. The ensemble mean of π_{00} is depicted in panel (a) of Figure 3.16 for the whole of Germany. This figure indicates that most of the Northeast German Plain comprising the area of the Elbe, Saale, and Mulde river basins, as well as large extensions along the Main and Rhine rivers, exhibit drought persistence greater than 0.8. The Northwest German Plain, comprising the Ems and Weser river basins, tend to have lower drought persistence than the eastern part of Germany, with an average value of π_{00} less than 0.7. The Alpine Foreland located within the Danube

basin and areas in and around the Black Forest, on the contrary, exhibit the largest variability in drought persistence within Germany ranging from less than 0.4 to 0.8. It is worth noting that those areas exhibiting large drought persistence have been also classified as areas with medium to high agricultural suitability according to a recent study conducted by UBA-PIK (www.pik.de). These regions comprise large plains within the Saale river basin around the cities of Halle and Magdeburg, and flood plains of the Rhine river on the western side of the Black Forest.

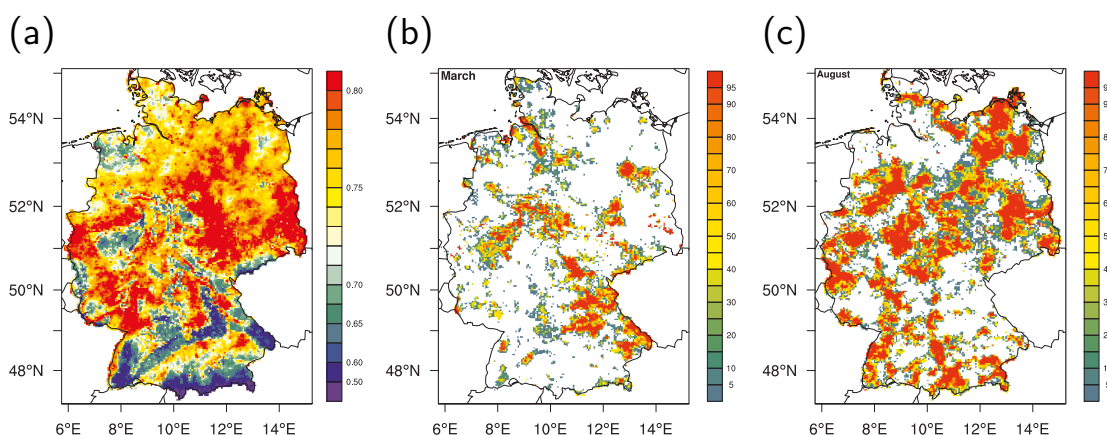


Figure 3.16: Persistence map of the SMI (a), and regions with positive (b) and negative (c) SMI trends (5% significance). Panels (b) and (c) depict the percentage of ensemble members indicating a significant trend.

Mann-Kendall tests on monthly $\overline{\text{SMI}}$ indicate that there are large extensions of the German territory showing positive trends (i.e. getting wetter) during winter months but negative trends in summer months, at 5% significance level. The largest areas exhibiting significant trends were detected in March and August as depicted in Figure 3.16, panels (b) and (c), respectively. It is worth noting that positive SMI trends tend to occur in areas with low persistence and negative trends in areas with high persistence. These trends are, in turn, related, with observed trends in temperature and precipitation. Further details on this aspect are beyond the scope of this paper.

3.6 Summary and Conclusions

In this study we have presented a method to derive a soil moisture index based on a process based hydrological model. This model uses a multiscale parametrization method that goes beyond standard calibration approaches. Great emphasis has been put on testing this model in all major river basins in Germany, especially with respect to the transferability of global parameters across locations and scales. Ongoing tests with Fluxnet and cosmic ray neutron probe data have also been

presented. Using this model a consistent ensemble of high resolution daily soil moisture fields for Germany since 1950 at a spatial resolution of 4×4 km were obtained.

Based on this soil moisture reconstruction, a soil moisture index (SMI) representing the corresponding monthly quantile was estimated with the kernel density approach. The derived SMI exhibits high correspondence with total grain yield of Germany and allows to identify major drought events in Germany, that have also been identified using other techniques (e.g. tree rings) and reported in the literature (Büntgen et al., 2010). This approach has advantages over standard empirical approaches or those obtained from satellite derived products, which are too coarse to account for soil moisture at high spatio-temporal resolutions and quite uncertain because the algorithms used to infer soil moisture do not take into account the water balance of large river basins. Consequently, the proposed technique has a large potential to be used as a monitoring tool in the future. More research is, however, needed to evaluate the SMI against times series of annual crop yield at regional scale. Further research is also required to identify potential driving mechanisms, the feedback effects, and the spatio-temporal correlations of soil moisture with other hydrological state variables such a snow depth, and climatic variables.

The effects of other sources of uncertainty stemming from model structure and quality of meteorological data on the soil moisture index should be further investigated. Potential benefits of using ensembles of multi-model, multi-parameter soil moisture simulations should be also carried out. Both issues, however are out of the scope of this study.

Based on the results of this study, the following conclusions were drawn. 1) The main source of parametric uncertainty of the soil moisture index is related with global model parameters. This uncertainty is seasonally and regionally varying. This corroborates, findings of other researchers who have advocated for multi-model ensembles to account for model uncertainty. In summary, one single model run is not enough for estimating benchmark events. 2) The uncertainty of overall statistics used for estimating drought events are highly sensitive to this kind of uncertainty. This sensitivity is the result of non-linear relations and branching effects caused by the clustering method. 3) Events peaking during summer with at most 6 months duration tend to exhibit a much large uncertainty than those peaking during winter. 4) The SMI is not a stationary variable. Many regions in Germany exhibited significant trends during the study period. Potential triggering mechanisms and drivers behind these trends might be the observed changes of precipitation and temperature, as well as, other feedback mechanisms. A detailed trend attribution, however, is out of the scope of this study. 5) The identification of benchmark drought events should be based on combined criteria such as SAD or intensity duration curves. Robust estimates can only be made with an ensemble SMI due to the uncertainty mentioned before.

Chapter 4

Calibration of a Hydrological Model using Patterns of Satellite Derived Land Surface Temperature

This chapter is largely based on an unpublished manuscript, which will be submitted to an ISI listed Journal:

Zink, M., Mai, J., Cuntz, M., and Samaniego, L.: Calibration of a Hydrological Model using Patterns of Satellite Derived Land Surface Temperature

4.1 Abstract

Hydrologic models are usually calibrated with observed river discharge at the catchment outlet. Discharge is only observed at a few points worldwide and further represent an integral response of the entire catchment. This approach does not consider the spatio-temporal variability of hydrologic fluxes and state variables, like evapotranspiration. Satellite data in contrast include these variabilities, are broadly available, and hence may help to better constrain model parameters. Within this study we assess the predictive skill of satellite derived land surface temperature (T_s) regarding river runoff (Q). We further investigate the effect on the parametric uncertainty if the model is jointly calibrated with Q and T_s . A diagnostic land surface temperature module was developed and implemented because the herein used hydrologic model mHM was not capable for estimating T_s . To focus the parameter optimization on spatial patterns of T_s we developed a bias insensitive pattern matching criterion. The proposed method was extensively tested in six distinct German river basins and cross validated in 222 additional catchments. The average Nash Sutcliffe Efficiency (NSE) is 0.51 and 0.4 for the six and 222 catchments, respectively, if the model is calibrated only with T_s . We conclude that land surface temperature has a predictive skill regarding discharge, which could be meaningful for calibrating a hydrologic model in ungauged locations. The combined calibration with Q and T_s reduced the root mean squared error in predicted evapotranspiration by 5% compared to flux tower observations but reduced the skill, i.e., NSE, of river runoff predictions by 6% on average for the six basins. Our results show that patterns of T_s do better constrain model parameters when considered in a calibration next to Q , but also that T_s alone has a predictive skill regarding river discharge.

4.2 Introduction

Hydrologic models are usually calibrated against runoff at the catchment outlet and thus only consider an integral signal of the entire catchment. This procedure ensures the fulfillment of the mass balance but has no control on the spatial distribution of hydrologic fluxes and states, like evapotranspiration or soil moisture, within the catchment. However, hydrologic applications like drought and flood monitoring or forecasting rely on spatially representative simulations of evapotranspiration and soil moisture. A calibration with river flow leads to sufficient estimations in discharge, but other fluxes such as evapotranspiration, are lacking accuracy (Rakovec et al., 2016; Zink et al.). To overcome these deficiencies the calibration of a hydrologic model with spatially distributed satellite observations is investigated within this study.

Spatially distributed ground observations of land surface fluxes and states do not

yet exist on the regional scale or larger. Thus, satellite data remain the only resource for spatially explicit observations of the earth surface. From the perspective of a hydrologic modeler satellite soil moisture or evapotranspiration observations are preferable for constraining hydrologic models because these variables are already model inherent. These data, however, have several disadvantages. First, the estimation of satellite soil moisture and evapotranspiration is based on modeling approaches (e.g., Bastiaanssen et al., 1998; Mu et al., 2007; Wagner et al., 2007), which convert the satellite signal to hydrologic variables. These models are sensitive to the parameterization of the soil and vegetation. Thus, constraining soil and vegetation parameters of hydrologic models is dependent on the modeling scheme and parameterization of these products. Second, these satellite retrievals still underlie big uncertainties and inaccuracies (Sheffield and Wood, 2011). And third, the spatio-temporal resolution of satellite soil moisture and evapotranspiration is coarse ($\geq 25 \text{ km}$, $\geq 1 \text{ mon}$) compared to the resolution of 4 km and 1 d of the hydrologic model used herein.

An alternative source of data is land surface temperature, which is based on satellite based thermal-infrared (TIR) observations. TIR is directly interlinked with T_s through the radiative temperature equation (Li et al., 2013). This equation is only dependent on corrections for atmospheric and emissivity effects (Li et al., 2013), but not on soil or vegetation characterizations. In particular, the temperature and water vapor profile of the atmosphere, the cloud cover and the land surface emissivity have to be known to estimate T_s . Therefore, we consider T_s as a more certain source of satellite information compared to soil moisture or evapotranspiration retrievals.

This study is based on land surface temperature (T_s) which is defined as the temperature of the interface between the Earth's surface and its atmosphere (Niçlòs et al., 2011). We will use it herein to improve the spatial representativeness of evapotranspiration. T_s is directly connected to evapotranspiration via the energy balance. Additionally, Lakshmi (2000), for example, showed a close relationship of soil moisture and land surface temperature. By calibrating a land surface model he improved soil moisture estimations. Thus, land surface temperature is a promising variable for improving the spatial representation of evapotranspiration or soil moisture in hydrologic models.

McCabe et al. (2005) observed a change in the spatial distribution of evapotranspiration when calibrating a land surface model with land surface temperature T_s . Boni et al. (2001) and Reichle et al. (2010) assimilated land surface temperature using a variational assimilation scheme and Ensemble Kalman Filtering, respectively. Both studies employed land surface models which are already implicitly solving the energy balance and thus already depend on T_s . Boni et al. (2001) concluded that surface control on evaporation is feasible whereas Reichle et al. (2010) did not observe any effect on surface energy fluxes.

A calibration of a hydrologic model with land surface temperature is proposed by

Crow et al. (2003). They found that consideration of spatially averaged evapotranspiration, next to discharge, improves monthly evapotranspiration predictions up to 20%. Similar efforts are done by Corbari et al. (2010, 2015), and Silvestro et al. (2013, 2014). All of them found improvements in evapotranspiration estimates if land surface temperature was considered when calibrating their models.

All of these studies have in common that they only considered selected model parameters in the calibration process and fixed the remaining parameters with prior knowledge (transfer from remote locations or expert knowledge). The models in use did already explicitly solve the energy balance and thus inherently depend on land surface temperature. Additionally, these studies did not explicitly focus on the spatial distribution of T_s . They either calibrated the model using catchment averaged T_s (Silvestro et al., 2013, 2014) or compared observations and simulations using standard error measures like bias or root mean squared error (Corbari et al., 2010, 2015). Contrarily, Reichle et al. (2010); Stisen et al. (2011), and Koch et al. (2015) suggested to use bias insensitive measures which only consider the spatial patterns of land surface temperature. This is due to the fact that T_s is known to be biased compared to ground observations (Trigo et al., 2008; Reichle et al., 2010; Niclòs et al., 2011; Li et al., 2013).

The herein used mesoscale Hydrologic Model (mHM) was not capable of estimating land surface temperature. We developed a diagnostic land surface temperature model which can be coupled to any hydrologic model. Further, we developed a bias insensitive, non parametric pattern matching criterion for calibration purposes. The mHM model, augmented by the diagnostic T_s module, is calibrated using this pattern matching criterion, first using land surface temperature only, and second with discharge (Q) and T_s simultaneously.

First, with the calibration with T_s alone we want to verify, if land surface temperature has a predictive skill regarding discharge. Therefore, we calibrate the hydrologic model mHM in six distinct German river basins and evaluate the model performance regarding discharge. The estimated parameter sets are transferred to 222 catchments, which have not been used during model calibration, to further investigate the predictive skill of the estimated parameter sets regarding discharge.

Second, we hypothesize that the parametric uncertainty of the hydrologic model mHM will decrease when Q and T_s are calibrated simultaneously. Especially for parameters connected to surface processes, as e.g., evapotranspiration, will be constrained better. The parametric uncertainty is assessed by conducting 20 independent model calibrations and comparing the resulting parameter ranges with the initial ranges for each parameter.

Third, we postulate that simultaneous calibration of mHM with Q and T_s would impact the spatial distribution of evapotranspiration and improve evapotranspiration estimations when compared to eddy flux measurements.

4.3 Study Domain and Data

4.3.1 Meteorological Data

The forcings needed for the hydrologic model are provided by the German Meteorological Service (DWD). The approximately 5000 precipitation and 2000 temperature stations covering Germany were interpolated using external drift kriging (Ahmed and De Marsily, 1987). A digital elevation model was used as external drift. The potential evapotranspiration is estimated based on the Hargreaves-Samani equation (Hargreaves and Samani, 1985) using the interpolated fields of minimum, maximum and average daily air temperature. The precipitation, average temperature and potential evapotranspiration are the main forcings for solving the water balance within the hydrologic model mHM. The spatial resolution is $4 \times 4 \text{ km}^2$ since we consider this as the lowest resolution supported by the station input data.

The hydrologic model mHM augmented by a land surface temperature module requires additional data for calibration. In the first place observed land surface temperature is needed, but additionally the net radiation is required to estimate land surface temperature within the new module. Unfortunately, land surface temperature and radiation observations are not available or too sparse as there are only 57 radiation measurement stations within Germany. Thus, additional data sources have been reviewed. Eligible data sources are required to be of a similar spatial resolution as the above mentioned meteorological forcings, and to have at least a daily temporal resolution to cope with data gaps, which, e.g., arise from cloudiness. Since reanalysis data are typically coarser than 0.25° , their spatial resolutions are not appropriate. Another source of data are satellite retrievals. Whereas, the spatial resolution (e.g., 1 km) of polar orbiting satellites, like TERRA, is high and equidistant, its temporal resolutions are coarse (one to two overpasses per day). Geostationary satellites (e.g., Meteosat), however, have a high temporal (≥ 15 minutes) but lower spatial resolution which decreases with increasing distance from the satellite. For Germany, data of Meteosat Second Generation (MSG) have an average spatial resolution of $3.5 \times 6.5 \text{ km}^2$ and a temporal resolution of 15 or 30 minutes depending on the data product.

Thus, we decided to use data from MSG which have been processed by the Land Surface Analysis - Satellite Application Facility (LSA-SAF). LSA-SAF provides ready to use interpretations for land surface temperature and radiation components from MSG data. Net radiation can not be inferred from satellite observations directly. Therefore, the net radiation is estimated based on downwelling short- and longwave radiation, land surface temperature, emissivity, and albedo products from LSA-SAF (see section 4.4.2, Equations 4.5a-4.5c).

The shortwave incoming radiation data of LSA-SAF have been evaluated using

data of 32 available station observations in 2009 provided by the German Meteorological Service (Deutscher Wetterdienst (DWD), 2011). With an average Pearson correlation coefficient of 0.93 (standard deviation=0.04) and a relative bias of 5% (standard deviation=2%) the satellite shortwave radiation compares well to ground observations. The satellite retrieved land surface temperature is validated at two eddy covariance stations, i.e., stations E2 and E4 (Figure 4.1), where radiometric temperature is measured (Kutsch et al., 2008; Rebmann et al., 2010). This comparison revealed a bias of the satellite retrieval of about 2.7 K. This compares well to literature which reports a bias of 2 K to 3 K for satellite retrieved land surface temperature (Trigo et al., 2008; Reichle et al., 2010; Niclòs et al., 2011; Li et al., 2013).

4.3.2 Study Domain and Land Surface Properties

The broader scope of the study domain is the territory of Germany. Intense analyses will be presented for the six inner German river basins presented in Figure 4.1. These are the largest inner German catchments and differ in size, hydrologic behavior and climatic conditions. They range from a flat, agricultural dominated, maritime influenced catchment in Northern Germany (i.e., Ems) to a snow influenced, more continental catchment with distinct slopes in the South (i.e., Neckar). A detailed description of the catchments can be found in Zink et al..

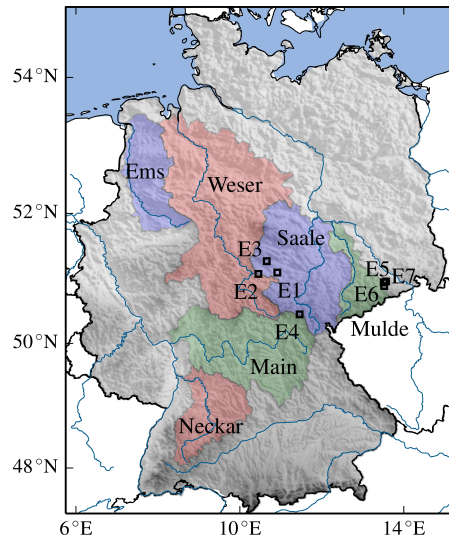


Figure 4.1: The main catchments used for parameter inference and numerical experiments. The six major inner German river basins span over a climate gradient ranging from maritime influence in the Ems to continental climate in Main and Neckar. The points E1 to E7 depict the location of eddy flux tower observations, which have been used for evaluating the simulated evapotranspiration.

The land surface is characterized by a digital elevation model provided by the Federal Agency for Cartography and Geodesy (BKG) (2010), a soil and hydrogeological map offered by the Federal Institute for Geosciences and Natural Resources (BGR) (1998, 2009), and land cover information from the European Environmental Agency (EEA) (2009). This data are discretized to a spatial resolution of $100 \times 100 \text{ m}^2$. The Global Runoff Data Centre (GRDC) (2011) and the European Water Archive (EWA) (2011) provided the discharge data.

4.4 Methodology

4.4.1 The mesoscale Hydrologic Model mHM

The computational experiments of this study were conducted employing the mesoscale Hydrologic Model mHM (Samaniego et al., 2010; Kumar et al., 2013b). It is a process-based and spatially distributed model which was developed for the estimation of hydrologic fluxes and state variables on the land surface. These states and fluxes are derived by closing the water balance on every grid cell. Within a grid cell the governing processes are conceptualized as discrete reservoir models for the different compartments of the hydrologic cycle, e.g., interception, snow accumulation, soil moisture, and evapotranspiration among others. The estimation of hydrologic fluxes and states is highly dependent on the quality of the evapotranspiration estimate, since it is the second most important flux in the water balance besides precipitation.

The evapotranspiration within mHM is estimated by scaling the available water within the interception, surface water, and soil water reservoir sequentially with a potential evapotranspiration (PET). Thus, PET is reduced consecutively by evapotranspiration from the beforehand mentioned reservoirs, respectively. Therein, interception and surface water retention are minor sources of evaporative water, whereas the water of the soil reservoir is the main source. Within the soil the amount of evaporative water is determined by scaling the remainder of PET with the available water within the different soil layers and a root fraction parameter sequentially from the top to the bottom layer. The root fraction parameter varies for the three land cover classes within the model (urban, mixed, and forest). Because the evapotranspiration estimation is highly dependent on the conceptualization of the soil water processes within land surface models, their representation within mHM will be described in the following.

The number and depth of the soil layers needed by the model are defined externally whereas the depth of the deepest soil layer is derived by mHM from the soil map and thus varies between different grid cells. For this study, three soil layers have been used. The first layer ends in 5 cm, the second in 25 cm below the surface and the third is the soil map dependent layer.

Besides soil textural properties (bulk density, sand, and clay content) the soil water content depends on the organic matter of the soil layers. The organic matter is derived using the formulation of Rawls (1983). The evapotranspiration of the single soil layers is subsequently estimated as a function of (a) potential evapotranspiration, (b) soil water content, (c) soil hydraulic properties (permanent wilting point, field capacity, saturated soil moisture content) and (d) the fraction of roots. This functional relationship contains several model parameters.

These parameters are derived by employing the Multiscale Parameter Regionalization (MPR) technique (Samaniego et al., 2010; Kumar et al., 2013b). In general, this parameter estimation approach is based on transfer functions which are dependent on transfer function parameters. This transfer function parameters are also called super- or *global parameters* (Pokhrel et al., 2008). They are space- and time-invariant and are the parameters which are adjusted during a calibration process.

In MPR the transfer functions (e.g., the pedotransfer functions for the estimation of soil parameters) are connected to the morphological input (e.g., soil textural properties) and thus lead to model parameters (e.g., porosity or soil hydraulic conductivity). In the example the *global parameters* are the coefficients of the pedotransfer functions. The model parameter estimation is performed on the resolution of the morphological input (e.g., $100 \times 100 \text{ m}^2$). They have to be upscaled to determine the model parameters on the hydrologic model resolution (e.g., $4 \times 4 \text{ km}^2$). The applied upscaling rules are different for the various model parameters (e.g., the geometric mean for the porosity and soil hydraulic conductivity).

Compared to other parameter estimation approaches, like hydrologic response units (Flügel, 1995), the advantages of MPR are (1) the ability to choose flexible model resolutions without the necessity to rescale the input, (2) the transferability of the *global parameters* across locations (Samaniego et al., 2013; Rakovec et al., 2016; Zink et al.), and (3) the transferability across scales (Kumar et al., 2013b,a) without recalibrating the model.

4.4.2 Development of a Land Surface Temperature Module

A goal of this study is to incorporate spatially distributed information into the hydrologic model mHM to improve the spatial representativeness of the hydrologic fluxes and states. Herein, we will focus on the evapotranspiration since it has a high impact on the water balance. Therefore, we considered satellite derived land surface temperature fields within mHM. The spatio-temporal distribution of land surface temperature is used to constrain mHM in addition to discharge.

Since the purpose of mHM is to solve the water balance equation, land surface temperature is not required to be estimated yet. By closing the water balance, evapotranspiration (E) is estimated. The energy balance is used to simulate land

surface temperature, since the evapotranspiration is the common variable of the energy and the water balance.

The following section will introduce a parsimonious module for estimating land surface temperature based on modeled evapotranspiration. This module is called land surface temperature module in the following. It can be coupled to any hydrologic model and will be adjoined with mHM.

On the one hand the evapotranspiration E [$mm\ d^{-1}$] is determined by closing the water balance

$$E = P - Q - \Delta S \quad (4.1)$$

with mHM. Where P is precipitation [$mm\ d^{-1}$], Q is river runoff [$mm\ d^{-1}$], and ΔS [$mm\ d^{-1}$] is the change in the storages, e.g., soil moisture. On the other hand the energy balance is defined as

$$R_n = LE + H + G + S \quad (4.2)$$

in which R_n denotes the net radiation [$W\ m^{-2}$], LE is the latent heat flux [$W\ m^{-2}$], H is the sensible heat flux [$W\ m^{-2}$], G is the soil heat flux [$W\ m^{-2}$] and S are the storage terms [$W\ m^{-2}$], e.g., photosynthetic or biomass heat storage. The latent heat flux LE is determined by converting the mass flux of evapotranspiration E estimated by mHM (Equation 4.1) to an energy flux. This conversion is calculated by

$$LE = \rho LE. \quad (4.3)$$

In which the L is the latent heat of vaporization [$kJ\ kg^{-1}$] and ρ is the density of water ($\rho = 1000\ kg\ m^{-3}$). The latent heat of vaporization L is approximated by $L = 2501 - 2.37T_a$ using the air temperature T_a in [$^{\circ}C$] (Dyck and Peschke, 1995).

The estimation of land surface temperature is performed using the temporal resolution of one day, because this is the temporal resolution of the meteorological input. For daily time steps it is assumed that the soil heat flux G and the storage terms S are negligible (Haverd et al., 2007). Therefore Equation 4.2 simplifies to

$$H = R_n - LE. \quad (4.4)$$

Because mHM is not estimating energy fluxes, the net radiation R_n has to be provided as an input to be able to estimate the sensible heat flux H . Since spatially comprehensive measurements of the net radiation are not available, an alternative source of data is required. One possible source are radiation products obtained

from satellite data. A straight satellite product for net radiation is not available. Therefore, it is determined by the single components of the radiation budget, which are derived from satellite measurements, as

$$R_n = Q_S^{(in)} - Q_S^{(out)} + Q_L^{(in)} - Q_L^{(out)} \quad (4.5a)$$

$$Q_S^{(out)} = \alpha Q_S^{(in)} \quad (4.5b)$$

$$Q_L^{(out)} = \epsilon \widehat{T}_s^4 \quad (4.5c)$$

where $Q_S^{(in)}$ and $Q_S^{(out)}$ are the incoming and outgoing short-wave radiation [$W m^{-2}$], respectively, and $Q_L^{(in)}$ and $Q_L^{(out)}$ are the incoming and outgoing long-wave radiation [$W m^{-2}$], respectively. The outgoing short-wave $Q_S^{(out)}$ radiation is estimated using Equation 4.5b, in which α is the albedo of the land surface [-]. The outgoing long-wave radiation $Q_L^{(out)}$ is approximated as emission of a gray body which can be calculated following the Stefan-Boltzmann law (Equation 4.5c). Therein, ϵ is the emissivity [-] and σ is the Stefan-Boltzmann constant ($\sigma = 5.67 \cdot 10^{-8} W m^{-2} K^{-4}$).

Thus, the estimation of the sensible heat flux H [$W m^{-2}$] (Equation 4.4) modifies to

$$H = (1 - \alpha)Q_S^{(in)} + Q_L^{(in)} - \epsilon\sigma\widehat{T}_s^4 - LE. \quad (4.6)$$

Further, the thermodynamical formulation of the sensible heat H is known by

$$H = \varrho_a c_p \frac{\widehat{T}_s - T_a}{r_a} \quad (4.7)$$

where T_a is the air temperature [K], \widehat{T}_s the model derived land surface temperature [K], r_a is the aerodynamic resistance [$s m^{-1}$], ϱ_a the density of air ($\varrho_a = 1.29 kg m^{-3}$) and c_p the specific heat capacity of air which has been assumed to be constant ($c_p = 1004 J kg^{-1} K$). Combining Equation 4.6 and 4.7 leads to a polynomial of forth degree in \widehat{T}_s

$$(1 - \alpha)Q_S^{(in)} + Q_L^{(in)} - LE + \frac{\varrho_a c_p}{r_a} T_a - \frac{\varrho_a c_p}{r_a} \widehat{T}_s - \epsilon\sigma\widehat{T}_s^4 = 0. \quad (4.8)$$

To sum up, \widehat{T}_s is the modeled variable of interest, $Q_S^{(in)}$, $Q_L^{(in)}$, α , and ϵ are satellite retrieved variables, ϱ_a , σ , and c_p are constants, T_a is measured air temperature which is an input for mHM, LE is derived by closing the water balance with mHM (Equations 4.1 and 4.3), and r_a is the aerodynamic resistance which is still unknown, but will be explained in the following.

4. Calibration using Patterns of Satellite Derived Land Surface Temperature

By solving Equation 4.8 four roots are obtained. The root which falls in the interval $[0 K, 500 K]$ is the feasible result for \widehat{T}_s . During all experiments it was found that only one of the four roots does fulfill this requirement.

Still there is one unknown variable, i.e., the aerodynamic resistance r_a in $[s m^{-1}]$, which is calculated using the equation of Allen et al. (1998):

$$r_a = \frac{\ln\left(\frac{z_m-d}{z_{0m}}\right) \ln\left(\frac{z_h-d}{z_{0h}}\right)}{k^2 u_z} \quad (4.9)$$

where z_h is the height of the humidity measurement $[m]$, d is the zero plane displacement height $[m]$, z_{0m} is the roughness length for momentum transfer $[m]$, z_{0h} is the roughness length for heat transfer $[m]$, k is the von Karman constant ($k = 0.41$), and u_z is the wind speed $[m s^{-1}]$ at the wind speed measurement height z_m in $[m]$. It is assumed that the measurement heights of wind speed and humidity are equal $z = z_m = z_h$.

The approximations of the three variables $d = \frac{2}{3}h_c$, $z_{0m} = 0.123h_c$, and $z_{0h} = 0.1z_{0m}$ are taken from Allen et al. (1998). The constants of d , z_{0m} and z_{0h} have been implemented as *global parameters* p_{48} , p_{49} , and p_{50} in the land surface temperature module, respectively. These parameters need to be calibrated whereas their ranges are chosen to be between $\pm 10\%$ of the values reported by Allen et al. (1998). Thus Equation 4.9 becomes

$$r_a = \frac{\ln\left(\frac{z-p_{48}h_c}{p_{49}h_c}\right) \ln\left(\frac{z-p_{48}h_c}{p_{49}p_{50}h_c}\right)}{k^2 u_z}. \quad (4.10)$$

This shows that besides the given height z and the measured windspeed u_z , r_a is dependent on the estimation of the parameters p_{48} , p_{49} , and p_{50} and the canopy height h_c .

Since no spatially comprehensive information about the canopy height h_c is available, the Multiscale Parameter Regionalization (MPR) technique has been employed to estimate h_c based on the land cover information. To account for the annual development of h_c the monthly evolution of the leaf area index (LAI) is taken into consideration. The functional relationship between canopy height and the LAI , i.e., for the mixed land cover class, is assumed to be

$$h_{c,mix}(i) = p_{47} \frac{LAI(i)}{\max_i LAI(i)}, \quad i = 1, \dots, 12. \quad (4.11)$$

in which $h_{c,mix}$ is the canopy height of the mixed land cover class $[m]$, $LAI(i)$ is the leaf area index $[m m^{-2}]$ for month i $[-]$ and p_{47} is the calibration parameter $[m]$ for

the estimation of the canopy height h_c for the mixed land cover class (*mix*). The mixed land cover class is a generalized class consisting of grasslands, agricultural areas and pastures.

Both other land cover classes (urban (*ur*) and forest (*for*)) are assumed to be constant in canopy height over the course of a year and do not depend on LAI

$$h_{c,for} = p_{45} \quad \text{and} \quad h_{c,ur} = p_{46} . \quad (4.12)$$

The estimation of the canopy height is conducted on the input resolution, i.e., $100 \times 100 \text{ m}^2$. For the upscaling to the model resolution, i.e., $4 \times 4 \text{ km}^2$, various upscaling operators have been tested and the arithmetic mean has proven to perform best.

To sum up, we have shown the development of a land surface temperature module which can be coupled to any environmental model. Satellite derived radiation components ($Q_S^{(in)}$ and $Q_L^{(in)}$), air temperature (T_a), wind speed (u_z), and modeled evapotranspiration (E) are used as input for the land surface temperature module. The necessary steps for estimating land surface temperature (\widehat{T}_s , Equation 4.8) are

1. The estimation of E as residual of the water balance (Equation 4.1) and
2. The calculation of \widehat{T}_s (Equation 4.8) based on the aerodynamic resistance (Equation 4.10).

To approximate the aerodynamic resistance r_a (Equation 4.10) the three *global parameters* p_{48} to p_{50} connected to the displacement height and the roughness lengths as well as the three *global parameters* p_{45} to p_{47} connected to the canopy height (Equation 4.11 and Equation 4.12) are necessary. An additional parameter p_{51} was introduced into Equation 4.8 to account for the bias, which has been observed in the satellite retrieved T_s . Finally, this parameter could be neglected because a bias insensitive error measure was designed for calibrating mHM with T_s .

These seven *global parameters* are estimated by an automated calibration of the model mHM. The difference between satellite derived T_s and simulated land surface temperature \widehat{T}_s is minimized during model calibration. The calibration procedure will be explained in the following.

4.4.3 Optimization of the Coupled mHM-Land Surface Temperature Model

For the calibration of mHM against the satellite retrieved land surface temperature the aforementioned T_s module is coupled to mHM. Thus, seven additional parameters are added to mHM and are included in the automated optimization of

the *global parameters*. For simplicity, the coupled mHM-land surface temperature model is denoted as mHM in the following. Furthermore, all parameters, including the *global parameters* of mHM (44 parameters) and the T_s module (7 parameters) are herein referred as mHM parameters. Hence, the coupled model has 51 *global parameters*.

The coupled model will be calibrated against land surface temperature or discharge or a combination of both. The performance regarding the two model outputs, i.e., discharge and land surface temperature, is estimated using a weighted objective function. In general the objective function Φ is estimated by

$$\Phi = \left(\sum_{i=1}^n w_i^p (\phi_i)^p \right)^{\frac{1}{p}} \quad (4.13)$$

where w_i is the weight ($\sum_{i=1}^n w_i = 1$) of the distance measure ϕ_i of n objectives. Different distance measures ϕ_i are considered, because discharge Q is only dependent on time, whereas T_s is a spatio-temporal variable. Following Duckstein (1984) the exponent p equal to 6 is included to the objective function to assure numerical stability and assure for a compromise solution. The different error measures ϕ for discharge and land surface temperature are described in the following.

Error Measure for Discharge Q The distance measure which is applied to the discharge estimations is the Nash-Sutcliffe Efficiency (NSE) (Nash and Sutcliffe, 1970). To get satisfying estimations of highflows as well as of lowflows, the NSE is determined for daily discharge (Equation 4.14) and the logarithm of daily discharge (Equation 4.15), respectively.

$$\phi_1 = NSE(Q) = 1 - \frac{\sum_{t=1}^T (\widehat{Q}_t - Q_t)^2}{\sum_{t=1}^T (Q_t - \bar{Q})^2} \quad (4.14)$$

$$\phi_2 = NSE(\ln Q) = 1 - \frac{\sum_{t=1}^T (\ln \widehat{Q}_t - \ln Q_t)^2}{\sum_{t=1}^T (\ln Q_t - \ln \bar{Q})^2} \quad (4.15)$$

where \widehat{Q}_t is the modeled and Q_t is the observed discharge [$m^3 s^{-1}$] at time step t [d] and \bar{Q} is the mean discharge of all time steps T of the observation.

For the optimization against discharge alone ϕ_1 and ϕ_2 are considered in the objective function. The weights are chosen to be equal for both criteria ($w_1 = w_2 = 0.5$).

Error Measure for Land Surface Temperature T_s To assess the model performance regarding the simulations of T_s an error measure for quantifying the differences between modeled and satellite retrieved T_s has to be found. The satellite

retrievals of T_s have an inherent bias of approximately 2 K to 3 K on the temporal resolution of one day compared to ground measurements (see section 4.3).

A bias correction of the satellite retrieved T_s was intended to be avoided, because an additional model accounting for the bias would have to be included into the coupled model. Such a bias model would need to be parameterized. To keep the number of parameters as low as possible the implementation of a bias correction model was avoided.

Hence, the application of common error measures like the mean squared error or any error measure which is sensitive to a bias are not considered. It is assumed that the patterns delivered by the satellite measurements are trustworthy. Thus, an objective comparing the patterns of the satellite retrieved and estimated land surface temperature qualitatively is targeted.

In hydrology common criteria used to determine pattern similarity are usually incorporating measures accounting for quantitative differences like the mean squared error (Hagen-Zanker, 2006; Wealands et al., 2005; Cloke and Pappenberger, 2008) and thus are inapplicable. A bias resistant, local and non-parametric measure denoted as pattern similarity (P) is developed. Mathematically, the pattern similarity criterion can be expressed as

$$\phi_3 = \frac{1}{NT} \sum_{t=1}^T \sum_{i,j \in \Omega} P_{ij}(t) \quad (4.16a)$$

$$P_{ij}(t) = \frac{1}{2 \cdot 8} \sum_{k=1}^8 \left[\text{sgn} \left(\widehat{T}_{s,ij}^{(k)}(t) - \widehat{T}_{s,ij}(t) \right) \text{sgn} \left(T_{s,ij}^{(k)}(t) - T_{s,ij}(t) \right) + 1 \right] \quad (4.16b)$$

where i and j are the elements of the spatial domain Ω , which in total consists of N cells, T is the number of time steps, $P_{ij}(t)$ is the pattern similarity criteria at cell (i, j) at a particular time step t , $T_{s,ij}^{(k)}$ is the land surface temperature of the k^{th} neighbor of the center cell (i, j) , and $T_{s,ij}$ is the land surface temperature of the center cell itself. The Pattern Similarity criterion is normalized with 8, the number of neighbors of the center cell (i, j) . The notation without hat (T_s) is used for the satellite derived land surface temperature, while the model simulated temperature is denoted with a hat (\widehat{T}_s). The sgn operation determines the sign of the argument a as

$$\text{sgn}(a) = \begin{cases} 1 & \text{if } a > 0 \\ -1 & \text{if } a \leq 0 \end{cases} \quad (4.17)$$

An example for the pattern similarity criterion is depicted in Fig. 4.2.

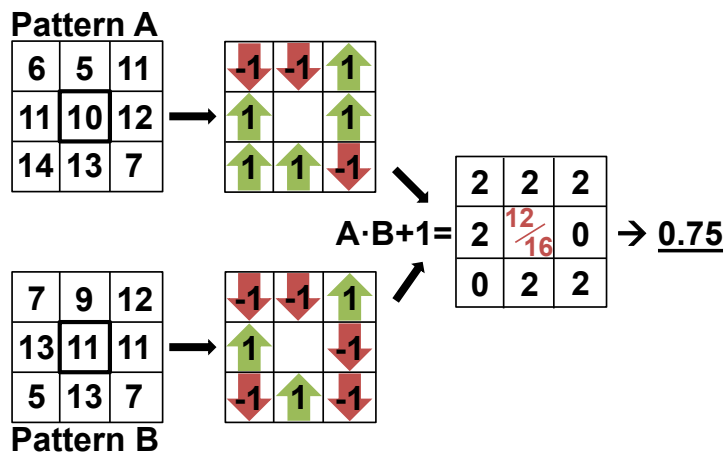


Figure 4.2: Schematic description of the pattern similarity criterion according to Equation 4.16b. In the upper left row an example Pattern A with the center pixel having the value 10 is illustrated (e.g., satellite retrieved T_s). Next to it, on its right, the sign of the comparison between the center pixel with its neighboring pixels is shown. If the respective neighboring pixel is larger than the center pixel (green arrow) the value 1 is assigned to this pixel (e.g., 5 pixels in Pattern A), otherwise (red arrow) the value -1 is assigned to them (e.g., 3 pixels in Pattern A). This analysis is repeated for a pattern B (e.g., simulation of \hat{T}_s), as depicted in the lower row. The results of both comparisons are multiplied and increased by 1. Thus, the dissimilar pixels between pattern A and pattern B become 0, while similar become 2. The elements of the resulting matrix are summed up and divided by twice of the number of neighbors (e.g., 8). For the given example, the pattern similarity criterion is 0.75, meaning that three quarter of the neighbors showed the same relation to its center value.

The criterion is based on a 3×3 pixel search raster. Its center cell is subtracted from the eight neighboring cells. The difference becomes negative and the $\text{sgn} = -1$, if the value of the center cell is greater than the neighbor. In the opposite case the sign becomes positive ($\text{sgn} = 1$). This procedure is applied to both fields under comparison, i.e., the satellite retrieved T_s and the modeled land surface temperature \hat{T}_s . The two resulting 3×3 signum matrices are multiplied with each other. The resulting matrix has a negative entry (-1) where the elements of both factors had different signs and a positive entry (+1) where the factors had the same sign.

Thus, a negative entry appears when the modeled grid cell shows a different tendency compared to the measured land surface temperature. The entry is positive, when the grid cell tendencies are in correspondence. In order to avoid the results to be canceled out when summed up, the eight single results are increased by one.

Hence, for full correspondence the sum of the elements of the search raster yields 16 while it is zero for full disagreement. Finally, the sum is scaled between zero and one. Hence, a $P_{ij}(t)$ of 1 means full agreement of patterns, i.e., no dissimilarity.

The scaling assures comparability to other error measures like the Nash Sutcliffe Efficiency or the correlation coefficient. The pattern similarity of 0 does not only correspond to full dissimilarity, but means that the two patterns are inverse to each other. A $P_{ij}(t)$ of 0.5 marks randomly diverging patterns.

The 3×3 local search window is applied to every cell (i, j) within the domain Ω and all time steps t of the patterns under comparison. The overall pattern similarity is then calculated as the mean of the single values (see Equation (4.16a)).

Numerical tests showed that a combination of the pattern similarity criteria with another bias resistant criteria, i.e., the Pearson correlation coefficient, result in the best model performances regarding discharge and land surface temperature. Thus, a fourth error measure is considered in the objective function

$$\phi_4 = \rho = \frac{\text{Cov}(T_s, \widehat{T}_s)}{\sigma_{T_s} \sigma_{\widehat{T}_s}} \quad (4.18)$$

where ρ denotes the Pearson correlation coefficient, $\text{Cov}(T_s, \widehat{T}_s)$ the covariance between the spatio-temporal fields of T_s and \widehat{T}_s , and σ_{T_s} and $\sigma_{\widehat{T}_s}$ denotes the standard deviation of the satellite retrieved T_s and modeled land surface temperature \widehat{T}_s , respectively.

The criteria for pattern similarity ϕ_3 and ϕ_4 are equally weighted ($w_3 = w_4 = 0.5$) in the objective function if applied for calibration against the land surface temperature (only ϕ_3 and ϕ_4 are considered in the objective function).

The calibration with respect to a combination of land surface temperature and discharge data are conducted using all four error measures ϕ_1 , ϕ_2 , ϕ_3 , and ϕ_4 as objective. The weights are defined as $w_1 = w_2 = \frac{1}{3}$ and $w_3 = w_4 = \frac{1}{6}$. The higher weighting of discharge error measures is chosen to ensure the partitioning of water to the different fluxes and states of the hydrologic cycle. In comparison with other weighting schemes this setup has proven to perform best.

To avoid the dominance of any objective ϕ_i ($i = 1, \dots, 4$) the objectives are normalized by their potential ranges:

$$\phi_i = \frac{\phi_i - \phi_i^{\min}}{\phi_i^{\max} - \phi_i^{\min}} \quad (4.19)$$

where *min* and *max* denote the upper and the lower bound of the particular objective i , respectively. ϕ_i^{\min} and ϕ_i^{\max} are determined based on 55 000 simulations in two of the catchments under investigation, i.e., Ems and Neckar, using random

parameters. To ensure sampling over the entire parameter domain a stratified sampling strategy was applied to generate 55 000 parameter sets (Morris, 1991).

4.4.4 Experimental Design

In order to address three different hypothesis several numerical experiments were conducted, which will be explained within this section. In common to all of the experiments are the six catchments under investigation depicted in Figure 4.1. To address the issue of parameter estimation uncertainty, all experiments are designed as ensemble simulations based on 20 independent parameter optimization runs. The standard calibration of hydrologic models with river discharge will serve as a reference or baseline scenario. All model calibrations are conducted with the Dynamically Dimensioned Search Algorithm (Tolson and Shoemaker, 2007).

To verify if land surface temperature T_s has a predictive skill regarding discharge we calibrate the hydrologic model mHM using T_s alone. The results are evaluated by comparison of estimated and observed discharge. The determined parameter sets are transferred to 222 ungauged locations to assess their validity and stability.

A second experiment aims to assess the impact of a combined calibration of discharge Q and land surface temperature T_s . It is expected that this approach has a high impact on the modeled evapotranspiration, since the land surface temperature characterizes the near surface atmospheric conditions and is directly connected to ET via Equation 4.8. Thus the conditioning of mHM with patterns of T_s should have an effect on the modeled evapotranspiration. We hypothesize that calibrating the hydrologic model mHM using land surface temperature and discharge will lead to a better constrain of parameters. By applying the aforementioned framework the model performance regarding discharge should not deteriorate significantly. The degree of parameter constraints are determined by analyzing 20 independent model calibrations. The resulting parameter estimation uncertainty is assessed by dividing the spread of the ensemble parameters with its initial ranges. To avoid influential effects of outliers, the spread of ensemble parameters is determined using the difference between 95th and 5th percentile.

$$R_r^i = 1 - \frac{r_{95}^i - r_5^i}{r_{max}^i - r_{min}^i}, i = 1, \dots, n \quad (4.20)$$

where r_5 and r_{95} are the 5th and 95th percentile of the ensemble of a optimized parameter i , r_{min} and r_{max} denote the minimum and maximum initial range for optimization of this parameter i out of n model parameters. Thus, R_r^i expresses the reduction of parameter ranges after model calibration if compared to the initial ranges. If the parameter range reduction R_r equals 1, the parameter range converges to a single value in all 20 independent runs. If $R_r = 0$ the optimized parameter spreads over the entire initial range.

Additionally to the parameter ranges, the effect on evapotranspiration E is studied. We hypothesize that the spatial variability of the resulting evapotranspiration fields will reduce by using patterns of land surface temperature complementary to discharge for parameter inference. On the one hand, this hypothesis stems from the knowledge that the land surface temperature is mainly governed by air temperature, which has high spatial covariances. On the other hand, we expect that constraining model parameters with an integral discharge signal could lead to spatial inconsistencies, but nevertheless fulfills the catchment water balance. In consequence, the magnitude of E will be comparable, whereas the spatial variability will not. The spatial variability of modeled E is estimated using the signal to noise ratio, which is defined as

$$SNR_E(t) = \frac{\mu_E(t)}{\sigma_E(t)} \quad (4.21)$$

where μ denotes the mean and σ the standard deviation of an evapotranspiration field E at a particular time step t . An evaluation with observed fields of evapotranspiration would be desirable, but spatially distributed measurements of evapotranspiration do not exist. An alternative could be evapotranspiration products which were derived from satellites. But first, they still underlie large uncertainties and second, either their spatial (e.g., 1°) or temporal (e.g., months) resolution is too coarse compared to the high resolution simulation of $4 \times 4 \text{ km}^2$ and 1 day of this study.

Next to the spatial variability of E , we will present an evaluation of the evapotranspiration estimates at eddy flux towers (see Figure 4.1). To be comparable to the footprint of the flux observation, which is several 10 m to several 100 m, the spatial resolution of the model is reduced to $100 \times 100 \text{ m}^2$ and the modeling period is extended to the period of the evapotranspiration observations. The flux tower observations have been corrected to fulfill the energy balance. This methodology is analogous to that described in Zink et al..

The calibration period is limited to the year 2009 due to availability of discharge and land surface temperature observations. All simulations have a model spin up period of 5 years. The majority of analyzes focus on the year 2009, but the predictive skill of discharge is assessed by comparing with all runoff observations available in the 222 catchments. The separation of the time series into calibration and validation period is unnecessary, because this study focuses on the benefit of using T_s for parameter inference compared to classical Q calibration.

4.5 Results and Discussion

4.5.1 The Predictive Skill of Land Surface Temperature Regarding River Runoff

In this section we will present results obtained by calibrating the hydrologic model mHM with patterns of land surface temperature as described in section 4.4.3 in order to assess the predictive skill of land surface temperature regarding river runoff.

An ensemble of 20 parameters, calibrated in each catchment, is used for a forward run to predict discharge. Figure 4.3 shows exemplarily the observed and simulated discharge time series of the two basins Ems and Main out of the six basins under investigation (Figure 4.1). For comparison, Figure 4.3 also shows discharge predictions obtained by classical calibration with river runoff (top row). As can be seen, the performance decreases if mHM is calibrated with T_s (bottom row). Especially low flow periods are usually overestimated (July to September). This overestimation results from insufficient estimated slow interflow and baseflow. These hydrologic processes are insufficiently modeled because T_s is non informative regarding them. This means parameters which are connected to slow interflow and baseflow are insensitive to a calibration with land surface temperature. Similar studies, using T_s for model calibration, limit the number of calibrated parameters to those connected to soil water storage and evapotranspiration (Crow et al., 2003; Gutmann and Small, 2010; Silvestro et al., 2013, 2014; Corbari and Mancini, 2014; Corbari et al., 2015). In these studies all other parameters are determined by prior knowledge, e.g., transfer from remote locations or expert knowledge.

The uncertainty arising from the parameter estimation process is depicted as grey bands in Figure 4.3. The runoff uncertainty increases for the T_s calibration compared to the classical calibration with discharge. In case of the Ems river basin the highflows of the flood event in spring 2009 are within the uncertainty bands for the T_s calibration, which was not the case for the Q calibration. On the contrary, some of the parameter sets from T_s calibration performed very poor in estimating flood events, e.g., in spring in the Main catchment (Figure 4.3 panel D). The high uncertainty in river runoff simulations is reasoned in the weak estimation of routing parameters when the model is calibrated with land surface temperature (see section 4.5.2). This approach shows stronger pronounced flood peaks as compared to Q calibration. This indicates that the direct runoff and fast interflow component are enabled more rapidly. The uncertainty ranges are, however, acceptable if considering runoff itself was not involved in model calibration. The median discharge estimated from T_s calibrations, shows unexpected good mapping of the observed discharge, revealing NSEs off 0.8 and 0.54 for the Ems and Main catchment, respectively.

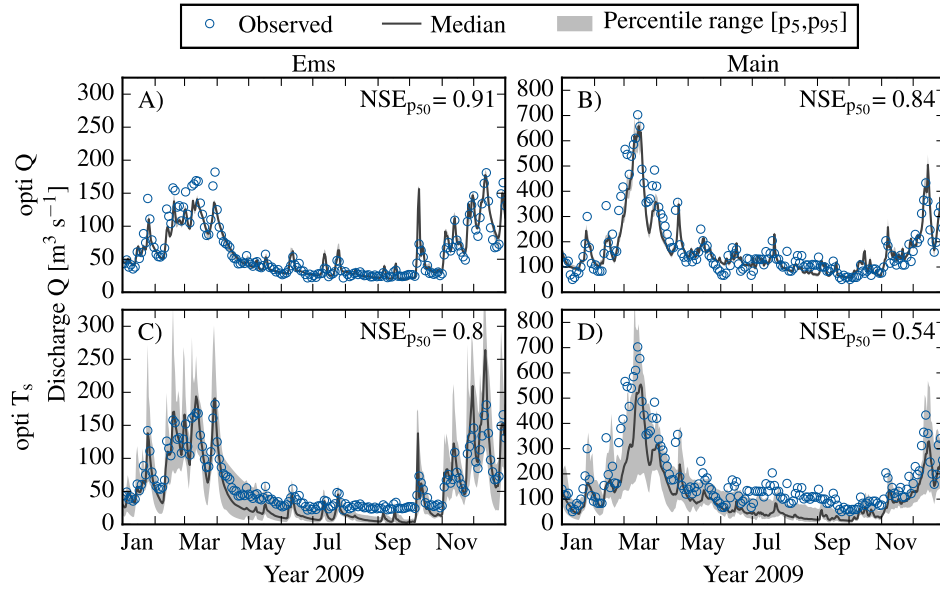


Figure 4.3: Simulated daily discharge when calibrating the hydrologic model mHM with discharge Q (panels A and B) and with land surface temperature T_s (panels C and D) for the catchments Ems (panels A and C) and Main (panels B and D). The grey bands depict the uncertainty of 20 ensemble model simulations assessed by the range of the 5th and 95th percentile of the estimated discharge. The dark grey line is the median of the ensemble discharge simulation. Its performance is given in the top right corner of each panel.

The median NSE of the 20 model calibrations with T_s varies between 0.36 and 0.66 within the six catchments and is in average 0.51 (Figure 4.4 panel A). Note that this is the median of NSEs obtained from the 20 calibrated parameter sets, compared to the NSE obtained from the median discharge time series reported above. Considering that discharge was not used for model parameter inference this is a satisfactory result and shows that T_s has some predictive skill regarding river discharge. But, the variations of the performance criteria are substantially high with an average standard deviation of 0.22. These uncertainties even increase (standard deviation=0.26) if the model parameters are transferred to remote locations (Figure 4.4 panel B). One reason is the five times higher number of ensemble simulations using 100 parameter sets, consisting of 20 parameter sets from each of the other five catchments. Another reason is that some transferred parameters will not be well adjusted for transfer to another location because different hydrologic processes are important in distinct catchments. The Neckar catchment, for example, has a significant groundwater contribution to the runoff process due to the karstic nature of the subsurface. Such processes will play a minor role in, e.g., the Ems basin, which is mainly located on a ground moraine. Hence, some subsurface parameters are not well constrained in the Ems basin and will lead to

an insufficient representation of karstic processes in the Neckar catchment. Still, the median NSEs are comparable to the on-site calibrations (Figure 4.4 panel A) which confirms the transferability and stability of the inferred parameters.

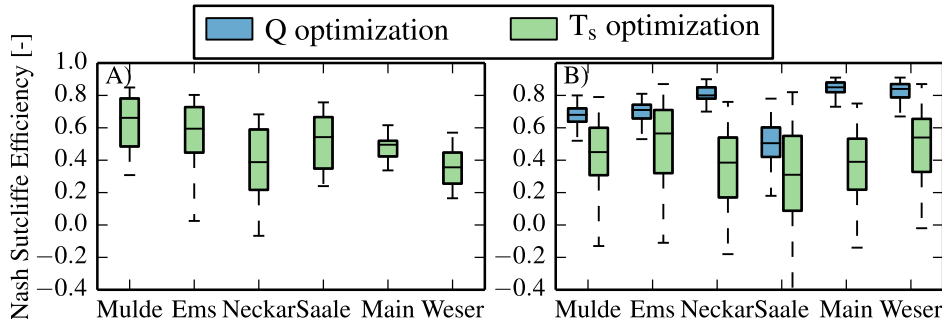


Figure 4.4: A) shows the performance of the model regarding discharge if the model is calibrated with land surface temperature (T_s). For each of the six catchments 20 independent calibration runs lead to the variability of the Nash-Sutcliffe performance criteria. B) depicts the model performance when calibrating mHM with either Q or T_s and transferring the parameters to the other catchments. Thus, the variability arises from 100 parameter sets, which are derived from the five different donor basins.

The comparison of transferred parameters obtained by Q calibration with those acquired by T_s calibration show an average deterioration of the median of 39%. This behavior was expected because a cross validation of land surface temperature inferred model parameters with river discharge can not outperform the calibration employing Q . However, for most of the catchments the upper edges of the box-plots at least reach the median model performance of the Q calibration.

The 120 optimized parameter sets (20 from each catchment) are transferred to 222 additional catchments to assess their ability to reproduce discharge observations (Figure 4.5). This cross validation experiment will assess the predictive power of T_s optimized model parameters because this catchments were not involved in the parameter inference process (Klemeš, 1986). For these catchments the average median model performance is 0.4. Whereas 91% of all catchments show positive median NSEs for daily discharge. These results further confirm that T_s has a predictive skill regarding discharge. But the performances may not be sufficient for reliable water balance predictions on a daily basis. For scenarios where no discharge data are at hand, the proposed procedure may help to get a first indication of the catchment's water balance.

Using satellite derived land surface temperature for calibrating hydrologic models fits to efforts to predict river runoff in ungauged basins (Sivapalan et al., 2003; Hrachowitz et al., 2013). The broadly available T_s can give first indications of a catchments water balance. Especially the results of the six study catchments

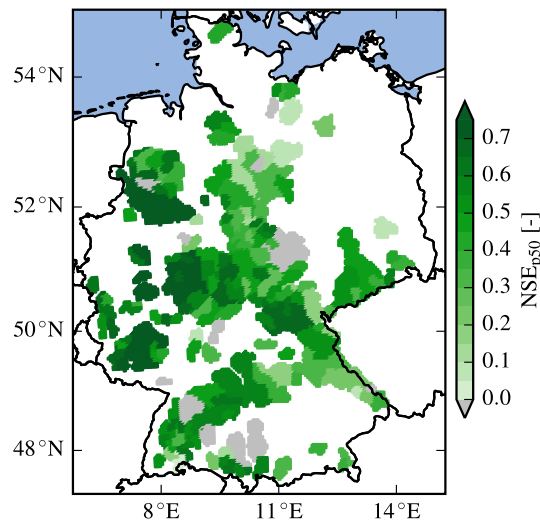


Figure 4.5: Meidan performance of ensemble discharge predictions in 222 catchments spread over Germany. These catchments have not been used for parameter inference. The 20 parameter sets of the six donor basins presented in Figure 4.1 are used for determining these results. The 120 parameter sets from the donor basins are based on calibrations only using land surface temperature.

(Figure 4.3) show that T_s has a moderate predictive skill for river discharge.

Corbari and Mancini (2014) found similar results for the calibration of a distributed Energy-Water Balance model. In their study the calibration with T_s did not outperform the discharge estimation with the standard parameterization of Energy-Water Balance model. Silvestro et al. (2014) also found that a land surface temperature calibration lead to performance losses if compared to streamflow calibrations. The deterioration shown within these studies is lower than the above mentioned. This can, however, be attributed to the used calibration procedure. Corbari and Mancini (2014) and Silvestro et al. (2014) restricted the number of parameters to be calibrated only to those connected to soil moisture and evapotranspiration. The remaining parameters have been estimated from prior knowledge with the assumption that they are insensitive to T_s . To restrict the calibration to a subset parameters, is a good idea in general but implies a risk. The parameters which remain for calibration may be insensitive or have low sensitivities with regard to T_s if compared to these excluded from calibration (see, e.g., Cuntz et al., 2015). A proper sensitivity analysis or parameter screening should be performed before excluding parameters from calibration. Therefore, within this study all parameters have been purpose to optimization, which may also include parameters which are insensitive regarding T_s , but get important for discharge prediction.

4.5.2 Calibration of mHM with River Runoff and Land Surface Temperature

The impact of simultaneously calibrating mHM with land surface temperature and river discharge is investigated within this section. Therefore, we analyze the effect on the identifiability of model parameters, the spatial variability of evapotranspiration, the estimation of river runoff, and the estimation of evapotranspiration at eddy flux towers.

Identifiability of Model Parameters: Parameter Range Reduction

The parameter range reduction for the calibration of the model with a) discharge, b) discharge and land surface temperature, and c) land surface temperature are determined according to Equation 4.20. One hypothesis of this study is that adding a diagnostic land surface temperature model to an existing hydrologic model helps to better constrain the model parameters. As indicated in section 4.4.3 only the patterns of T_s were involved in model calibration of mHM through the pattern similarity criterion (Equation 4.16). The spread of the ensemble parameters normalized with its initial ranges is shown in Figure 4.6. Dark red colors characterize well constrained model parameters, whereas light yellow colors identify parameters which are almost randomly drawn from their initial ranges. This figure gives some indications of the identifiability, and hence the sensitivity of the parameters regarding the various variables used for calibration (Q , T_s , or both). The interpretation of the sensitivity is analogous to the parameter range reduction: If the parameter range is reduced the particular parameter is sensitive with respect to the individual variable.

The most obvious difference between the three optimization strategies can be observed in the group of the soil moisture evapotranspiration parameters (p_{19} to p_{24}). These parameters primarily govern the water extraction from the soil due to evapotranspiration. They are constrained best if calibrated with T_s (Figure 4.6 bottom panel). The ranges also narrow significantly when mutually calibrated with Q and T_s (Figure 4.6 center panel). Two out of the three evapotranspiration parameters (parameters 25 and 26) show a similar behavior. These results confirm that using patterns of satellite derived land surface temperature for parameter optimization helps to better constrain model parameters, especially those which are connected to evapotranspiration.

The results shown in Figure 4.6 also indicate that using T_s only for parameter optimization may not be sufficient because some parameters are not well constrained. The snow threshold temperature (parameter 2), for example, is not as good constrained if Q is not considered in model calibration. The snow threshold temperature parameter defines the aggregate state of the precipitation. If the air temperature is below this threshold, precipitation is treated as snow, otherwise it

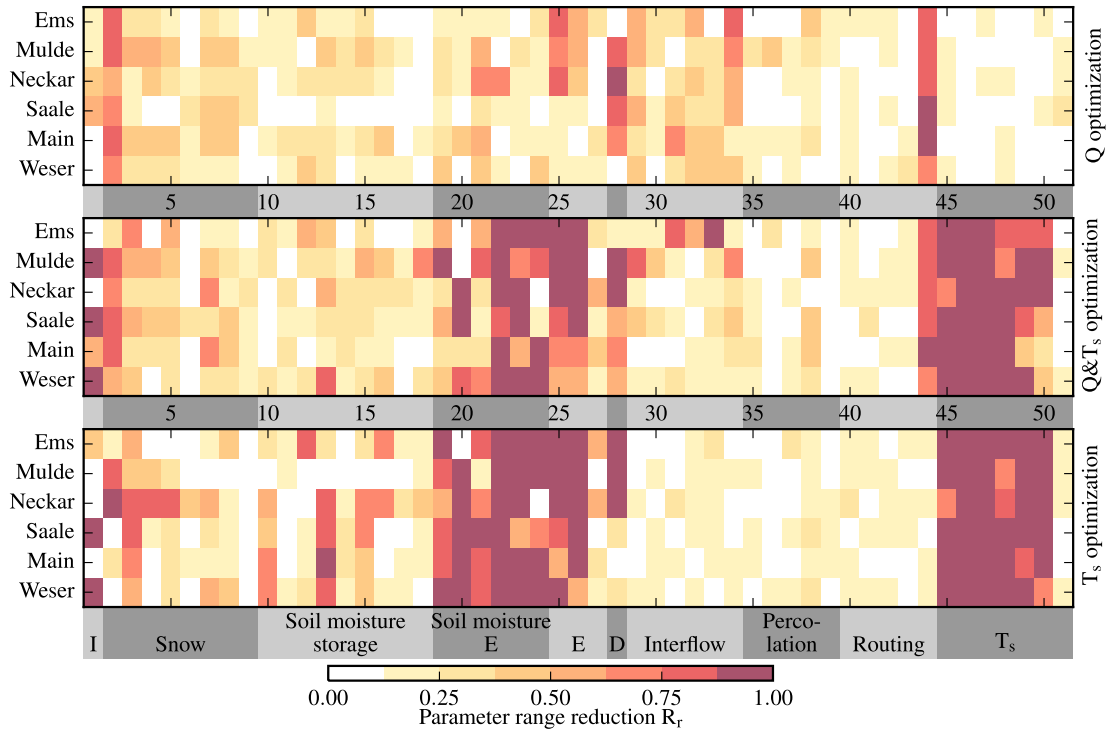


Figure 4.6: The parameter range reduction if mHM is calibrated against discharge (upper row), discharge and land surface temperature (middle row), or land surface temperature (lower row). The parameter range reduction is assessed by scaling the range of a particular parameter resulting from 20 independent calibration runs with the initial parameter range (see Equation 4.20). A low value (light yellow) indicates a small range reduction, whereas a high value (dark red) indicates a well constrained parameter. The parameters are grouped according to their appearance in different model processes. Abbreviations: I - interception, D - direct runoff.

is considered as rain. T_s is a bad estimator for the snow threshold temperature because this parameter only gets important in winter. During the cold season evapotranspiration is low and in consequence the impact of T_s on the modeled water fluxes is low too.

The last routing parameter, i.e., parameter 44, is almost insensitive to T_s (Figure 4.6 bottom panel). Further, the interflow parameters (parameters 31-34) show a lower range reduction to parameter optimizations including Q observations. These insensitivities explain the mismatches in low flows observed in Figure 4.3. Moreover, the strongly pronounced peaks in Figure 4.6 are reasoned in the lousy estimation of the threshold for activating/deactivating the fast inflow process (parameter 29 in Figure 4.6).

The high parameter range reduction of the parameters 45-50 confirms the proper implementation and parameterization of the diagnostic land surface temperature module. This is an important aspect, since increasing the number of model parameters due to the implementation of a new process should not lead to a distraction of the optimization algorithm caused by insensitive parameters.

Parameter 51, which also belongs to the newly introduced T_s parameters, characterizes a bias correction parameter for T_s . This parameter was implemented during the investigation of different objective functions, in which we also tested bias sensitive error measures, e.g., NSE or SSE. The fact that this parameter is not well constrained underpins that the pattern similarity criterion is bias insensitive.

These results confirm the hypothesis that the consideration of spatially distributed, satellite retrieved land surface temperature fields improve the identifiability of parameters of the hydrologic model mHM.

Spatial Patterns of Evapotranspiration

The results of the calibration with discharge and land surface temperature are compared to those which were obtained by classical calibration with discharge. Hence, this section will analyze the impacts of additionally constraining mHM with T_s on the spatial distribution of evapotranspiration.

Figure 4.7 shows the evapotranspiration of summer 2009 in the catchment Main. Whereas panel A displays the result of an optimization with discharge, panel B shows the result of the calibration with discharge and land surface temperature. It can be seen that the pattern of the evapotranspiration of calibration using discharge shows a higher spatial variability compared that using Q and T_s . Next to its reduced spatial variability, E is on average higher if the model was calibrated with Q and T_s . The average evapotranspiration for Q and Q and T_s calibration are $246 \text{ mm season}^{-1}$ and $262 \text{ mm season}^{-1}$ in summer, respectively. Nonetheless, the discharge performance for the Main catchment does not decrease (results will be presented later in section 4.5.2). The locations with evapotranspiration values less than $210 \text{ mm season}^{-1}$ are urban areas.

The visual comparison in Figure 4.7 supports the hypothesis that the spatial field of evapotranspiration has a higher spatial variability if the model is optimized with discharge only. The spatial variability of the evapotranspiration decreases if land surface temperature, which carries some information about the spatial distribution, is included in the calibration process. McCabe et al. (2005) also found that T_s had an effect on spatial variability of evapotranspiration, but did not quantify it.

In this study we quantify the impact on the spatial fields of evapotranspiration by the signal to noise ratio (SNR, see Equation 4.21). For the two example catchments, Ems and Main, the smoothed signal to noise ratio over the course of the

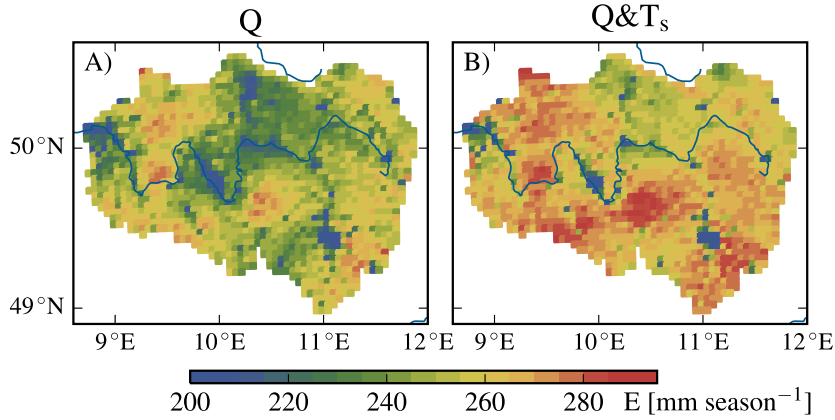


Figure 4.7: Comparison of the simulated evapotranspiration if the model is calibrated with A) discharge or B) discharge and land surface temperature simultaneously. The plot shows the sum of evapotranspiration in summer 2009 (June, July, August) for the Main catchment (see Figure 4.1).

year 2009 is shown in Figure 4.8. The SNR is higher for the calibration with river runoff and land surface temperature. This means the fields of E are smoother and do not have as much spatial variability as these obtained by calibration with discharge. This smoothing is not only caused by T_s , but to a significant extent by the air temperature, which is a very sensitive variable in Equation 4.8. Air temperature has very high spatial covariance, i.e., low spatial variability, compared to, e.g., precipitation, which propagates to the evapotranspiration in the proposed framework.

A significant impacts of the calibration procedure on simulated evapotranspiration can only be observed between April and September (Figure 4.8). During winter evapotranspiration is very low and thus uncertain model parameters do not have a significant effect on neither the magnitude nor the spatial variability of E . Anyway, the uncertainty of the modeled E is low during this period.

Figure 4.9 panel A presents the average signal to noise ratios of the year 2009 for the six catchments. To compare the impact of the $Q - T_s$ calibration on both E and river runoff Q , Figure 4.9 panel B presents the NSE of river runoff. As panel A shows the SNR is higher for all of the $Q - T_s$ calibrations. Further, the uncertainty bands are smaller compared to the Q calibration for all basins with exception of the Mulde. Figures 4.8 and 4.9 conform that the spatial variability of evapotranspiration is reduced, if land surface temperature is considered during model calibration.

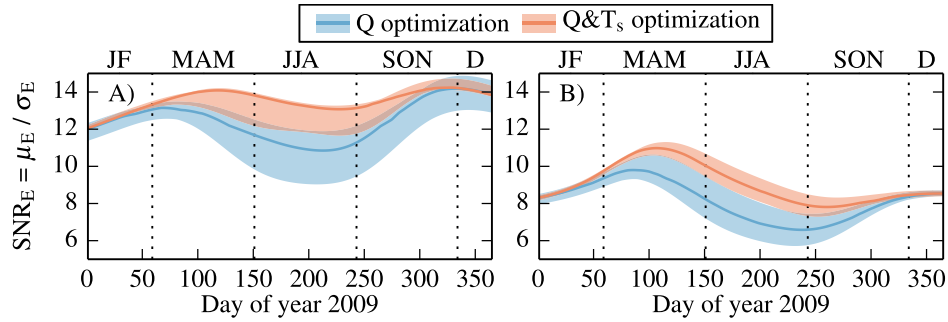


Figure 4.8: Kernel smoothed signal to noise ratio (SNR, Equation 4.21) of evapotranspiration fields for the catchments A) Ems and B) Main. Low values characterize noisy fields, whereas high values describe spatially smooth patterns. The uncertainty bands depict the difference between the 5th and 95th percentile of the signal to noise ratio of the 20 on-site calibrated parameter sets.

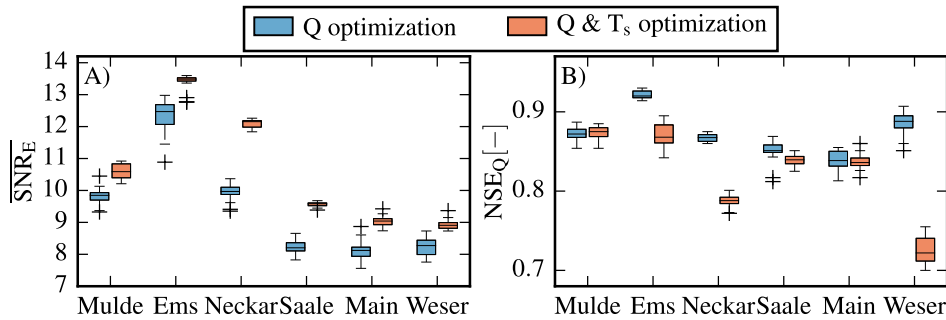


Figure 4.9: Comparison of optimization strategies using Q only or Q and T_s regarding A) the average spatial variability of evapotranspiration and B) Nash-Sutcliffe performance criterion (NSE) of daily discharge (panel B). Panel A is estimated by averaging the daily signal to noise ratio of 2009 (e.g., Figure 4.8). Panel B shows the estimated discharge of 2009 using the above mentioned calibration objectives. The uncertainty stems from 20 independent parameter estimations.

River Runoff

Finding a comprise solution for optimizing the hydrologic model with Q and T_s should not deteriorate the discharge simulation significantly. Figure 4.9 panel B shows that for four out of six catchments this condition is fulfilled. For the Neckar and Weser catchment the discharge deteriorates significantly by more than 5% for the simultaneous calibration. One reason for that could be the weighting scheme between the two objectives Q and T_s . For some catchments it may be necessary to increase the weighting of the objective function considering discharge, i.e., ϕ_1 and ϕ_2 in Equation 4.13. Crow et al. (2003) studied the effect of weighting Q and T_s differently and found that the model performance differs based on the chosen weighting scheme. The herein proposed weighting was determined during a lot of test for the Ems and Neckar catchment and showed good results for these test cases. Generally, the weighting of different objectives can be argued in one way or another. Ideally a Pareto optimization would give a closer insight to the offset between both objectives. However, the decision which objective should be preferred stays a subjective choice. With exception of the Mulde, in none of the catchments the NSE could be improved by assimilating T_s (Figure 4.9 panel B). On average the median runoff performance deteriorates by 6% if T_s is considered in the calibration. A range of -11% to 14% performance difference was found by Corbari and Mancini (2014) if the model is calibrated by T_s and Q simultaneously. Thus, our findings are comparable to this study.

Evapotranspiration at Eddy Flux Towers

Figure 4.10 compares the performances for simulated evapotranspiration of the classical discharge calibration with the combined $Q - T_s$ calibration. The Pearson correlation coefficient between observations and simulation is increasing if mHM is calibrated with both Q and T_s , as Figure 4.10 panel A shows. The medians of the correlation and the RMSE improve 5% and 8%, respectively. The major improvements are achieved in summer when the evapotranspiration is highest, for example, the median correlation coefficient in summer improves from 0.36 to 0.67 at station E3.

Another important effect is the reduction of uncertainty of the evapotranspiration simulations (Figure 4.10). At some stations the uncertainty bands are hardly visible for the $Q - T_s$ calibration. This behavior can be directly attributed to the parameter range reduction (see section 4.5.2). The uncertainty of the E estimates has to decrease because the parameter estimation uncertainty of parameters related to evapotranspiration decreased (parameters 19 to 27 in Figure 4.6). Comparing the improvement in E estimation and the deterioration in Q simulation it is difficult to draw a conclusion. We consider a combined calibration with Q and T_s as beneficial based on the tradeoff of performances of the two major water balance

variables E and Q and, moreover, the improved parameter identifiability.

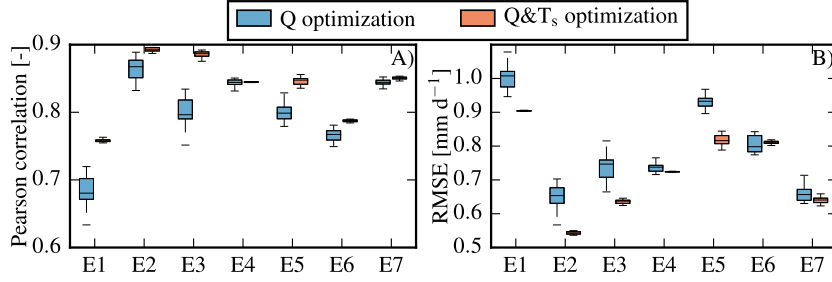


Figure 4.10: Evaluation of evapotranspiration (E) estimates at 7 eddy flux towers (Figure 4.1). A) shows the Pearson correlation coefficient and B) shows the root mean squared error (RMSE) between flux tower observations and model simulations using 20 parameter sets inferred by either calibration with discharge (blue) or discharge and land surface temperature (orange). The flux tower observation periods range from 3 to 10 years and are on average 6 years. Note that high Pearson correlation coefficients are beneficial, while the opposite is true for the RMSE.

4.6 Summary and Conclusions

This study focused on the development and implementation of a diagnostic land surface temperature module for hydrologic models. The T_s module is meant to account for spatial patterns of satellite observations within the model calibration process. Therefore, the herein applied hydrologic model mHM has been calibrated using three different strategies. First, as a reference mHM was classically calibrated with observed streamflow. Second, a calibration with land surface temperature aimed to assess the predictive power of this method regarding streamflow. And third, a combined calibration with Q and T_s was intended to better constrain model parameters, i.e., reduce the ranges of the ensemble parameter sets. All experiments have been conducted by consideration of parameter estimation uncertainty which was realized by 20 independent parameter optimization runs.

The results of the study confirm that only by accounting for spatial variability of land surface temperature in the parameter inference process results in moderate model performances. This is a step forward towards predictions in ungauged basins. Land surface temperature data are broadly and freely available over the entire globe and thus represent a valuable source of information for hydrologic modeling.

A second finding of this study is that calibrating the hydrologic model mHM with Q and T_s lead to better constrained model parameters, even if the implementa-

tion of the diagnostic land surface temperature model requires additional model parameters. Especially parameters connected to evapotranspiration were better constrained if compared to discharge only calibrations. This confirms that the classical calibration of hydrologic model should be reviewed. The calibration with river runoff concentrates on the integral signal at the basin outlet without considering the spatial representativeness of the model.

The herein presented methodology is a step forward to consider such spatially distributed observations, even if they are inherently biased. The developed pattern similarity criterion is a first attempt to assess the spatial structure of spatially distributed observations.

But also limitations of this methodology could be observed. Counterintuitively, the model performance with regard to runoff decreased despite the fact that model parameters have been better constrained. At the same time the model performance regarding evapotranspiration increases at the seven eddy flux measurement sites.

Parameters connected to interflow and routing could not be sufficiently constrained if only T_s was considered in the calibration process. Further research has to be done to explore other sources of satellite data, which may overcome this discrepancy. GRACE data, for example, seem to be a promising alternative to assess subsurface model parameters.

Some research has further to be dedicated for investigating new measures to incorporate either spatial or temporal information of satellite data. Cloke and Pappenberger (2008) and Koch et al. (2015) did already some efforts in this direction, but the literature about bias-insensitive pattern matching criteria in hydrology is still rare.

Another approach to make better use of satellite information could be a two step calibration approach. In a first step a sensitivity analysis has to identify the model parameters which are sensitive to the respective model variable, e.g., discharge or land surface temperature. Based on that knowledge the hydrologic model is calibrated first with land surface temperature and second with discharge by only considering the sensitive parameters for the respective variable.

Chapter 5

The German Drought Monitor

This chapter is largely based on the publication:

Zink, M., Samaniego, L., Kumar, R., Thober, S., Mai, J., Schäfer, D., and Marx, A. (2016): The German Drought Monitor. *Environmental Research Letters*, 11(7): 074002, doi:10.1088/1748-9326/11/7/074002.

5.1 Abstract

The 2003 drought event in Europe had major implications on many societal sectors, including energy production, health, forestry and agriculture. The reduced availability of water accompanied by high temperatures led to substantial economic losses on the order of 1.5 Billion Euros, only in agriculture. Furthermore, soil droughts have considerable impacts on ecosystems, forest fires and water management. Monitoring soil water availability in near real-time and at high-resolution, i.e., $4 \times 4 \text{ km}^2$, enables water managers to mitigate the impact of these extreme events. The German Drought Monitor was established in 2014 as an online platform. It uses an operational modeling system that consists of four steps: (1) a daily update of observed meteorological data by the German Weather Service, with consistency checks and interpolation; (2) an estimation of current soil moisture using the mesoscale Hydrological Model (mHM); (3) calculation of a quantile-based Soil Moisture Index (SMI) based on a 60 year data record; and (4) classification of the SMI into five drought classes ranging from abnormally dry to exceptional drought. Finally, an easy to understand map is produced and published on a daily basis on www.ufz.de/droughtmonitor. Analysis of the ongoing 2015 drought event, which garnered broad media attention, shows that 75% of the German territory underwent drought conditions in July 2015. Regions such as Northern Bavaria and Eastern Saxony, however, have been particularly prone to drought conditions since autumn 2014. Comparisons with historical droughts show that the 2015 event is amongst the ten largest drought events observed in Germany since 1954 in terms of its spatial extent, magnitude and duration.

5.2 Introduction

Drought is a natural phenomenon that results from deficiencies in precipitation compared to the expected or normal (Wilhite, 2005). It may translate to water scarcity, a discrepancy between the actual demand and the corresponding availability of water for environmental and societal needs. Compared to other natural disasters, droughts have the largest spatial extent and longest duration (Sheffield and Wood, 2011). These creeping events easily persist over several years and can reach national to continental spatial coverage (Sheffield and Wood, 2011; Samaniego et al., 2013). According to the EM-DAT database (Guha-Sapir et al., 2015), droughts affected 2.2 billion people worldwide between 1950 and 2014, thus making droughts the second most important natural disaster after floods (3.6 billion people affected). In Europe, for example, the costs per event during this period are estimated to be 621 Mio. EUR, the costliest amongst all natural disasters that occurred in this region (Guha-Sapir et al., 2015). Droughts have impacts on many societal sectors, including forestry, water resources management, energy generation, and health. Their impacts can be divided into direct and indirect impacts

(Wilhite et al., 2007). Examples of direct impacts are reduced crop yield and forest productivity, increased forest fire hazard, reduced water levels, and increased mortality rates for livestock, wildlife and fish. They can usually be quantified, though the assessment of indirect impacts is often challenging. An example of indirect drought impact is variable food prices due to market effects in the agricultural sector. As a result, it is difficult to estimate the total costs and losses at the regional and national levels. Furthermore, the indirect losses of droughts often exceed those of the direct ones (Wilhite et al., 2007).

From an economic perspective, droughts affect mainly agriculture, food and energy production, inland navigation, and tourism. The agro-economic impact is typically highest, due to losses in crop yield and livestock. Energy production is negatively affected if the water temperature rises above a critical threshold and, consequently, the availability of cooling water for energy plants is limited. Wilhite et al. (2000) considered droughts to be one of the most damaging natural hazards in terms of economic costs. Widespread, long-term drought events, in particular, not only have an impact on the regional agricultural sector but may also have international impacts on commodity prices and food security (EEA, 2012b).

According to the European Commission, the frequency of droughts has increased since 1980 and will, very likely, further increase (EEA, 2012a). To date, 11% of the European population and 17% of the area of the EU have been affected by water scarcity (European Commission, 2007, 2010). For example, the 2003 drought event, which covered major parts of Europe, caused 7,000 fatalities in Germany alone (European Commission, 2012) and had an agro-economic impact of 1.5 billion EUR. On the European level, the death toll was estimated to exceed 70,000 (Robine et al., 2008), and the agro-economical impact was estimated to be 15 billion EUR (COPA-COGECA, 2003). This severe drought impacted many components of societal life. It disrupted irrigation, inland navigation, and power plant cooling (Fink et al., 2004; Parry et al., 2007). The current 2015 soil drought event in Germany caused losses in crop yield and increased forest fire risk. An analysis of the evolution of this event is presented in this study.

A precise and generally accepted definition of drought does not exist (Wilhite, 2005) because drought impacts are specific to the region of its occurrence and to the field of interest. For example, an agricultural production engineer would interpret a drought event in a different manner than a water resources manager would. According to the WMO (2006) and Mishra and Singh (2010), four different types of drought can usually be found in the scientific literature: meteorological, hydrological, agricultural and socioeconomic droughts. Additionally, groundwater drought (van Lanen and Peters, 2000; Kumar et al., 2015) is important on longer timescales. Meteorological droughts relate to a deficiency of precipitation for a defined period of time, whereas hydrological drought focuses on the availability of surface and subsurface water (e.g., water levels of river and lakes). A meteorological drought is often assessed by the Standardized Precipitation Index (SPI,

McKee et al. (1993)). Groundwater droughts are characterized by exceptionally low groundwater levels, groundwater recharge and baseflow. Agricultural drought is connected to soil water availability for plants. A low amount of soil water being available for plants can lead to crop yield reduction or crop failure. Furthermore, socio-economic drought can emerge from all of the aforementioned drought types. It is characterized by a shortfall in water supply (water scarcity), meaning that the water demand could not be covered, leading to monetary losses. In terms of duration, precipitation drought has the shortest occurrence, followed by agricultural drought and finally hydrological and groundwater droughts.

A drought monitoring system that delivers timely information about the onset, extent, duration and intensity could help to reduce both drought-related fatalities and economic and ecological damages (Wilhite, 1993). The German Drought Monitor (GDM) presented herein focuses on agricultural droughts, which are highly relevant for Germany because they induce substantial agro-economic losses. In situ soil moisture observations are usually unavailable at regional or national scales and in near real-time. Alternatively, remotely sensed products are available over large areas, but contain uncertainties (Sheffield et al., 2014), cover only short time periods, are limited to sensor overflight times, depend on cloudiness and do not close the water balance. Hence, this study presents a drought identification and classification framework based on a distributed hydrologic model simulation.

5.2.1 Existing Drought Monitoring Systems

Several drought monitors for large parts of the world are currently available to the public. On the continental scale, drought monitoring or forecasting systems exist for North America (Lawrimore et al., 2002), Europe (Horion et al., 2012), and Africa (Sheffield et al., 2014). On a national scope, online platforms for India (Shah and Mishra, 2015), the Czech Republic (Trnka et al., 2014), and the United States of America (Svoboda et al., 2002; Luo and Wood, 2007; Wood, 2008) are available. Efforts to monitor drought evolution on the global scale have been made by Pozzi et al. (2013) and Hao et al. (2014).

A variety of input data, spatial and temporal resolutions and estimated drought indices can be found among these monitoring systems. The longest established system is the US drought monitor launched in 1999. The weekly published map is a composite of different indices based on meteorological observations, i.e., standardized precipitation index, the Palmer drought severity index, soil moisture percentiles derived from hydrologic model simulations, and expert knowledge from more than 130 people (Svoboda et al., 2002). Thus, local experts like agricultural and water resources managers can add information and help verify the drought map. The North American drought monitor was implemented in 2002 based on experience with the US drought monitor (Lawrimore et al., 2002). It enlarges the investigated domain to include Canada and Mexico and delivers monthly drought

maps. The drought monitors of the University of Washington (Wood, 2008) and Princeton University (Luo and Wood, 2007) cover the continental United States, showing simulations and forecasts of soil moisture, snow and runoff at $1/8^\circ$ spatial resolution derived using the Variable Infiltration Capacity (VIC) model (Liang et al., 1994).

Systems established for India (Shah and Mishra, 2015) and Africa (Sheffield et al., 2014) are based on bias-corrected satellite precipitation with the latter including a seasonal forecasting capability. These systems are running on $1/4^\circ$ resolution using the VIC model and provide drought indices based on precipitation, soil moisture, and streamflow. The Czech drought monitor (Trnka et al., 2014) is based on modeled root zone soil moisture, which is derived from local meteorological observations. Maps are published on a weekly basis and have a spatial resolution of 500 m.

The European Drought Observatory (EDO) publishes the current drought status for Europe at a ten-day interval based on a combined drought indicator composed of the standardized precipitation index (SPI) as well as soil moisture and vegetation conditions (Horion et al., 2012). The soil water and vegetation status are assessed by its anomalies, which are calculated as the deviation of the long-term mean divided by the standard deviation. EDO uses local observations to derive the SPI and the hydrologic model LISFLOOD (De Roo et al., 2000) to estimate soil moisture. The status of the vegetation is estimated based on the fraction of Absorbed Photosynthetically Active Radiation (fAPAR) retrieved from ENVISAT. The spatial resolutions of precipitation, soil moisture and fAPAR are 25 km, 5 km and 1 km, respectively, whereas their reference periods are 1981-2010, 1990-2010, and 1997-2010, respectively (Horion et al., 2012).

5.2.2 Justification for a German Drought Monitor

The implementation of a national drought monitoring system goes beyond the capabilities of the existing systems. In our work with regional stakeholders from agriculture and forestry, the need for a high-resolution regional monitoring system was expressed. Therefore, the drought monitoring system presented herein is based on data provided by the German Meteorological Service (Deutscher Wetterdienst (DWD), 2015), which are the most dense and reliable meteorological data available for this region. Furthermore, due to the long-term availability of these data, we are able to use a 60-year reference period for the estimation of drought indices for every grid cell and day of the year. This is substantially longer than can be found in other existing systems for this region. The estimation of drought indices is based on monthly soil moisture percentiles instead of anomalies, which allows for a better quantification of the drought in terms of drought magnitude and ranking using historical events. Finally, we expect that the implementation of a national drought monitor would encourage local experts, stakeholders and decision makers

to take part in the future developments and in the verification of the GDM.

5.3 Operational Drought Monitoring Framework

The German Drought Monitor (GDM) estimates drought conditions based on near realtime observed meteorological data (Deutscher Wetterdienst (DWD), 2015). These forcings drive the hydrologic model mHM (Samaniego et al., 2010; Kumar et al., 2013b) to estimate root-zone soil moisture conditions. A 60-year soil moisture data set for the period 1954-2013 is created to reconstruct historic drought conditions. This reconstruction is the statistical basis for estimating soil moisture percentiles for current conditions for every location and time point. Furthermore, it allows an evaluation of recent drought events with respect to historical events. A similar framework to that used in the GDM is applied to rank historic drought events in Germany (Samaniego et al., 2013) and for seasonal drought predictions in Europe (Thober et al., 2015).

The operational system consists of four processing steps (Figure 5.1). In the first step, local observations from the German Meteorological Service are retrieved every morning (Deutscher Wetterdienst (DWD), 2015). These data are initially quality checked by the DWD. Nevertheless, the GDM checks the downloaded data for consistency and detects outliers as a supplementary quality control. Currently, approximately 1700 precipitation and 500 climate stations, which observe the minimum, maximum, and average daily temperatures, are used to derive daily fields of meteorological input data for the hydrologic model. The daily data are interpolated by external drift kriging using terrain elevation as external drift. The spatial resolution of the resulting meteorological fields is a compromise between the demands for highly resolved hydrological predictions, which are required by stakeholders and practitioners, and the lowest reasonable resolution supported by the input data. The average minimal distance between two neighboring precipitation stations is approximately 6 km in Germany. Thus, we decided on a target resolution of $4 \times 4 \text{ km}^2$, which would provide high-resolution information without facing the risk of over-interpreting of the meteorological observations. These data are available with a time lag of four days. Due to the high persistency of soil moisture, this near real-time estimation is considered sufficient for agricultural or water management purposes.

In the second step, these interpolated fields are used to force the hydrological model mHM, a process-based model that treats grid cells as unique hydrological units. It comprises hydrological processes such as interception, snow accumulation and melting, infiltration, soil water dynamics, groundwater recharge and storage. The generated discharge of a model cell consists of direct runoff, baseflow, slow and fast interflow, which, after aggregating its components, is routed through the model domain using the Muskingum-Cunge flood routing algorithm (Chow et al.,

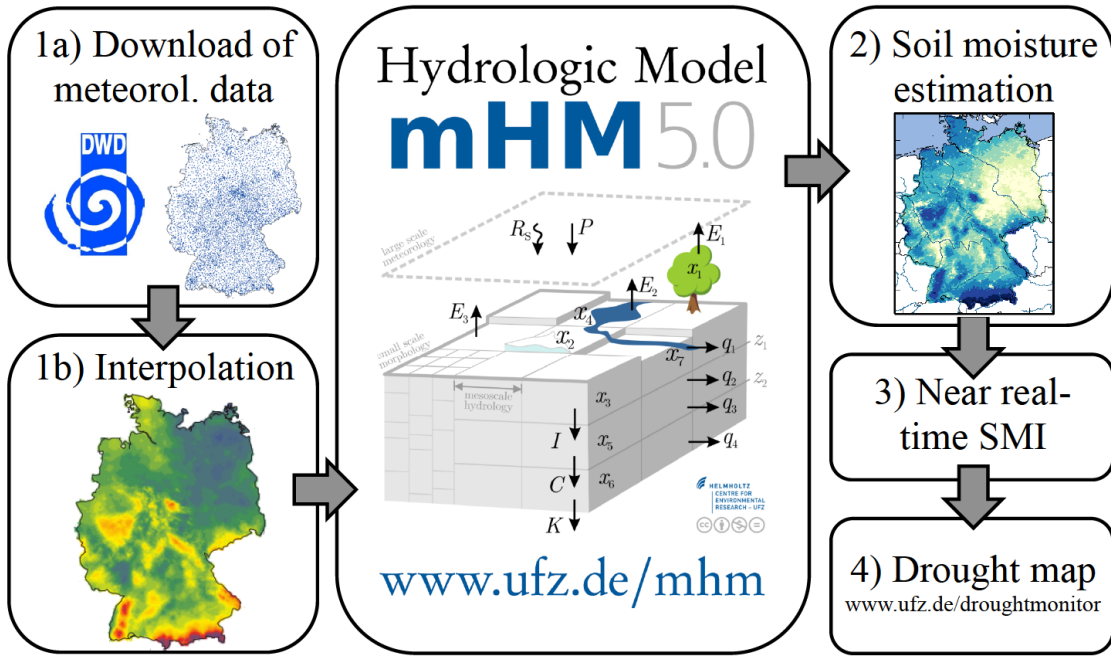


Figure 5.1: Framework of the German Drought Monitor. After 1) downloading and interpolating of the meteorological data from the National Weather Service (DWD) the data are fed to the hydrologic model mHM. 2) mHM estimates the soil moisture for the entire root zone on a daily basis which is used to 3) calculate the Soil Moisture Index (SMI). The SMI is 4) classified and visualized in a drought map published online.

1988; Todini, 2007a). By using the Multiscale Parameter Regionalization (MPR) technique (Samaniego et al., 2010; Kumar et al., 2013b), mHM directly accounts for the sub-grid variability of physiographic characteristics. The model parameters are estimated in a preliminary step on the lowest possible input resolution of the physiographic variables, i.e., $100 \times 100 \text{ m}^2$. In a second step, effective parameters at the hydrological modeling resolution of $4 \times 4 \text{ km}^2$ are estimated by applying particular upscaling operators. This technique makes mHM scale- and location-independent because it connects effective parameters to physiological inputs (Kumar et al., 2013b). In several studies, the model has shown to perform satisfactorily in a wide range of catchments with drainage areas ranging from 4 to 530,000 km^2 and with contrasting climatic regimes (Germany, India, USA, Europe) as has been shown (e.g., Samaniego et al. (2013, 2011); Kumar et al. (2013a); Rakovec et al. (2016)).

A soil moisture field, updated daily, is estimated by running the model with an internal time step of one hour. The soil water availability is estimated in three different layers. The thicknesses of the upper two layers are 5 cm and 20 cm. A third layer is spatially variable in depth, depending on the soil horizon properties specified in the input data. This variable depth, is on average, 1.8 m in Germany. The

estimated soil moisture of each single layer is used to estimate the total root zone soil moisture. The hydrological model stores specified state variables at the end of a model run. To calculate the soil moisture statistical reference, we performed a 60-year simulation from 1954 to 2013. Within the operational framework, we are currently performing hydrological simulations initialized with the model states of December 31, 2013. Thus computational time is minimized as the daily model simulation runs from January 1, 2014, onwards. An evaluation of the hydrologic model on the domain of Germany is provided by Samaniego et al. (2013).

The third step within the GDM is to transform the daily updated soil moisture into the Soil Moisture Index (SMI) by estimating the percentile of the updated soil moisture value with respect to its climatology. The daily updated soil moisture is estimated as the average of the soil conditions of the preceding 30 days. Therefore, it represents values that correspond to a time period of one month. The SMI is estimated using a non-parametric kernel-based cumulative distribution function based on a 60-year historic soil moisture reconstruction (1954-2013), as described by Samaniego et al. (2013). The calculation of the SMI is comparable to other indices such as the Standardized Precipitation Index (SPI, McKee et al. (1993)). It is estimated on every grid cell and for the particular time of the year (i.e., the average of the 30 days preceding the estimation day).

Finally, the fourth step consists of categorizing the estimated SMI into several drought classes and visualizing the results. A main requirement for the appearance of the publicly available drought map is intelligibility. For the visualization of drought events, we adapted the appearance of the German Drought Monitor to that of the US Drought Monitor (Svoboda et al., 2002), using five classes. Four classes define drought conditions, and the fifth class describes the pre-warning state of abnormally dry (Table 5.1). The four drought classes scale from moderate, (vegetation prone to water stress) to exceptional (high probability of losses of crops and increased forest fire risk).

The classes are derived using the thresholds of the Soil Moisture Index (Table 5.1). These thresholds reflect the occurrence of similar conditions in the past and thus indicate the potential impacts of these conditions. For example, the class of exceptional drought is defined by an upper threshold of 0.02. This implies that this soil moisture conditions were observed in less than 2% of the time within the 60-year reference period at this grid cell and time of the year. Thus, this drought condition only occurred in less than 1.2 cases over the last 60 years, which is equal to a return period of 50 a.

Because the SMI describes the status of the soil but not necessarily the impact on the vegetation, this classification scheme still requires further research. Crops cope with drought conditions better or worse at different stages of plant development and may not be influenced by heavy drought conditions. Revisiting this argument would mean that an effect of the Soil Moisture Index (SMI) on vegetation at different stages of plant development has to be investigated.

Table 5.1: The classification of droughts for the German Drought Monitor based on the Soil Moisture Index (SMI) (adapted from Svoboda et al. (2002)).

SMI class	Condition of the soil	Description of potential impacts
$0.30 \geq \text{SMI} > 0.20$	Abnormally Dry	conditions before or after a preceding drought
$0.20 \geq \text{SMI} > 0.10$	Moderate Drought	damages to crops and pastures possible
$0.10 \geq \text{SMI} > 0.05$	Severe Drought	losses in crops and pastures are likely
$0.05 \geq \text{SMI} > 0.02$	Extreme Drought	high probability of major losses in crops and pastures
$\text{SMI} \leq 0.02$	Exceptional Drought	high probability of exceptional losses in crops and pastures

The resulting maps are visualized and published online in the GDM. Currently, an up-to-date drought map is published every morning at 3 am CET on www.ufz.de/droughtmonitor.

5.4 Benchmark for the Recent 2015 Drought Event

Germany has experienced two drought events since the implementation of the GDM. The first took place in spring 2014, and the second occurred in summer/autumn 2015. These events are used to assess the performance of the GDM. The 2014 event (see Figure 5.2, upper row) had its largest spatial coverage in April 2014. In Germany, 70% of the area was under drought conditions ($\text{SMI} \leq 0.2$), with 25% of the total area being under exceptional drought ($\text{SMI} \leq 0.02$). The situation relaxed significantly in May 2014 due to above average rainfall, and the total drought area (moderate to exceptional drought) decreased to almost half of the area affected in April. Furthermore, the area under exceptional drought reduced to only 1%. As a consequence, the vegetation and, in particular, agricultural crops received sufficient amounts of water, especially during the crucial growing phase after seeding in April/May. In consequence, even the deterioration of drought conditions in June did not have a negative impact on yield in 2014. On the contrary, the Federal Ministry of Food and Agriculture (BMEL, 2014) reported that productivity of agriculture was superior to the preceding six years.

In 2015, the drought situation was different (Figure 5.2, lower row). In contrast to the situation in 2014, soils were not experiencing extreme to exceptional dry conditions in spring. The drought primarily evolved during spring and summer.

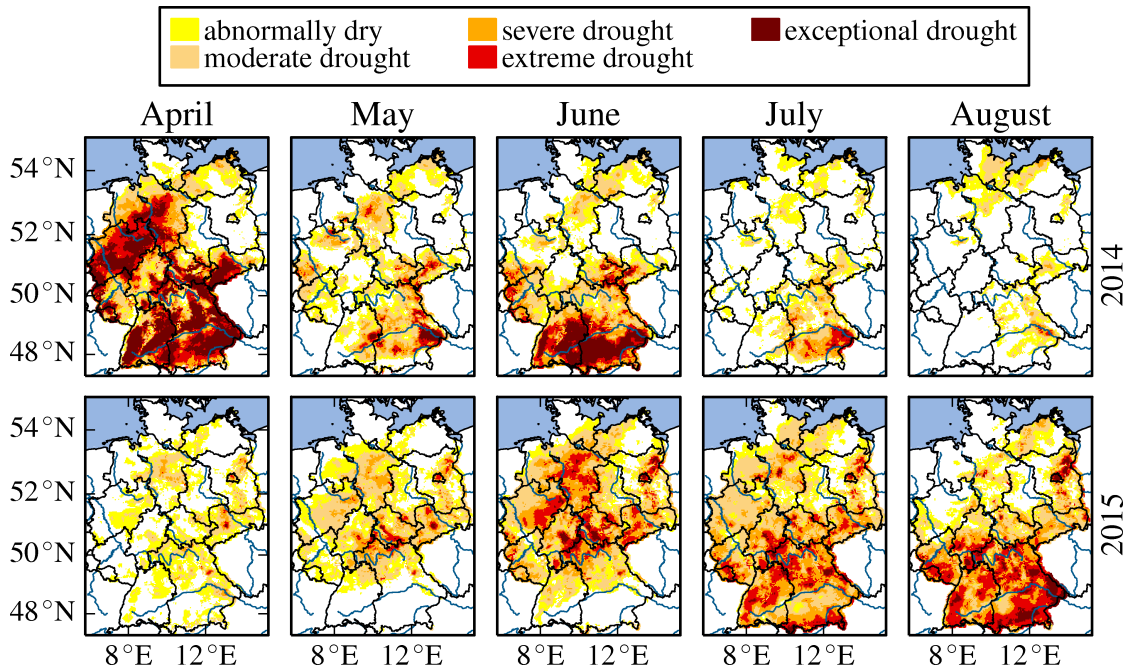


Figure 5.2: Soil water conditions from April to August in 2014 (upper row) and 2015 (lower row).

Nevertheless, the growing phase of some crops was already delayed by water shortage in May (BMEL, 2015). In some regions of Northern Bavaria and Eastern Saxony, soils were under drought conditions since autumn 2014. These regions were especially prone to losses in crop yield and to increased forest-fire risk. According to (BMEL, 2015), corn yield was 22% below the average yield between 2009 and 2014 in Germany. Additionally, some regions of Germany were prone to losses in animal food production, so they faced the decision of either buying additional food or reducing livestock (BMEL, 2015). Due to the low water levels, inland navigation was stopped on the Elbe River. A hotspot for very dry conditions was Berlin (Figure 5.2, lower row), where trees had already started shedding their leaves in the middle of August. Reports on economic consequences have not been published yet, but there were extensive fire watch activities due to very high forest fire risk and losses in crops such as corn, which led to increased expenses. Almost 75% of the area of Germany was under at least moderate drought in July 2015. During August 2015, the total area under drought decreased, but the areas of extreme and exceptional drought conditions increased to 22% and 5%, respectively.

The benchmark of the 2015 event with respect to historical drought events is shown in Figure 5.3. The left graph of this figure is created by applying the cluster identification algorithm proposed by Samaniego et al. (2013). This three-step algorithm uses the duration, spatial extent and drought intensity to calculate a dimensionless drought magnitude. The drought intensity is calculated as the

negative deviation from the SMI value 0.2, whereas the magnitude is the integral of drought intensity over time and space. The results show that the ongoing 2014-2015 event ranks among the 10 largest events observed in Germany since 1954.

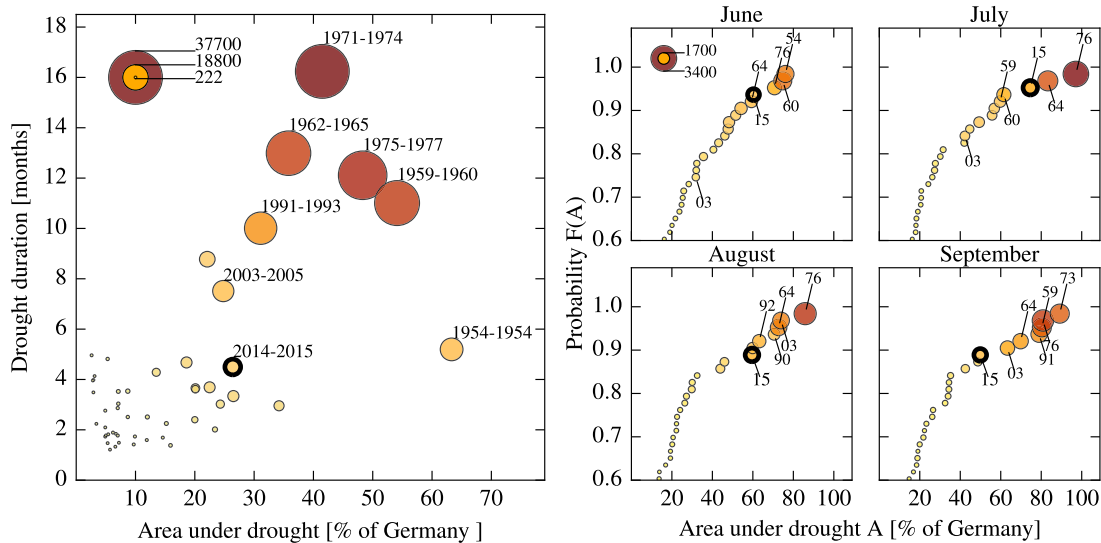


Figure 5.3: Ranking of the recently ongoing drought event in 2015. The panel on the left shows the relationship between the area, duration and magnitude of drought events since 1954. The 4 panels on the right show the drought area and magnitude at specific months over the last 62 years. The magnitudes are represented by the size of the bubble and the color code. The reference period for this figure is 1954/01/01-2015/10/31.

A more detailed insight can be obtained from the 4 panels on the right in Figure 5.3. In these graphs, the event duration is fixed to one particular month, and only the area and magnitude are variable and analyzed. The drought conditions in June and July 2015, rank within the four largest events with respect to spatial extent. The magnitude is highly correlated to the area under drought; hence, between June and September, the 2015 event ranks among the 7 largest events for the respective months. The displayed 2003 event is well remembered in Germany due to its large socio-economic impacts. In 2003, the drought event evolved more slowly than the 2015 one did, but the former peaked in August, with a magnitude $M=2067$, which is greater than the maximum magnitude reached by the 2015 event in July ($M=1770$).

5.5 Conclusion and Outlook

The German Drought Monitor (GDM) provides an easily accessible agricultural drought information system on both the regional and national levels. This information is available online since 2014. Feedback from regional stakeholders indicated

that the main user groups are from regional agencies, agriculture and forestry. Furthermore, during the 2015 drought, the GDM was widely used by the media when drought consequences became visible in Germany (e.g., in tree leaf coloring in summer).

The GDM is driven by an observational dataset, which enables drought estimates on a high spatial resolution of $4 \times 4 \text{ km}^2$. The operation of the system allows for estimates of the soil moisture on a daily basis. A drought map for Germany is released to the public on a daily basis, with a latency of 4 days. This map is intended to be easily understandable and easy to access via a web browser. The information presented within the GDM may help agricultural planners or water resources managers to optimize their actions. Furthermore, it enables the public to obtain timely information concerning the drought conditions within their region on an open access basis.

Benchmarking of recent or ongoing drought events with historical observations helps to understand their severity and indicate potential impacts. Although we intend to address agricultural drought in particular, further research should investigate the impact of low soil moisture status on agricultural yields and thereby improve drought monitoring and prediction. Therefore, a collaborative effort with agricultural engineers, water resources managers, hydrologists, policy makers, and stakeholders should be brought into focus. This will improve the reliability of drought information and increase the acceptance of the monitor. Additionally, stakeholders could improve the information content and readability of the produced drought maps through adaptation to their needs. Therefore, we plan to jointly identify 1) how to improve the visualization of drought information (e.g., readability and information content of the maps); 2) which additional information or drought indices may be beneficial (e.g., SPI) and how to present them in a comprehensible, easy to understand manner, and 3) how to implement local expert knowledge into the daily published product. An additional field of work remains in handling predictive uncertainties. These uncertainties stem from the input data uncertainty, the model's structural uncertainty and the parametric uncertainty (e.g., Samaniego et al. (2013)). Further research is necessary to investigate how to communicate this additional information without counteracting the GDM's simplicity and intelligibility.

The German Drought Monitor presented above is an important step for the delivery of a high-resolution, near real-time drought information in Germany.

Chapter 6

Discussion and Outlook

This study presents the development of a drought monitoring system for Germany from scratch. This implicated the development of a method to estimate continuous hydrological fluxes and states such as soil moisture on the national domain of Germany based on hydrologic modeling. For this purpose a parameter selection approach based on filtering well performing model parameters within the major inner seven river basins in Germany was proposed. An uncertainty assessment was presented which revealed parametric uncertainties in routed river runoff simulations as well as in gridded fields of hydrologic fluxes and states. The analysis regarding the spatio-temporal distribution of uncertainties indicated that the spatial distribution of uncertainties is highly correlated with the dryness index.

A consecutive investigation identified benchmark drought events in Germany based on the uncertain estimations of soil moisture. These uncertainties of soil moisture propagate to the identification of drought events and lead to significant classification errors of drought characteristics such as drought area or intensity. Drought area, for example, was found to have a standard deviation of up to approximately 7% of the area of Germany for particular events only due to parametric uncertainty.

A study using patterns of satellite derived land surface temperature for model calibration investigated the ability to reduce uncertainties in hydrologic predictions. This method has the capability to better constrain several model parameters, which will finally reduce overall uncertainty in hydrologic predictions, i.e., evapotranspiration. Reducing the uncertainty of evapotranspiration estimates directly impacts the estimated soil moisture, since it is the major source of evaporative water.

A final effort was dedicated to the implementation of an agricultural drought monitoring system for Germany, the German Drought Monitor (GDM). This system delivers information about soil moisture availability which has not been accessible on regional or national scale in Germany before. This Information complement data from local authorities about meteorological and hydrological drought conditions and thus better inform them about potential drought impacts. The German Drought Monitor got high attention from media due to its large spatial coverage

and up-to-dateness. Local to national newspapers and broadcasting companies appreciated the comprehensible maps of the GDM and republished them (Figure 6.1).

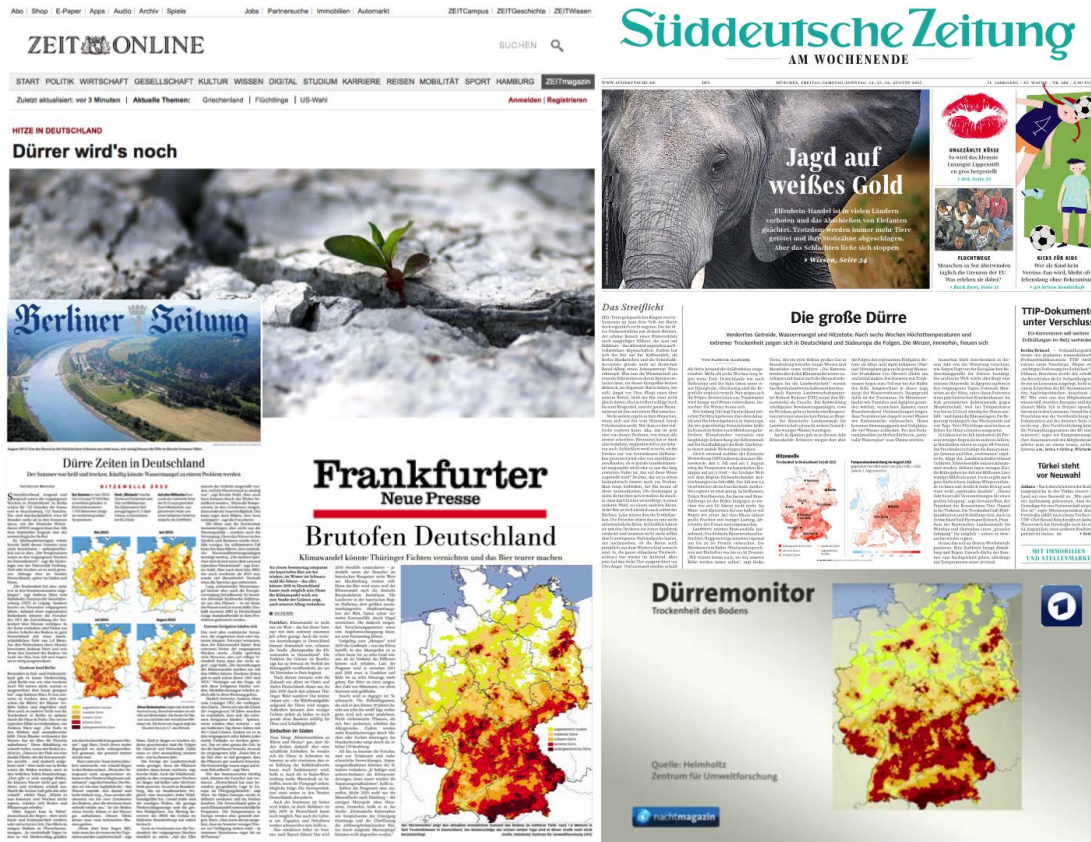


Figure 6.1: Media coverage of the German Drought Monitor at the drought event 2015. The maps produced by the German Drought Monitor were used from several newspapers and television broadcasters having regional to national coverage.

The following sections discuss the current state of my research and gives an outlook on how it can complement developments in near future.

6.1 Discussion

A main focus of this study was attributed to the parametric uncertainty of hydrologic models, which is only one source of uncertainties for hydrologic predictions. A holistic framework for the assessment of predictive uncertainties has to account for model structural and input uncertainties additional to parametric uncertainty. In the following, particular aspects of predictive uncertainties are discussed.

A substantial degree of uncertainty in the above-mentioned simulated hydrologic variables originates from the interchange of parameters between the major German river basins. This parameter transfer assures the validity of the parameters on the national scale. However, transferring parameters among distinct catchments can lead to the application of inappropriate parameters in the receiver catchment. The direct runoff parameter, for example, is almost insensitive for the Ems basin, but has a high sensitivity in the Neckar basin. This behavior can be explained by a quick response to precipitation events in the steeply sloped Neckar compared to the almost flat Ems basin. Transferring this parameter from the Ems to the Neckar will introduce uncertainties for hydrologic predictions. A simultaneous calibration of multiple, distinct catchments would yield in better constrained parameters, which are valid beyond catchment boundaries.

Another source of parametric uncertainty is attributed to the choice of the optimization algorithm. Within this study, the Dynamically Dimensioned Search (DDS) algorithm was chosen for model calibration. This algorithm terminates after a user specified number of model iterations. DDS converges very fast to a good objective function value, but does not necessarily find its optimum. Due to that reason, the estimated parametric uncertainty is sensitive to the iteration budget. Herein, we ensured appropriate iteration budgets by checking the convergence of the objective function values between several independent calibration runs. Other optimization algorithms, e.g, the Shuffled Complex Evolution algorithm, terminate if reaching a threshold of the remaining searchable space (the complex). This approach converges to optimal objective function values but needs much higher runtimes. DDS was an appropriate choice for this study due to its lower computational costs for achieving satisfying model performances.

Knowledge about the implementation and operation of several hydrologic models has to be gained, to assess model structural uncertainties. This is usually a big challenge since operating a single hydrologic model on large spatial domains is already a big effort. Therefore, a model platform is emphasized which allows for different representations and parameterizations of the same process. Efforts to develop such a model platform were undertaken. The mesoscale Hydrologic Model mHM was restructured and rewritten with significant contribution of the author of this study. Thus, mHM became the ideal test platform for investigating multiple model hypothesis as discussed in scientific literature (Niu et al., 2011; Clark et al., 2011, 2015). As a first attempt, different representations of the potential evapotranspiration approaches were implemented to mHM and applied to several catchments in Europe. Future developments aim on the implementation of different soil moisture approaches such as a variable infiltration capacity approach.

Beside the investigation of reducing and assessing predictive uncertainties, further research is needed on how to communicate them. The German Drought Monitor is designed to integrate scientists, stakeholders and decision makers. It is based on a single model realization neglecting the afore-mentioned uncertainties. This

is due to the fact that there is a lack of knowledge concerning the communication of uncertainties to decision makers and the public (Ramos et al., 2010). A collaborative effort of many disciplines is needed to investigate potential communication approaches. Natural scientists and social scientists have to work jointly on the communication and the education of stakeholders to interpret uncertainties in drought characteristics.

6.2 Outlook

It is planned to expand the study for reducing parameter uncertainties based on satellite retrieved land surface temperature with several other observations. Constraining a hydrological model with various data from different sources will lead to higher certainty for hydrologic predictions. In-situ observations of soil moisture and evapotranspiration are one potential source. These variables have major influence on the water balance and thus can be used to better constrain model parameters. New technologies like cosmic ray neutron sensing and soil moisture retrievals from ground truth stations of the Global Navigation Satellite System, are thrilling opportunities to strengthen the predictive power of hydrologic models.

Satellite retrieved soil moisture and evapotranspiration data unreliable in terms of accuracy and temporal continuity, yet. However, satellites deliver valuable information about the spatial and temporal distribution of the afore-mentioned variables. Satellite earth observations are a promising source of reliable information in future. Hydrologic models should be ready to make use of this broadly available data resource. Approaches for calibrating mHM on soil moisture data are focus of my current research.

An additional promising data source is the Gravity Recovery and Climate Experiment (GRACE). GRACE observes the changes in the earth's gravity field. These changes can be directly attributed to the total water storage, which describes the mass of the surface and subsurface water. Total water storage observations have already shown high potential to improve hydrologic predictions if considered in the parameter estimation process. Unfortunately, these data are very coarse in temporal (100-400 km) and spatial resolution (1 month).

So far, the German Drought Monitor is based on assessing the current state of the soil moisture in Germany. A seasonal forecasting system would be beneficial to planning purposes and mitigation measures. The most straightforward way to make seasonal drought forecasts is to design an Ensemble Streamflow Prediction system. This system uses past observations of meteorological variables, e.g., precipitation, instead of a numerical weather forecasts. The future development of the monitor will focus on the implementation of an Ensemble Streamflow Prediction

system, while a subsequent development will aim on the integration of probabilistic numerical weather forecasts.

The need for the implementation of indices, e.g., Standardized Precipitation Index or Runoff Index, will be assessed during stakeholder consultations. Therefore, the *Climate Office of Central Germany*, seated at our department, aims to bring together natural and social scientists as well as decision makers and stakeholders. This cooperation will determine additional requirements on the German Drought Monitor and will significantly influence its's future appearance.

Summarizing, the implementation of the German Drought Monitor was a step forward for informing the public and decision makers about agricultural droughts. The historic reconstruction of droughts enables the evaluation of ongoing events using benchmark drought events. Thus, potential negative impacts of drought events may be mitigated based on information delivered by the herein developed and published operational system.

Bibliography

- Abbott, M. B. and Refsgaard, J. C., editors. *Distributed hydrological modelling*. Kluwer Academic Publishers, Dordrecht, Netherlands, 1996.
- Ahmed, S. and De Marsily, G. Comparison of geostatistical methods for estimating transmissivity using data on transmissivity and specific capacity. *Water Resources Research*, 23(9):1717–1737, 1987. doi:10.1029/WR023i009p01717.
- Allen, R. G. R., Pereira, L., Raes, D., and Smith, M. Crop evapotranspiration - Guidelines for computing crop water requirements - FAO Irrigation and drainage paper 56. Technical Report 56, FAO - Food and Agriculture Organization of the United Nations, Rome, 1998.
- Andreadis, K. M., Clark, E. A., Wood, A. W., Hamlet, A. F., and Lettenmaier, D. P. Twentieth-Century Drought in the Conterminous United States. *Journal of Hydrometeorology*, 6(6):985–1001, 2005. doi:10.1175/JHM450.1.
- Andreadis, K. M. and Lettenmaier, D. P. Trends in 20th century drought over the continental United States. *Geophysical Research Letters*, 33(10):n/a–n/a, 2006. doi:10.1029/2006GL025711.
- Bastiaanssen, W., Menenti, M., Feddes, R., and Holtslag, A. A remote sensing surface energy balance algorithm for land (SEBAL). 1. Formulation. *Journal of Hydrology*, 212-213(1-4):198–212, 1998. doi:10.1016/S0022-1694(98)00253-4.
- Berg, A. A., Famiglietti, J. S., Rodell, M., Reichle, R. H., Jambor, U., Holl, S. L., and Houser, P. R. Development of a hydrometeorological forcing data set for global soil moisture estimation. *International Journal of Climatology*, 25(13):1697–1714, 2005. doi:10.1002/joc.1203.
- Bergström, S. Development and application of a conceptual runoff model for Scandinavian catchments. Technical report, University of Lund, Norrköping, Sweden, 1976.
- Beven, K. Editorial: Future of distributed modelling. *Hydrological Processes*, 6(3):253–254, 1992. doi:10.1002/hyp.3360060302.
- Beven, K. Prophecy, reality and uncertainty in distributed hydrological modelling. *Advances in Water Resources*, 16(1):41–51, 1993. doi:10.1016/0309-1708(93)90028-E.

- Beven, K. *Environmental Modelling: An Uncertain Future?* CRC Press, Boca Raton, 2008.
- Beven, K. *Rainfall-Runoff Modelling*. John Wiley & Sons, Ltd, Chichester, UK, 2 edition, 2012. ISBN 9781119951001. doi:10.1002/9781119951001.
- Beven, K. and Freer, J. Equifinality, data assimilation, and uncertainty estimation in mechanistic modelling of complex environmental systems using the GLUE methodology. *Journal of Hydrology*, 249(1-4):11–29, 2001. doi:10.1016/S0022-1694(01)00421-8.
- Beven, K. J. and Cloke, H. L. Comment on Hyperresolution global land surface modeling: Meeting a grand challenge for monitoring Earth’s terrestrial water by Eric F. Wood et al. *Water Resources Research*, 48(1):W01801, 2012. doi:10.1029/2011WR010982.
- Bierkens, M. F. P., Bell, V. a., Burek, P., Chaney, N., Condon, L. E., David, C. H., de Roo, A., Döll, P., Drost, N., Famiglietti, J. S., Flörke, M., Gochis, D. J., Houser, P., Hut, R., Keune, J., Kollet, S., Maxwell, R. M., Reager, J. T., Samaniego, L., Sudicky, E., Sutanudjaja, E. H., van de Giesen, N., Winsemius, H., and Wood, E. F. Hyper-resolution global hydrological modelling: what is next? Everywhere and locally relevant. *Hydrological Processes*, (October):n/a–n/a, 2014. doi:10.1002/hyp.10391.
- BMEL. Erntebericht 2014: Mengen und Preise. Technical Report August, Federal Ministry of Food and Agriculture, Bonn, 2014.
- BMEL. Erntebericht 2015 : Mengen und Preise. Technical Report August, Federal Ministry of Food and Agriculture, Bonn/Berlin, 2015.
- Boni, G., Entekhabi, D., and Castelli, F. Land data assimilation with satellite measurements for the estimation of surface energy balance components and surface control on evaporation. *Water Resources Research*, 37(6):1713, 2001. doi:10.1029/2001WR900020.
- Box, G. E. P., Jenkins, G. M., and Reinsel, G. C. *Time Series Analysis*. John Wiley & Sons, Inc., Hoboken, NJ, 4 edition, 2008. ISBN 9781118619193. doi:10.1002/9781118619193.
- Budyko, M. I. *Climate and Life*. Academic Press, New York, 1974.
- Büntgen, U., Trouet, V., Frank, D., Leuschner, H. H., Friedrichs, D., Luterbacher, J., and Esper, J. Tree-ring indicators of German summer drought over the last millennium. *Quaternary Science Reviews*, 29(7-8):1005–1016, 2010. doi:10.1016/j.quascirev.2010.01.003.

- Burnash, R. J. C., Ferral, R. L., and McGuire, R. A. *A generalized streamflow simulation system: conceptual modeling for digital computers*. U. S. Dept. of Commerce, National Weather Service, Sacramento, 1973.
- Carpenter, T. M. and Georgakakos, K. P. Intercomparison of lumped versus distributed hydrologic model ensemble simulations on operational forecast scales. *Journal of Hydrology*, 329(1-2):174–185, 2006. doi:10.1016/j.jhydrol.2006.02.013.
- Chen, T. H., Henderson-Sellers, A., Milly, P. C. D., Pitman, A. J., Beljaars, A. C. M., Polcher, J., Abramopoulos, F., Boone, A., Chang, S., Chen, F., Dai, Y., Desborough, C. E., Dickinson, R. E., Dümenil, L., Ek, M., Garratt, J. R., Gedney, N., Gusev, Y. M., Kim, J., Koster, R., Kowalczyk, E. A., Laval, K., Lean, J., Lettenmaier, D., Liang, X., Mahfouf, J.-F., Mengelkamp, H.-T., Mitchell, K., Nasonova, O. N., Noilhan, J., Robock, A., Rosenzweig, C., Schaake, J., Schlosser, C. A., Schulz, J.-P., Shao, Y., Shmakin, A. B., Verseghy, D. L., Wetzell, P., Wood, E. F., Xue, Y., Yang, Z.-L., and Zeng, Q. Cabauw Experimental Results from the Project for Intercomparison of Land-Surface Parameterization Schemes. *Journal of Climate*, 10(6):1194–1215, 1997. doi:10.1175/1520-0442(1997)010<1194:CERFTP>2.0.CO;2.
- Chow, V. T., Maidment, D. R., and Mays, L. W. *Applied hydrology*. McGraw-Hill, New York, 1988.
- Clark, M. P., Kavetski, D., and Fenicia, F. Pursuing the method of multiple working hypotheses for hydrological modeling. *Water Resources Research*, 47(9):n/a–n/a, 2011. doi:10.1029/2010WR009827.
- Clark, M. P., Nijssen, B., Lundquist, J. D., Kavetski, D., Rupp, D. E., Woods, R. a., Freer, J. E., Gutmann, E. D., Wood, A. W., Brekke, L. D., Arnold, J. R., Gochis, D. J., and Rasmussen, R. M. A unified approach for process-based hydrologic modeling: 1. Modeling concept. *Water Resources Research*, 51(4):1–17, 2015. doi:10.1002/2015WR017200.A.
- Cloke, H. L. and Pappenberger, F. Evaluating forecasts of extreme events for hydrological applications: an approach for screening unfamiliar performance measures. *Meteorological Applications*, 15(1):181–197, 2008. doi:10.1002/met.58.
- COPA-COGECA. Assessment of the impact of the heat wave and drought of the summer 2003 on agriculture and forestry. Technical report, Committee of Agricultural Organisations in the European Union, Brussels, 2003.
- Corbari, C. and Mancini, M. Calibration and Validation of a Distributed Energy-Water Balance Model Using Satellite Data of Land Surface Temperature and Ground Discharge Measurements. *Journal of Hydrometeorology*, 15(1):376–392, 2014. doi:10.1175/JHM-D-12-0173.1.

- Corbari, C., Mancini, M., Li, J., and Su, Z. Can satellite land surface temperature data be used similarly to river discharge measurements for distributed hydrological model calibration? *Hydrological Sciences Journal*, 60(2):202–217, 2015. doi:10.1080/02626667.2013.866709.
- Corbari, C., Sobrino, J. a., Mancini, M., and Hidalgo, V. Land surface temperature representativeness in a heterogeneous area through a distributed energy-water balance model and remote sensing data. *Hydrology and Earth System Sciences*, 14(10):2141–2151, 2010. doi:10.5194/hess-14-2141-2010.
- Crow, W. T., Wood, E., and Pan, M. Multiobjective calibration of land surface model evapotranspiration predictions using streamflow observations and spaceborne surface radiometric temperature retrievals. *Journal of Geophysical Research*, 108(D23):4725, 2003. doi:10.1029/2002JD003292.
- Cuntz, M., Mai, J., Zink, M., Thober, S., Kumar, R., Schäfer, D., Schrön, M., Craven, J., Rakovec, O., Spieler, D., Prykhodko, V., Dalmasso, G., Musuuza, J., Langenberg, B., Attinger, S., and Samaniego, L. Computationally inexpensive identification of noninformative model parameters by sequential screening. *Water Resources Research*, 51(8):6417–6441, 2015. doi:10.1002/2015WR016907.
- Dawson, C. and Wilby, R. Hydrological modelling using artificial neural networks. *Progress in Physical Geography*, 25(1):80–108, 2001. doi:10.1191/030913301674775671.
- Day, G. N. Extended Streamflow Forecasting Using NWSRFS. *Journal of Water Resources Planning and Management*, 111(2):157–170, 1985. doi:10.1061/(ASCE)0733-9496(1985)111:2(157).
- De Roo, A. P. J., Wesseling, C. G., and Van Deursen, W. P. A. Physically based river basin modelling within a GIS: the LISFLOOD model. *Hydrological Processes*, 14(11-12):1981–1992, 2000. doi:10.1002/1099-1085(20000815/30)14:11/12<1981::AID-HYP49>3.0.CO;2-F.
- Dee, D., Fasullo, J., Shea, D., Walsh, J., and National Center for Atmospheric Research Staff. The Climate Data Guide: Atmospheric Reanalysis: Overview & Comparison Tables. 2016.
- Demuth, S. and Heinrich, B. Temporal and spatial behaviour of drought in south germany. In *Friend97 Regional Hydrology Concepts and Models for Sustainable Water Resource Management*, pp. 151–157. 1997.
- Deutscher Wetterdienst (DWD). Global irradiance. 2011.
- Deutscher Wetterdienst (DWD). REGNIE: Verfahrensbeschreibung und Nutzeranleitung. 2013.
- Deutscher Wetterdienst (DWD). Climate station data. 2015.

- Döring, S., Döring, J., Borg, H., and Böttcher, F. Vergleich von Trockenheitsindizes zur Nutzung in der Landwirtschaft unter den klimatischen Bedingungen Mitteldeutschlands. *Hercynia*, 44(2):145–168, 2011.
- Dracup, J. A. Drought monitoring. *Stochastic Hydrology and Hydraulics*, 5(4):261–266, 1991. doi:10.1007/BF01543134.
- Dracup, J. A., Lee, K. S., and Paulson, E. G. On the definition of droughts. *Water Resources Research*, 16(2):297–302, 1980. doi:10.1029/WR016i002p00297.
- Duan, Q., Sorooshian, S., and Gupta, V. Effective and efficient global optimization for conceptual rainfall-runoff models. *Water Resources Research*, 28(4):1015–1031, 1992. doi:10.1029/91WR02985.
- Duckstein, L. Multiobjective Optimization in Structural Design: The Model Choice Problem. In Atrek, E., Gallagher, R. H., Ragsdell, K. M., and Zienkiewicz, O. C., editors, *New directions in optimum structural design*, pp. 459–481. John Wiley, New York, 1984. doi:10.1002/oca.4660060212.
- Dyck, S. and Peschke, G. *Grundlagen der Hydrologie*. Verlag für Bauwesen, Berlin, 3 edition, 1995.
- EEA. Climate change, impacts and vulnerability in Europe 2012: an indicator-based report. Technical Report 12, European Environment Agency, Copenhagen, Denmark, 2012a. doi:10.2800/66071.
- EEA. Water resources in Europe in the context of vulnerability: EEA 2012 state of water assessment. Technical Report 11, European Environment Agency, Copenhagen, Denmark, 2012b. doi:10.2800/65298.
- Entin, J. K., Robock, A., Vinnikov, K. Y., Hollinger, S. E., Liu, S., and Namkhai, A. Temporal and spatial scales of observed soil moisture variations in the extratropics. *Journal of Geophysical Research: Atmospheres*, 105(D9):11865–11877, 2000. doi:10.1029/2000JD900051.
- European Commission. Water Scarcity and Droughts - In-Depth Assessment. Technical report, European Commission, 2007.
- European Commission. Water Scarcity and Drought in the European Union. 2010.
- European Commission. Final Report Gap Analysis of the Water Scarcity and Droughts Policy in the EU European Commission. Technical report, European Commission, 2012.
- European Commission - Joint Research center (JRC). CCM River and Catchment Database. 2007.
- European Environmental Agency (EEA). CORINE Land Cover 1990, 2000 and 2006. 2009.

- European Water Archive (EWA). Runoff data. 2011.
- Fan, Y. and van den Dool, H. Climate Prediction Center global monthly soil moisture data set at 0.5?? resolution for 1948 to present. *Journal of Geophysical Research D: Atmospheres*, 109(D10):D10102, 2004. doi:10.1029/2003JD004345.
- Federal Agency for Cartography and Geodesy (BKG). Digital Elevation Model (DEM). 2010.
- Federal Environmental Agency. Climate Change in Germany: Vulnerability and Adaption of Climate sensitive Sectors: Research Report 201 41 253. Technical report, Federal Environmental Agency (Umweltbundesamt), Dessau, Germany, 2005.
- Federal Institute for Geosciences and Natural Resources (BGR). Digital soil map of Germany 1:1,000,000 (BUEK 1000). 1998.
- Federal Institute for Geosciences and Natural Resources (BGR). Hydrogeological map of Germany 1:200,000 (HUEK 200). 2009.
- Federal Ministry for the Environment Nature Conservation Building and Nuclear Safety. *Hydrological Atlas of Germany (HAD)*. Bonn, 2003. ISBN 3000056246.
- Field, J. O. Drought, the famine process, and the phasing of interventions. In Willhite, D. A., editor, *Drought: a global assessment*, pp. 273–284. Routledge Hazards and Disasters Series (UK), Vol. 2, 2000. ISBN 0-415-21418-1.
- Fink, A. H., Bruecher, T., Krueger, A., Leckebusch, G. C., Pinto, J. G., and Ulbrich, U. The 2003 European summer heatwaves and drought-synoptic diagnosis and impacts. *Weather*, 59(2004):209–216, 2004. doi:10.1256/wea.73.04.
- Flügel, W.-A. Delineating Hydrological Respons Units by Geographical Information System Analysis for Regional Hydrological Modelling using PRMS/MMS in the Drainage Basin of the River Bröl, Germany. *Hydrological Processes*, 9(January 1994):423–436, 1995. doi:10.1002/hyp.3360090313.
- Foken, T. The energy balance closure problem: An overview. *Ecological Applications*, 18(September):1351–1367, 2008. doi:10.1890/06-0922.1.
- Franke, J., Goldberg, V., Eichelmann, U., Freydank, E., and Bernhofer, C. Statistical analysis of regional climate trends in Saxony, Germany. *Climate Research*, 27(2):145–150, 2004. doi:10.3354/cr027145.
- Gerrits, A. M. J., Savenije, H. H. G., Veling, E. J. M., and Pfister, L. Analytical derivation of the Budyko curve based on rainfall characteristics and a simple evaporation model. *Water Resources Research*, 45(4):1–15, 2009. doi:10.1029/2008WR007308.

- Global Runoff Data Centre (GRDC). Runoff data. 2011.
- Guha-Sapir, D., Below, R., and Hoyois, P. EM-DAT: The OFDA/CRED International Disaster Database. 2015.
- Gupta, H. V., Sorooshian, S., and Yapo, P. O. Status of Automatic Calibration for Hydrologic Models: Comparison with Multilevel Expert Calibration. *Journal of Hydrologic Engineering*, 4(2):135–143, 1999. doi:10.1061/(ASCE)1084-0699(1999)4:2(135).
- Gutmann, E. D. and Small, E. E. A method for the determination of the hydraulic properties of soil from MODIS surface temperature for use in land-surface models. *Water Resources Research*, 46(6):n/a–n/a, 2010. doi:10.1029/2009WR008203.
- Hagen-Zanker, A. Comparing continuous valued raster data A cross disciplinary scan. Technical report, Research Institute for Knowledge Systems bv, Maastricht, 2006.
- Hao, Z., AghaKouchak, A., Nakhjiri, N., and Farahmand, A. Global integrated drought monitoring and prediction system. *Scientific Data*, 1:1–10, 2014. doi:10.1038/sdata.2014.1.
- Hargreaves, G. and Samani, Z. Reference crop evapotranspiration from ambient air temperature. *American Society of Agricultural Engineers*, 1(85-2517):96–99, 1985.
- Haug, G. H., Günther, D., Peterson, L. C., Sigman, D. M., Hughen, K. A., and Aeschlimann, B. Climate and the Collapse of Maya Civilization. *Science*, 299(5613):1731–1735, 2003. doi:10.1126/science.1080444.
- Haverd, V., Cuntz, M., Leuning, R., and Keith, H. Air and biomass heat storage fluxes in a forest canopy: Calculation within a soil vegetation atmosphere transfer model. *Agricultural and Forest Meteorology*, 147(3-4):125–139, 2007. doi:10.1016/j.agrformet.2007.07.006.
- Hodell, D. a., Curtis, J., H., and Brenner, M. Possible role of climate in the collapse of Classic Maya civilization. *Nature*, 375(6530):391–394, 1995. doi:10.1038/375391a0.
- Horion, S., Singleton, A., Barbosa, P., and Vogt, J. JRC experience on the development of Drought Information Systems. Technical report, Joint Research Centre, 2012. doi:10.2788/15761.
- Hrachowitz, M., Savenije, H., Blöschl, G., McDonnell, J., Sivapalan, M., Pomeroy, J., Arheimer, B., Blume, T., Clark, M., Ehret, U., Fencia, F., Freer, J., Gelfan, A., Gupta, H., Hughes, D., Hut, R., Montanari, A., Pande, S., Tetzlaff, D.,

- Troch, P., Uhlenbrook, S., Wagener, T., Winsemius, H., Woods, R., Zehe, E., and Cudennec, C. A decade of Predictions in Ungauged Basins (PUB)a review. *Hydrological Sciences Journal*, 58(6):1198–1255, 2013. doi:10.1080/02626667.2013.803183.
- Huang, S., Krysanova, V., Österle, H., and Hattermann, F. F. Simulation of spatiotemporal dynamics of water fluxes in Germany under climate change. *Hydrological Processes*, 24(23):3289–3306, 2010. doi:10.1002/hyp.7753.
- Hundecha, Y. and Bárdossy, A. Modeling of the effect of land use changes on the runoff generation of a river basin through parameter regionalization of a watershed model. *Journal of Hydrology*, 292(1-4):281–295, 2004. doi:10.1016/j.jhydrol.2004.01.002.
- IPCC. Managing the Risks of Extreme Events and Disasters to Advance Climate Change Adaptation. Technical report, 2012.
- Keyantash, J. and Dracup, J. a. The quantification of drought: An evaluation of drought indices. 2002. doi:10.-0477.
- Klemeš, V. Operational testing of hydrological simulation models. *Hydrological Sciences Journal*, 31(1):13–24, 1986. doi:10.1080/02626668609491024.
- Koch, J., Jensen, K. H., and Stisen, S. Toward a true spatial model evaluation in distributed hydrological modeling: Kappa statistics, Fuzzy theory, and EOF-analysis benchmarked by the human perception and evaluated against a modeling case study. *Water Resources Research*, 51(2):1225–1246, 2015. doi:10.1002/2014WR016607.
- Kollet, S. J. and Maxwell, R. M. Integrated surfacegroundwater flow modeling: A free-surface overland flow boundary condition in a parallel groundwater flow model. *Advances in Water Resources*, 29(7):945–958, 2006. doi:10.1016/j.advwatres.2005.08.006.
- Koster, R. D., Guo, Z., Yang, R., Dirmeyer, P. a., Mitchell, K., and Puma, M. J. On the Nature of Soil Moisture in Land Surface Models. *Journal of Climate*, 22(16):4322–4335, 2009. doi:10.1175/2009JCLI2832.1.
- Kuczera, G. and Mroczkowski, M. Assessment of hydrologic parameter uncertainty and the worth of multiresponse data. *Water Resources Research*, 34(6):1481–1489, 1998. doi:10.1029/98WR00496.
- Kumar, R. *Distributed Hydrologic Model Parameterization: Application in a Mesoscale River Basin*. Ph.D. thesis, Friedrich Schiller University Jena, 2010.
- Kumar, R., Livneh, B., and Samaniego, L. Toward computationally efficient large-scale hydrologic predictions with a multiscale regionalization scheme. *Water Resources Research*, 49(9):5700–5714, 2013a. doi:10.1002/wrcr.20431.

- Kumar, R., Musuuza, J. L., Van Loon, A. F., Teuling, A. J., Barthel, R., Ten Broek, J., Mai, J., Samaniego, L., and Attinger, S. Multiscale evaluation of the standardized precipitation index as a groundwater drought indicator. *Hydrology and Earth System Sciences Discussions*, 12(8):7405–7436, 2015. doi:10.5194/hessd-12-7405-2015.
- Kumar, R., Samaniego, L., and Attinger, S. The effects of spatial discretization and model parameterization on the prediction of extreme runoff characteristics. *Journal of Hydrology*, 392(1-2):54–69, 2010. doi:10.1016/j.jhydrol.2010.07.047.
- Kumar, R., Samaniego, L., and Attinger, S. Implications of distributed hydrologic model parameterization on water fluxes at multiple scales and locations. *Water Resources Research*, 49(1):360–379, 2013b. doi:10.1029/2012WR012195.
- Kutsch, W. L., Kolle, O., Rebmann, C., Knohl, A., Ziegler, W., and Schulze, E.-D. Advection and resulting CO₂ exchange uncertainty in a tall forest in central Germany. *Ecological Applications*, 18(6):1391–1405, 2008. doi:10.1890/06-1301.1.
- Laio, F., Porporato, A., Ridolfi, L., and Rodriguez-Iturbe, I. On the seasonal dynamics of mean soil moisture. *Journal of Geophysical Research*, 107(D15):ACL 8–1–ACL 8–9, 2002. doi:10.1029/2001JD001252.
- Lakshmi, V. A simple surface temperature assimilation scheme for use in land surface models. *Water Resources Research*, 36(12):3687, 2000. doi:10.1029/2000WR900204.
- van Lanen, H. A. J. and Peters, E. Definition, effects and assessment of groundwater droughts. In Vogt, J. V. and Somma, F., editors, *Drought and Drought Mitigation in Europe*, pp. 49–61. Kluwer Academic Publishers, Dordrecht, Netherlands, 2000.
- Lawrimore, J., Heim, R. R., Svoboda, M., Swail, V., and Englehart, P. J. Beginning a new era of drought monitoring across North America. 2002. doi:10.1175/1520-0477(2002)083<1191:BANEOD>2.3.CO;2.
- Li, Z.-L., Tang, B.-H., Wu, H., Ren, H., Yan, G., Wan, Z., Trigo, I. F., and Sobrino, J. a. Satellite-derived land surface temperature: Current status and perspectives. *Remote Sensing of Environment*, 131:14–37, 2013. doi:10.1016/j.rse.2012.12.008.
- Liang, X., Lettenmaier, D. P., Wood, E. F., and Burges, S. J. A simple hydrologically based model of land surface water and energy fluxes for general circulation models. *Journal of Geophysical Research*, 99(D7):14415–14428, 1994. doi:10.1029/94JD00483.

- Liang, X., Wood, E. F., and Lettenmaier, D. P. Surface soil moisture parameterization of the VIC-2L model: Evaluation and modification. *Global and Planetary Change*, 13(1-4):195–206, 1996. doi:10.1016/0921-8181(95)00046-1.
- Liu, Y., Dorigo, W., Parinussa, R., de Jeu, R., Wagner, W., McCabe, M., Evans, J., and van Dijk, A. Trend-preserving blending of passive and active microwave soil moisture retrievals. *Remote Sensing of Environment*, 123(October 2006):280–297, 2012. doi:10.1016/j.rse.2012.03.014.
- Liu, Y. and Gupta, H. V. Uncertainty in hydrologic modeling: Toward an integrated data assimilation framework. *Water Resources Research*, 43(7):n/a–n/a, 2007. doi:10.1029/2006WR005756.
- Livneh, B., Rosenberg, E. a., Lin, C., Nijssen, B., Mishra, V., Andreadis, K. M., Maurer, E. P., and Lettenmaier, D. P. A Long-Term Hydrologically Based Dataset of Land Surface Fluxes and States for the Conterminous United States: Update and Extensions*. *Journal of Climate*, 26(23):9384–9392, 2013. doi:10.1175/JCLI-D-12-00508.1.
- Luo, L. and Wood, E. F. Monitoring and predicting the 2007 U.S. drought. *Geophysical Research Letters*, 34(22):1–6, 2007. doi:10.1029/2007GL031673.
- Luterbacher, J., Dietrich, D., Xoplaki, E., Grosjean, M., and Wanner, H. European Seasonal and Annual Temperature Variability, Trends, and Extremes Since 1500. *Science*, 303(5663):1499–1503, 2004. doi:10.1126/science.1093877.
- Maurer, E. P., Wood, A. W., Adam, J. C., Lettenmaier, D. P., and Nijssen, B. A Long-Term Hydrologically Based Dataset of Land Surface Fluxes and States for the Conterminous United States*. *Journal of Climate*, 15(22):3237–3251, 2002. doi:10.1175/1520-0442(2002)015<3237:ALTHBD>2.0.CO;2.
- McCabe, G. J. and Palecki, M. A. Multidecadal climate variability of global lands and oceans. *International Journal of Climatology*, 26(7):849–865, 2006. doi:10.1002/joc.1289.
- McCabe, M. F., Kalma, J. D., and Franks, S. W. Spatial and temporal patterns of land surface fluxes from remotely sensed surface temperatures within an uncertainty modelling framework. *Hydrology and Earth System Sciences*, 9(5):467–480, 2005. doi:10.5194/hess-9-467-2005.
- McDonald, M. G. and Harbaugh, A. W. A modular three-dimensional finite-difference ground-water flow model. Technical report, U.S. Geological Survey, 1984.
- McKee, T. B., Doesken, N. J., and Kleist, J. The relationship of drought frequency and duration to time scales. In *Proceedings of the 8th Conference of Applied Climatology*, 1, pp. 179–184. American Meteorological Society, Anaheim, CA, 1993.

- Meng, L. and Quiring, S. M. A Comparison of Soil Moisture Models Using Soil Climate Analysis Network Observations. *Journal of Hydrometeorology*, 9(4):641–659, 2008. doi:10.1175/2008JHM916.1.
- Mishra, A. K. and Singh, V. P. A review of drought concepts. *Journal of Hydrology*, 391(1-2):202–216, 2010. doi:10.1016/j.jhydrol.2010.07.012.
- Mishra, V., Cherkauer, K. A., and Shukla, S. Assessment of Drought due to Historic Climate Variability and Projected Future Climate Change in the Mid-western United States. *Journal of Hydrometeorology*, 11(1):46–68, 2010. doi:10.1175/2009JHM1156.1.
- Mo, K. C., Chen, L.-C., Shukla, S., Bohn, T. J., and Lettenmaier, D. P. Uncertainties in North American Land Data Assimilation Systems over the Contiguous United States. *Journal of Hydrometeorology*, 13(3):996–1009, 2012. doi:10.1175/JHM-D-11-0132.1.
- Morris, M. D. Factorial Sampling Plans for Preliminary Computational Experiments. *Technometrics*, 33(2):161, 1991. doi:10.2307/1269043.
- Mu, Q., Heinsch, F. A., Zhao, M., and Running, S. W. Development of a global evapotranspiration algorithm based on MODIS and global meteorology data. *Remote Sensing of Environment*, 111(4):519–536, 2007. doi:10.1016/j.rse.2007.04.015.
- Nash, J. and Sutcliffe, J. River flow forecasting through conceptual models part I A discussion of principles. *Journal of Hydrology*, 10(3):282–290, 1970. doi:10.1016/0022-1694(70)90255-6.
- Neumann, J. and Wycisk, P. Mean annual ground water recharge data. 2003.
- Nicholson, S. Land surface processes and Sahel climate. *Reviews of Geophysics*, 38(1):117–139, 2000. doi:10.1029/1999RG900014.
- Niclòs, R., Galve, J. M., Valiente, J. a., Estrela, M. J., and Coll, C. Accuracy assessment of land surface temperature retrievals from MSG2-SEVIRI data. *Remote Sensing of Environment*, 115(8):2126–2140, 2011. doi:10.1016/j.rse.2011.04.017.
- Nijssen, B., Schnur, R., and Lettenmaier, D. P. Global retrospective estimation of soil moisture using the variable infiltration capacity land surface model, 1980–93. *Journal of Climate*, 14(8):1790–1808, 2001. doi:10.1175/1520-0442(2001)014<1790:GREOSM>2.0.CO;2.
- Niu, G.-Y., Yang, Z.-L., Mitchell, K. E., Chen, F., Ek, M. B., Barlage, M., Kumar, A., Manning, K., Niyogi, D., Rosero, E., Tewari, M., and Xia, Y. The community Noah land surface model with multiparameterization options (Noah-MP): 1.

- Model description and evaluation with local-scale measurements. *Journal of Geophysical Research*, 116(D12):1–16, 2011. doi:10.1029/2010JD015139.
- Nykanen, D. K. and Foufoula-Georgiou, E. Soil moisture variability and scale-dependency of nonlinear parameterizations in coupled land-atmosphere models. *Advances in Water Resources*, 24(9-10):1143–1157, 2001. doi:10.1016/S0309-1708(01)00046-X.
- Ol’dekop, E. M. On evaporation from the surface of river basins. *Transactions on Meteorological Observations*, 4:200, 1911.
- Palmer, W. C. Meteorological Drought. 1965.
- Parry, M., Canziani, O., Palutikof, J., van der Linden, P., Hanson, C., and Eds. The impact of the European 2003 heatwave. Technical report, Intergovernmental Panel on Climate Change (IPCC), Cambridge, UK, 2007.
- Pokhrel, P., Gupta, H. V., and Wagener, T. A spatial regularization approach to parameter estimation for a distributed watershed model. *Water Resources Research*, 44(12):n/a–n/a, 2008. doi:10.1029/2007WR006615.
- Pozzi, W., Sheffield, J., Stefanski, R., Cripe, D., Pulwarty, R., Vogt, J. V., Heim, R. R., Brewer, M. J., Svoboda, M., Westerhoff, R., Van Dijk, A. I. J. M., Lloyd-Hughes, B., Pappenberger, F., Werner, M., Dutra, E., Wetterhall, F., Wagner, W., Schubert, S., Mo, K., Nicholson, M., Bettio, L., Nunez, L., Van Beek, R., Bierkens, M., De Goncalves, L. G. G., De Mattos, J. G. Z., and Lawford, R. Toward global drought early warning capability: Expanding international cooperation for the development of a framework for monitoring and forecasting. *Bulletin of the American Meteorological Society*, 94(June):776–785, 2013. doi:10.1175/BAMS-D-11-00176.1.
- Rakovec, O. *Improving operational flood forecasting using data assimilation*. Ph.D. thesis, Wageningen University, 2014.
- Rakovec, O., Kumar, R., Mai, J., Cuntz, M., Thober, S., Zink, M., Attinger, S., Schäfer, D., Schrön, M., and Samaniego, L. Multiscale and Multivariate Evaluation of Water Fluxes and States over European River Basins. *Journal of Hydrometeorology*, 17(1):287–307, 2016. doi:10.1175/JHM-D-15-0054.1.
- Ramos, M.-H., Mathevet, T., Thielen, J., and Pappenberger, F. Communicating uncertainty in hydro-meteorological forecasts: mission impossible? *Meteorological Applications*, 17(2):223–235, 2010. doi:10.1002/met.202.
- Rauthe, M., Steiner, H., Riediger, U., Mazurkiewicz, A., and Gratzki, A. A Central European precipitation climatology Part I: Generation and validation of a high-resolution gridded daily data set (HYRAS). *Meteorologische Zeitschrift*, 22(3):235–256, 2013. doi:10.1127/0941-2948/2013/0436.

- Rawls, W. Estimating Soil Bulk Density From Particle Size Analysis and Organic Matter Content. *Soil Science*, 135(2):123–125, 1983.
- Rebmann, C., Zeri, M., Lasslop, G., Mund, M., Kolle, O., Schulze, E.-D., and Feigenwinter, C. Treatment and assessment of the CO₂-exchange at a complex forest site in Thuringia, Germany. *Agricultural and Forest Meteorology*, 150(5):684–691, 2010. doi:10.1016/j.agrformet.2009.11.001.
- Reichle, R. H., Kumar, S. V., Mahanama, S. P. P., Koster, R. D., and Liu, Q. Assimilation of Satellite-Derived Skin Temperature Observations into Land Surface Models. *Journal of Hydrometeorology*, 11(5):1103–1122, 2010. doi:10.1175/2010JHM1262.1.
- Rivera Villarreyes, C. A., Baroni, G., and Oswald, S. E. Integral quantification of seasonal soil moisture changes in farmland by cosmic-ray neutrons. *Hydrology and Earth System Sciences*, 15(12):3843–3859, 2011. doi:10.5194/hess-15-3843-2011.
- Robine, J., Cheung, S. L. K., Le Roy, S., Van Oyen, H., Griffiths, C., Michel, J.-P., and Herrmann, F. R. Death toll exceeded 70,000 in Europe during the summer of 2003. *Comptes Rendus Biologies*, 331(2):171–178, 2008. doi:10.1016/j.crvi.2007.12.001.
- Rodell, M., Houser, P. R., Berg, a. a., and Famiglietti, J. S. Evaluation of 10 Methods for Initializing a Land Surface Model. *Journal of Hydrometeorology*, 6(2):146–155, 2005. doi:10.1175/JHM414.1.
- Rodriguez-Iturbe, I., Entekhabi, D., and Bras, R. L. Nonlinear Dynamics of Soil Moisture at Climate Scales: 1. Stochastic Analysis. *Water Resources Research*, 27(8):1899–1906, 1991. doi:10.1029/91WR01035.
- Rosero, E., Gulden, L. E., Yang, Z.-L., De Goncalves, L. G., Niu, G.-Y., and Kaheil, Y. H. Ensemble Evaluation of Hydrologically Enhanced Noah-LSM: Partitioning of the Water Balance in High-Resolution Simulations over the Little Washita River Experimental Watershed. *Journal of Hydrometeorology*, 12(1):45–64, 2011. doi:10.1175/2010JHM1228.1.
- Samaniego, L., Kumar, R., and Attinger, S. Multiscale parameter regionalization of a grid-based hydrologic model at the mesoscale. *Water Resources Research*, 46(5):W05523, 2010. doi:10.1029/2008WR007327.
- Samaniego, L., Kumar, R., and Jackisch, C. Predictions in a data-sparse region using a regionalized grid-based hydrologic model driven by remotely sensed data. *Hydrology Research*, 42(5):338–355, 2011. doi:10.2166/nh.2011.156.
- Samaniego, L., Kumar, R., and Zink, M. Implications of Parameter Uncertainty on Soil Moisture Drought Analysis in Germany. *Journal of Hydrometeorology*, 14(1):47–68, 2013. doi:10.1175/JHM-D-12-075.1.

- Schaake, J. C. An intercomparison of soil moisture fields in the North American Land Data Assimilation System (NLDAS). *Journal of Geophysical Research*, 109(D1):D01S90, 2004. doi:10.1029/2002JD003309.
- Schindler, D. and Mayer, H. Forest meteorological investigation of the drought 2003 in the Southwest of Germany. *Allgemeine Forst und Jagdzeitung*, 178(2-3):21–37, 2007.
- Schindler, U., Steidl, J., Müller, L., Eulenstein, F., and Thiere, J. Drought risk to agricultural land in Northeast and Central Germany. *Journal of Plant Nutrition and Soil Science*, 170(3):357–362, 2007. doi:10.1002/jpln.200622045.
- Schreiber, P. Über die Beziehungen zwischen dem Niederschlag und der Wasserführung der Flüsse in Mitteleuropa. *Zeitschrift für Meteorologie*, 21(10):441–452, 1904.
- Scott, D. W. and Sain, S. R. Multidimensional Density Estimation. In Rao, C. R., editor, *Handbook of Statistics*, pp. 229–261. 2005. doi:10.1016/S0169-7161(04)24009-3.
- Shah, R. D. and Mishra, V. Development of an Experimental Near-Real-Time Drought Monitor for India. *Journal of Hydrometeorology*, 16(1):327–345, 2015. doi:10.1175/JHM-D-14-0041.1.
- Sheffield, J., Andreadis, K. M., Wood, E. F., and Lettenmaier, D. P. Global and Continental Drought in the Second Half of the Twentieth Century: Severity-Area-Duration Analysis and Temporal Variability of Large-Scale Events. *Journal of Climate*, 22(8):1962–1981, 2009. doi:10.1175/2008JCLI2722.1.
- Sheffield, J., Goteti, G., Wen, F., and Wood, E. F. A simulated soil moisture based drought analysis for the United States. *Journal of Geophysical Research*, 109(D24):D24108, 2004. doi:10.1029/2004JD005182.
- Sheffield, J., Goteti, G., and Wood, E. F. Development of a 50-Year High-Resolution Global Dataset of Meteorological Forcings for Land Surface Modeling. *Journal of Climate*, 19(13):3088–3111, 2006. doi:10.1175/JCLI3790.1.
- Sheffield, J. and Wood, E. F. Characteristics of global and regional drought, 1950–2000: Analysis of soil moisture data from offline simulation of the terrestrial hydrologic cycle. *Journal of Geophysical Research*, 112(D17):D17115, 2007. doi:10.1029/2006JD008288.
- Sheffield, J. and Wood, E. F. *Drought: Past Problems and Future Scenarios*. Taylor & Francis, New York, 2011.
- Sheffield, J., Wood, E. F., Chaney, N., Guan, K., Sadri, S., Yuan, X., Olang, L., Amani, A., Ali, A., Demuth, S., and Ogallo, L. A Drought Monitoring and

-
- Forecasting System for Sub-Sahara African Water Resources and Food Security. *Bulletin of the American Meteorological Society*, 95(6):861–882, 2014. doi:10.1175/BAMS-D-12-00124.1.
- Shiklomanov, I. World fresh water resources. In Gleick, P. H., editor, *Water in Crisis: A Guide to the World's Fresh Water Resources*, pp. 14–24. Oxford University Press, New York, 1993.
- Shukla, S., Steinemann, A. C., and Lettenmaier, D. P. Drought Monitoring for Washington State: Indicators and Applications. 2011. doi:10.1175/2010JHM1307.1.
- Shuttleworth, W. J. *Terrestrial Hydrometeorology*. John Wiley & Sons, 2012. ISBN 9780470659380. doi:10.1002/9781119951933.
- Silvestro, F., Gabellani, S., Delogu, F., Rudari, R., and Boni, G. Exploiting remote sensing land surface temperature in distributed hydrological modelling: the example of the Continuum model. *Hydrology and Earth System Sciences*, 17(1):39–62, 2013. doi:10.5194/hess-17-39-2013.
- Silvestro, F., Gabellani, S., Rudari, R., Delogu, F., Laiolo, P., and Boni, G. Uncertainty reduction and parameters estimation of a $\tilde{\sim}$ distributed hydrological model with ground and remote sensing data. *Hydrology and Earth System Sciences Discussions*, 11(6):6215–6271, 2014. doi:10.5194/hessd-11-6215-2014.
- Šimnek, J., van Genuchten, M. T., and Šejna, M. Development and Applications of the HYDRUS and STANMOD Software Packages and Related Codes. *Vadose Zone Journal*, 7(2):587, 2008. doi:10.2136/vzj2007.0077.
- Sivapalan, M., Takeuchi, K., Franks, S. W., Gupta, V. K., Karambiri, H., Lakshmi, V., Liang, X., McDonnell, J. J., Mendiondo, E. M., O’Connell, P. E., Oki, T., Pomeroy, J. W., Schertzer, D., Brook, S., and Zehe, E. IAHS Decade on Predictions in Ungauged Basins (PUB), 20032012: Shaping an exciting future for the hydrological sciences. *Hydrological Sciences Journal*, 48(6):857–880, 2003. doi:10.1623/hysj.48.6.857.51421.
- Soubeyroux, J.-m., Franchisteguy, L., Habets, F., Baillon, M., Regimbeau, F., Vidal, J.-p., Moigne, P. L., and Morel, S. Safran-Isba-Modcou - Un outil pour le suivi hydrométéorologique opérationnel et les études. *La Météorologie*, 63:40–45, 2008.
- Stahl, K. and Demuth, S. Linking streamflow drought to the occurrence of atmospheric circulation patterns. *Hydrological Sciences Journal*, 44(3):467–482, 1999. doi:10.1080/02626669909492240.

- Stisen, S., McCabe, M. F., Refsgaard, J. C., Lerer, S., and Butts, M. B. Model parameter analysis using remotely sensed pattern information in a multi-constraint framework. *Journal of Hydrology*, 409(1-2):337–349, 2011. doi:10.1016/j.jhydrol.2011.08.030.
- Svoboda, M., LeComte, D., Hayes, M., Heim, R., Gleason, K., Angel, J., Rippey, B., Tinker, R., Palecki, M., Stooksbury, D., Miskus, D., and Stephens, S. The drought monitor. *Bulletin of the American Meteorological Society*, 83(8):1181–1190, 2002. doi:10.1175/1520-0477(2002)083<1181:TDM>2.3.CO;2.
- Thober, S., Kumar, R., Sheffield, J., Mai, J., Schäfer, D., and Samaniego, L. Seasonal Soil Moisture Drought Prediction over Europe Using the North American Multi-Model Ensemble (NMME). *Journal of Hydrometeorology*, 16(6):2329–2344, 2015. doi:10.1175/JHM-D-15-0053.1.
- Thober, S., Mai, J., Zink, M., and Samaniego, L. Stochastic temporal disaggregation of monthly precipitation for regional gridded data sets. *Water Resources Research*, 50(11):8714–8735, 2014. doi:10.1002/2014WR015930.
- Todini, E. A mass conservative and water storage consistent variable parameter Muskingum-Cunge approach. *Hydrology and Earth System Sciences Discussions*, 4(3):1549–1592, 2007a. doi:10.5194/hessd-4-1549-2007.
- Todini, E. Hydrological catchment modelling: past, present and future. *Hydrology and Earth System Sciences*, 11(1):468–482, 2007b. doi:10.5194/hess-11-468-2007.
- Tokar, A. S. and Johnson, P. A. Rainfall-Runoff Modeling Using Artificial Neural Networks. *Journal of Hydrologic Engineering*, 4(3):232–239, 1999. doi:10.1061/(ASCE)1084-0699(1999)4:3(232).
- Tolson, B. A. and Shoemaker, C. A. Dynamically dimensioned search algorithm for computationally efficient watershed model calibration. *Water Resources Research*, 43(1):1–16, 2007. doi:10.1029/2005WR004723.
- Tongal, H. and Berndtsson, R. Impact of complexity on daily and multi-step forecasting of streamflow with chaotic, stochastic, and black-box models. *Stochastic Environmental Research and Risk Assessment*, 2016. doi:10.1007/s00477-016-1236-4.
- Trenberth, K. E., Dai, A., van der Schrier, G., Jones, P. D., Barichivich, J., Briffa, K. R., and Sheffield, J. Global warming and changes in drought. *Nature Clim. Change*, 4(1):17–22, 2014. doi:10.1038/NCLIMATE2067.
- Trigo, I. F., Monteiro, I. T., Olesen, F., and Kabsch, E. An assessment of remotely sensed land surface temperature. *Journal of Geophysical Research*, 113(D17):1–12, 2008. doi:10.1029/2008JD010035.

- Trnka, M., Hlavinka, P., Semerádová, D., Balek, J., Možný, M., Štěpánek, P., Zahradníček, P., Hayes, M., Eitzinger, J., and Žalud, Z. Drought monitor for the Czech Republic - www.intersucho.cz. In *Mendel and Bioclimatology*, pp. 630–638. 2014. ISBN 9788021069831.
- Vereecken, H., Huisman, J. a., Bogaert, H., Vanderborght, J., Vrugt, J. a., and Hopmans, J. W. On the value of soil moisture measurements in vadose zone hydrology: A review. *Water Resources Research*, 44:1–21, 2008. doi:10.1029/2008WR006829.
- Vidal, J.-P., Martin, E., Franchistéguy, L., Habets, F., Soubeyroux, J.-M., Blanchard, M., and Baillon, M. Multilevel and multiscale drought reanalysis over France with the Safran-Isba-Modcou hydrometeorological suite. *Hydrology and Earth System Sciences*, 14(3):459–478, 2010. doi:10.5194/hess-14-459-2010.
- Vogt, J., Soille, P., de Jager, A., Rimaviciute, E., Mehl, W., Foisneau, S., Bodis, K., Dusart, J., Paracchini, M.-L., Haastrup, P., and Bamps, C. *A pan-European river and catchment database*. European Commission - JRC, Luxembourg, 2007. ISBN 9789279069413.
- Wagener, T. and Gupta, H. V. Model identification for hydrological forecasting under uncertainty. *Stochastic Environmental Research and Risk Assessment*, 19(6):378–387, 2005. doi:10.1007/s00477-005-0006-5.
- Wagener, T., McIntyre, N., Lees, M. J., Wheater, H. S., and Gupta, H. V. Towards reduced uncertainty in conceptual rainfall-runoff modelling: dynamic identifiability analysis. *Hydrological Processes*, 17(2):455–476, 2003. doi:10.1002/hyp.1135.
- Wagner, W., Blöschl, G., Pampaloni, P., Calvet, J.-C., Bizzarri, B., Wigneron, J.-P., and Kerr, Y. Operational readiness of microwave remote sensing of soil moisture for hydrologic applications. *Nordic Hydrology*, 38(1):1, 2007. doi:10.2166/nh.2007.029.
- Wang, A., Bohn, T. J., Mahanama, S. P., Koster, R. D., and Lettenmaier, D. P. Multimodel ensemble reconstruction of drought over the continental United States. *Journal of Climate*, 22(10):2694–2712, 2009. doi:10.1175/2008JCLI2586.1.
- Wang, A., Lettenmaier, D. P., and Sheffield, J. Soil Moisture Drought in China, 1950–2006. *Journal of Climate*, 24(13):3257–3271, 2011. doi:10.1175/2011JCLI3733.1.
- Wealands, S. R., Grayson, R. B., and Walker, J. P. Quantitative comparison of spatial fields for hydrological model assessmentsome promising approaches. *Advances in Water Resources*, 28(1):15–32, 2005. doi:10.1016/j.advwatres.2004.10.001.

- Wilhite, D. A. The enigma of drought. In Wilhite, D. A., editor, *Drought assessment, management, and planning: Theory and Case Studies*, volume 2, pp. 3–15. Springer US, Boston, 1993. doi:10.1007/978-1-4615-3224-8_1.
- Wilhite, D. A., editor. *Drought and Water Crisis : Science, Technology, and Management Issues*. Taylor & Francis, Boca Raton, 2005. ISBN 9780824727710.
- Wilhite, D. A. and Glantz, M. H. Understanding: the Drought Phenomenon: The Role of Definitions. *Water International*, 10(3):111–120, 1985. doi:10.1080/02508068508686328.
- Wilhite, D. A., Sivakumar, M. V. K., and Wood, D. Early Warning Systems for Drought Preparedness and Drought Management. In *Proceedings of an Expert Group Meeting held in Lisbon*, p. 212. World Meteorological Organization, Geneva, Switzerland, 2000.
- Wilhite, D. A., Svoboda, M. D., and Hayes, M. J. Understanding the complex impacts of drought: A key to enhancing drought mitigation and preparedness. *Water Resources Management*, 21(5):763–774, 2007. doi:10.1007/s11269-006-9076-5.
- Wilks, D. S. *Statistical Methods in the Atmospheric Sciences*. Academic Press, Amsterdam, 3 edition, 2011.
- WMO. Drought monitoring and early warning: concepts, progress and future challenges. Technical Report 1006, World Meteorological Organisation, 2006.
- Wood, A. W. The University of Washington Surface Water Monitor: An experimental platform for national hydrologic assessment and prediction. In *22nd conference on hydrology*, p. 13. New Orleans, 2008.
- Wood, A. W. and Lettenmaier, D. P. An ensemble approach for attribution of hydrologic prediction uncertainty. *Geophysical Research Letters*, 35(14):L14401, 2008. doi:10.1029/2008GL034648.
- Wood, A. W., Leung, L. R., Sridhar, V., and Lettenmaier, D. P. Hydrologic Implications of Dynamical and Statistical Approaches to Downscaling Climate Model Outputs. *Climatic Change*, 62(1-3):189–216, 2004. doi:10.1023/B:CLIM.0000013685.99609.9e.
- Wood, E. F., Roundy, J. K., Troy, T. J., van Beek, L. P. H., Bierkens, M. F. P., Blyth, E., de Roo, A., Döll, P., Ek, M., Famiglietti, J., Gochis, D., van de Giesen, N., Houser, P., Jaffé, P. R., Kollet, S., Lehner, B., Lettenmaier, D. P., Peters-Lidard, C., Sivapalan, M., Sheffield, J., Wade, A., and Whitehead, P. Hyperresolution global land surface modeling: Meeting a grand challenge for monitoring Earth’s terrestrial water. *Water Resources Research*, 47(5):1–10, 2011. doi:10.1029/2010WR010090.

- Xu, C.-y. *Hydrologic Models*. Uppsala University, Uppsala, 2002.
- Zhang, X.-J., Tang, Q., Pan, M., and Tang, Y. A Long-Term Land Surface Hydrologic Fluxes and States Dataset for China. *Journal of Hydrometeorology*, 15(5):2067–2084, 2014. doi:10.1175/JHM-D-13-0170.1.
- Zhu, C. and Lettenmaier, D. P. Long-Term Climate and Derived Surface Hydrology and Energy Flux Data for Mexico: 1925–2004. *Journal of Climate*, 20(9):1936–1946, 2007. doi:10.1175/JCLI4086.1.
- Zink, M., Kumar, R., Cuntz, M., and Samaniego, L. A High-Resolution Dataset of Water Fluxes and States for Germany accounting for Parametric Uncertainty. *unpublished manuscript*.

List of Figures

1.1	Volumetric view on the Earth's water resources. The big sphere represents the volume of available water on, in, and above Earth (fresh and salt water) compared to the Earth's volume. The middle-size sphere on its right side depicts the available liquid fresh water resources on Earth including groundwater, lakes, swamps, and rivers. The smallest sphere, located below the former, shows the volume of surface fresh water (lakes and rivers) compared to the Earth's volume (source: http://water.usgs.gov/edu/earthhowmuch.html).	1
1.2	The hydrologic cycle. (adapted from: http://hydrogeology.glg.msu.edu)	3
1.3	The four different types of drought and their sequence of occurrence. (source: National Drought Mitigation Center, University of Nebraska-Lincoln, USA)	7
2.1	Study area showing the seven catchments used for estimation of common parameter sets for Germany. The points E1-E7 denote eddy covariance stations which are used for the evaluation of evapotranspiration and soil moisture.	16
2.2	Schematic view on the distributed, mesoscale Hydrologic Model mHM (www.ufz.de/mhm).	19
2.3	Model performance expressed as Nash Sutcliffe Efficiency (NSE) at daily (upper row) and monthly (lower row) resolution for the calibration period 2000-2004 (left hand side) and validation period 1965-1999 (right hand side). The white box plots show the results of the on-site calibration, whereas the gray box plots are simulations using the 100 ensemble parameter sets for Germany. Note that the y-axis starts at $NSE=0.5$	25
2.4	Observed and modeled monthly discharge for the seven catchments, which were used for parameter inference. The figure shows one decade (1990-1999) of the evaluation period. The solid dark gray line depicts the median model results and the light gray band depicts the range between the 5 th and 95 th percentile of the 100 ensemble simulations.	26

2.5	Budyko plot and performance maps for ensemble parameter sets at 222 catchments spread over Germany. The upper row depicts evaluations based on daily values (panels A, B, C), whereas the lower row depicts monthly discharge evaluation (panels D, E, F). In the first column the catchments are presented as Budyko plots (panels A, D) which are color-coded based on the ensemble median NSE for daily (panel A) and monthly (panel D) discharge values. The gray band envelops different estimations of the Budyko curve (Schreiber, 1904; Ol'dekop, 1911; Budyko, 1974). The center column depicts the location of the 222 catchments shown in the Budyko plots using the same color-code (panels B, E). The right column shows the range of the 5 th and 95 th ensemble percentiles for the NSE on daily (panel C) and monthly (panel F) basis. Panels A, B, D, E share the left color bar and panels C and F share the right color bar. The simulation period is adopted according to the available discharge observations, but is at least 10 years (average=42 years).	28
2.6	Observed ($E_{a,obs}$) versus ensemble median modeled evapotranspiration ($E_{a,mod}$) at seven eddy covariance stations (Figure 2.1).	29
2.7	Exemplary time series of observed and modeled monthly evapotranspiration and daily soil moisture anomalies at four eddy covariance stations. The solid dark gray line depicts the median model results and the light gray band depicts the range between the 5 th and 95 th percentile of the 100 ensemble simulations.	31
2.8	Comparison of mean annual groundwater recharge (R) modeled with A) mHM and from B) the Hydrologic Atlas of Germany (Federal Ministry for the Environment Nature Conservation Building and Nuclear Safety, 2003; Neumann and Wycisk, 2003). Panel C shows the difference (A-B) between both data sets. Units are [mm a ⁻¹] for all panels.	32
2.9	Water balance variables, their coefficients of variation as well as land surface characteristics for Germany. A) Mean annual precipitation P , B) ensemble mean annual evapotranspiration E_a , C) and per-grid-cell-generated runoff Q_G , D) dryness index E_p/P , E) sum of porosities (saturated soil water content) of all model layers, F) coefficient of variation from the ensemble of annual evapotranspiration and G) discharge, H) dominating land cover class on 4×4 km ² grid. The mean values and coefficients of variation are based on the period 1950-2010.	34

2.10	Normalized ranges of ensemble monthly climatology of hydrologic variables for different environmental zones within Germany. The locations of 11 environmental zones are depicted on the map on the upper right. The normalized ranges are determined as the differences of the 5 th and 95 th percentiles divided by the median (50 th percentile) of the ensemble. The hydrologic variables presented are evapotranspiration E_a , soil moisture SM , per-grid-cell-generated runoff Q_G , and groundwater recharge R	35
2.11	Superposition of parameter uncertainty through different model fluxes and states based on monthly, climatological values of E_a - evapotranspiration, SM - soil moisture, R - groundwater recharge, and Q_G - per-grid-cell-generated runoff. The uncertainty ranges and the median refer to the left ordinate, whereas the normalized uncertainty range refers to the right ordinate (blue). The geographical location of region 2, 4, 10, and 11 are depicted in Figure 2.10. . . .	37
3.1	Map of Germany indicating the main river basins used for this study. Selected locations for uncertainty analysis of the soil moisture climatology are depicted with a dot.	50
3.2	Ensemble monthly mean soil moisture fraction over Germany for the period 1950 to 2010.	57
3.3	Seasonality of the long-term soil moisture fraction x in the Rhine basin. Each point denotes the mean and the standard deviation of x at a given grid cell within this basin.	58
3.4	Parameter uncertainty of percentiles P_{10} and P_{90} of x at selected cells in Germany. The ensemble mean of these statistics is shown with a continuous line whereas their standard deviation is depicted in solid color. The location of the grid cells are shown in Figure 3.1. The position of the panels approximately resembles the geographic location of these grid cells.	59
3.5	Drought indices estimated with precipitation (a), runoff (b) and soil moisture (c) at 1960-08. Panel (d) depicts the time series of the averaged values over Germany from 1959 to 1969. The solid grey area indicates the drought occurrence.	60
3.6	Ensemble mean of the Pearson correlation coefficient (a) and mean coefficient of variation (b) between monthly soil moisture fraction estimated with rainfall products DWD1 and DWD2 but same model parameters.	61
3.7	Parameter uncertainty of SMI averaged over six major basins in Germany from 1971-01-01 to 1991-12-31. The light grey depicts the variability of the ensemble $\langle SMI \rangle$ and the black line represents the ensemble mean $\overline{\langle SMI \rangle}$	62

3.8	Panel (a): 12-month moving average of $\langle \text{SMI} \rangle$ over Germany and major river basins including uncertainty during the period from 1951-01-01 to 2010-12-31. Panel (b): Area under drought. The light grey line depicts the variability of the ensemble $\langle \text{SMI} \rangle$ and the black line represents the ensemble mean $\overline{\langle \text{SMI} \rangle}$	63
3.9	Panel (a): Probability of being at a drought severity class D0,...,D4 for May 1976. Panel (b): Most likely drought severity class based on the ensemble simulations. Classification according to the US Drought Monitor (http://droughtmonitor.unl.edu).	64
3.10	Area under drought, duration, and magnitude of the eight largest events in Germany since 1950 based on the ensemble $\langle \text{SMI} \rangle$	65
3.11	Sensitivity of the false positive rate (α) to ensemble size. In this example, α denotes the probability of rejecting the null hypothesis that the event from 1971-1974 ranks 1st among all drought events from 1950 to 2010. The size of the bootstrapping realizations was 1000.	68
3.12	Severity at the peak of the eight largest drought events from 1951-01-01 to 2010-12-31 based on the ensemble mean SMI.	68
3.13	Panel (a): Drought intensity evolution for the 10 largest drought events since 1950. Panel (b): Major drought events for a given duration and season of occurrence. The numbers denote the following events: 1: 1953-1954, 2: 1959-1960, 3: 1962-1965, 4: 1971-1974, 5: 1975-1978, 6: 1988-1991, 7: 1991-1993, 8: 1995-1997, 9: 2003-2005, 10: 2005-2007.	69
3.14	Top: Bivariate density functions between drought area and total drought magnitude of four major events. Panels (a) and (b) depict the most intense drought events with 6 months duration after its onset in winter and summer, respectively. Panels (c) and (d) correspond to the most intense drought events having a drought duration of at least 30 months, in winter and summer, respectively. Bottom: Predictive uncertainty and evolution of the area under drought for the selected events.	71
3.15	Panels (a) to (d): Ensemble averaged Severity-Area-Duration (SAD) curves of eight major drought events for 3, 6, 9, and 12 months duration since 1950 over Germany. Panel (e) depicts the predictive uncertainty of the SAD curves obtained for the event 2003-2005. In this panel, lines in red denote the ensemble mean.	72
3.16	Persistence map of the SMI (a), and regions with positive (b) and negative(c) SMI trends (5% significance). Panels (b) and (c) depict the percentage of ensemble members indicating a significant trend.	73

4.1	The main catchments used for parameter inference and numerical experiments. The six major inner German river basins span over a climate gradient ranging from maritime influence in the Ems to continental climate in Main and Neckar. The points E1 to E7 depict the location of eddy flux tower observations, which have been used for evaluating the simulated evapotranspiration.	81
4.2	Schematic description of the pattern similarity criterion according to Equation 4.16b. In the upper left row an example Pattern A with the center pixel having the value 10 is illustrated (e.g., satellite retrieved T_s). Next to it, on its right, the sign of the comparison between the center pixel with its neighboring pixels is shown. If the respective neighboring pixel is larger than the center pixel (green arrow) the value 1 is assigned to this pixel (e.g., 5 pixels in Pattern A), otherwise (red arrow) the value -1 is assigned to them (e.g., 3 pixels in Pattern A). This analysis is repeated for a pattern B (e.g., simulation of \hat{T}_s), as depicted in the lower row. The results of both comparisons are multiplied and increased by 1. Thus, the dissimilar pixels between pattern A and pattern B become 0, while similar become 2. The elements of the resulting matrix are summed up and divided by twice of the number of neighbors (e.g., 8). For the given example, the pattern similarity criterion is 0.75, meaning that three quarter of the neighbors showed the same relation to its center value.	90
4.3	Simulated daily discharge when calibrating the hydrologic model mHM with discharge Q (panels A and B) and with land surface temperature T_s (panels C and D) for the catchments Ems (panels A and C) and Main (panels B and D). The grey bands depict the uncertainty of 20 ensemble model simulations assessed by the range of the 5 th and 95 th percentile of the estimated discharge. The dark grey line is the median of the ensemble discharge simulation. Its performance is given in the top right corner of each panel.	95
4.4	A) shows the performance of the model regarding discharge if the model is calibrated with land surface temperature (T_s). For each of the six catchments 20 independent calibration runs lead to the variability of the Nash-Sutcliffe performance criteria. B) depicts the model performance when calibrating mHM with either Q or T_s and transferring the parameters to the other catchments. Thus, the variability arises from 100 parameter sets, which are derived from the five different donor basins.	96

4.5	Meidan performance of ensemble discharge predictions in 222 catchments spread over Germany. These catchments have not been used for parameter inference. The 20 parameter sets of the six donor basins presented in Figure 4.1 are used for determining these results. The 120 parameter sets from the donor basins are based on calibrations only using land surface temperature.	97
4.6	The parameter range reduction if mHM is calibrated against discharge (upper row), discharge and land surface temperature (middle row), or land surface temperature (lower row). The parameter range reduction is assessed by scaling the range of a particular parameter resulting from 20 independent calibration runs with the initial parameter range (see Equation 4.20). A low value (light yellow) indicates a small range reduction, whereas a high value (dark red) indicates a well constrained parameter. The parameters are grouped according to their appearance in different model processes. Abbreviations: I - interception, D - direct runoff.	99
4.7	Comparison of the simulated evapotranspiration if the model is calibrated with A) discharge or B) discharge and land surface temperature simultaneously. The plot shows the sum of evapotranspiration in summer 2009 (June, July, August) for the Main catchment (see Figure 4.1).	101
4.8	Kernel smoothed signal to noise ratio (SNR, Equation 4.21) of evapotranspiration fields for the catchments A) Ems and B) Main. Low values characterize noisy fields, whereas high values describe spatially smooth patterns. The uncertainty bands depict the difference between the 5 th and 95 th percentile of the signal to noise ratio of the 20 on-site calibrated parameter sets.	102
4.9	Comparison of optimization strategies using Q only or Q and T_s regarding A) the average spatial variability of evapotranspiration and B) Nash-Sutcliffe performance criterion (NSE) of daily discharge (panel B). Panel A is estimated by averaging the daily signal to noise ratio of 2009 (e.g., Figure 4.8). Panel B shows the estimated discharge of 2009 using the above mentioned calibration objectives. The uncertainty stems from 20 independent parameter estimations.	102
4.10	Evaluation of evapotranspiration (E) estimates at 7 eddy flux towers (Figure 4.1). A) shows the Pearson correlation coefficient and B) shows the root mean squared error (RMSE) between flux tower observations and model simulations using 20 parameter sets inferred by either calibration with discharge (blue) or discharge and land surface temperature (orange). The flux tower observation periods range from 3 to 10 years and are on average 6 years. Note that high Pearson correlation coefficients are beneficial, while the opposite is true for the RMSE.	104

5.1	Framework of the German Drought Monitor. After 1) downloading and interpolating of the meteorological data from the National Weather Service (DWD) the data are fed to the hydrologic model mHM. 2) mHM estimates the soil moisture for the entire root zone on a daily basis which is used to 3) calculate the Soil Moisture Index (SMI). The SMI is 4) classified and visualized in a drought map published online.	114
5.2	Soil water conditions from April to August in 2014 (upper row) and 2015 (lower row).	117
5.3	Ranking of the recently ongoing drought event in 2015. The panel on the left shows the relationship between the area, duration and magnitude of drought events since 1954. The 4 panels on the right show the drought area and magnitude at specific months over the last 62 years. The magnitudes are represented by the size of the bubble and the color code. The reference period for this figure is 1954/01/01-2015/10/31.	118
6.1	Media coverage of the German Drought Monitor at the drought event 2015. The maps produced by the German Drought Monitor were used from several newspapers and television broadcasters having regional to national coverage.	122

List of Tables

1.1	Main water reservoirs of the earth characterized by volume and turnover times (Shiklomanov, 1993; Shuttleworth, 2012).	2
2.1	Catchment properties and water balance characteristics of the seven major German river basins. The geographical location of the catchments is depicted in Figure 2.1.	17
2.2	Evaluation of evapotranspiration E_a and soil moisture SM at seven eddy stations. The evaluation is based on daily and monthly values for the available observation period. The location of the eddy flux stations is depicted in Figure 2.1.	30
3.1	Uncertainty of characteristics of major drought events in Germany since 1950. Uncertainty of the characteristics and mean \pm standard deviation.	66
3.2	Probability of finding a drought event in any of the top eight ranks. Here, only the eight largest events in Germany since 1950 were selected. The sum of the likelihood is not necessarily one due to the truncation of the table up to only the eighth rank. Values in bold represent the largest likelihood based on the ensemble simulations. .	67
5.1	The classification of droughts for the German Drought Monitor based on the Soil Moisture Index (SMI) (adapted from Svoboda et al. (2002)).	116

Selbstständigkeitserklärung

Ich erkläre, dass ich die vorliegende Arbeit selbstständig und unter Verwendung der angegebenen Hilfsmittel, persönlichen Mitteilungen und Quellen angefertigt habe.

Leipzig, 6. Dezember 2016



Matthias Zink

